

CONTRACTOR REPORT

MICROFICHE

e1

SAND94-1376
Unlimited Release
UC-721

WIPP Benchmark Calculations with the Large Strain SPECTROM Codes

G. D. Callahan, K. L. DeVries
RE/SPEC Inc.
Rapid City, SD 57709-0725

Prepared by
Sandia National Laboratories
Albuquerque, New Mexico 87185 and Livermore, California 94550
for the United States Department of Energy
under Contract DE-AC04-94AL85000

Approved for public release; distribution is unlimited.

Printed August 1995



102 p. (in various
pagings)

Issued by Sandia National Laboratories, operated for the United States Department of Energy by Sandia Corporation.

NOTICE: This report was prepared as an account of work sponsored by an agency of the United States Government. Neither the United States Government nor any agency thereof, nor any of their employees, nor any of their contractors, subcontractors, or their employees, makes any warranty, express or implied, or assumes any legal liability or responsibility for the accuracy, completeness, or usefulness of any information, apparatus, product, or process disclosed, or represents that its use would not infringe privately owned rights. Reference herein to any specific commercial product, process, or service by trade name, trademark, manufacturer, or otherwise, does not necessarily constitute or imply its endorsement, recommendation, or favoring by the United States Government, any agency thereof or any of their contractors or subcontractors. The views and opinions expressed herein do not necessarily state or reflect those of the United States Government, any agency thereof or any of their contractors.

Printed in the United States of America. This report has been reproduced directly from the best available copy.

Available to DOE and DOE contractors from
Office of Scientific and Technical Information
PO Box 62
Oak Ridge, TN 37831

Prices available from (615) 576-8401, FTS 626-8401

Available to the public from
National Technical Information Service
US Department of Commerce
5285 Port Royal RD
Springfield, VA 22161

NTIS price codes
Printed copy: A06
Microfiche copy: A01

WIPP Benchmark Calculations with the Large Strain SPECTROM Codes

G.D. Callahan
K.L. DeVries
RE/SPEC Inc.
Rapid City, SD 57709-0725

ABSTRACT

This report provides calculational results from the updated Lagrangian structural finite-element programs **SPECTROM-32** and **SPECTROM-333** for the purpose of qualifying these codes to perform analyses of structural situations in the Waste Isolation Pilot Plant (WIPP). Results are presented for the Second WIPP Benchmark (Benchmark II) Problems (Morgan et al., 1981) and for a simplified heated room problem used in a parallel design calculation study (Munson and Morgan, 1986). The Benchmark II problems consist of an isothermal room problem and a heated room problem. The stratigraphy involves 27 distinct geologic layers including ten clay seams of which four are modeled as frictionless sliding interfaces. The analyses of the Benchmark II problems consider a 10-year simulation period.

The evaluation of nine structural codes used in the Benchmark II problems shows that inclusion of finite-strain effects is not as significant as observed for the simplified heated room problem, and a variety of finite-strain and small-strain formulations produced similar results. The simplified heated room problem provides stratigraphic complexity equivalent to the Benchmark II problems but neglects sliding along the clay seams. The simplified heated problem does, however, provide a calculational check case where the small strain-formulation produced room closures about 20 percent greater than those obtained using finite-strain formulations.

A discussion is given of each of the solved problems, and the computational results are compared with available published results. In general, the results of the two **SPECTROM** large strain codes compare favorably with results from other codes used to solve the problems.

CONTENTS

1.0 INTRODUCTION	1
2.0 CODE DESCRIPTION	3
2.1 General Structure and Capabilities	3
2.1.1 SPECTROM-32	3
2.1.2 SPECTROM-333	5
2.2 Initial Stresses	6
2.3 Slide Lines	6
2.4 Thermal Structural Modeling	7
2.5 Verification Problem	7
3.0 PROBLEM DESCRIPTIONS	11
3.1 Benchmark II Isothermal Room Configuration	11
3.2 Benchmark II Heated Room Configuration	13
3.3 Simplified Heated Parallel Problem Configuration	16
4.0 COMPUTATIONAL RESULTS	21
4.1 Benchmark II Isothermal Room Results	23
4.1.1 Structural Mesh Statistics	23
4.1.2 Displacement Histories and Deformed Mesh	23
4.1.3 Relative Displacements Across the Slide Lines	30
4.1.4 Stress Profiles	35
4.2 Benchmark II Heated Room Results	35
4.2.1 Temperature Calculations	35
4.2.2 Structural Mesh Statistics	41
4.2.3 Displacement Histories and Deformed Mesh	41
4.2.4 Relative Displacements Across the Slide Lines	45
4.2.5 Stress Profiles	53
4.3 Simplified Heated Room Calculation Results	53
4.3.1 Thermal Calculations	53
4.3.2 Structural Mesh Statistics	60

CONTENTS (Continued)

4.3.3 Displacement Histories and Deformed Mesh	60
4.3.4 Stress Profiles	64
5.0 CONCLUSIONS	71
5.1 Benchmark II Isothermal Room	71
5.2 Benchmark II Heated Room	71
5.3 Simplified Heated Room	72
5.4 Summary	73
6.0 REFERENCES	75
APPENDIX A: MATERIAL CHARACTERIZATION	A-1

Tables

3-1 Mechanical properties for the simplified heated parallel calculation	18
3-2 Thermal properties for the simplified heated parallel calculation	19
4-1 Features of finite element codes and mesh statistics	22
A-1 Mechanical properties for the Benchmark II problem (upper level, nominal 655 m)	A-3
A-2 Thermal properties for the Benchmark II problem	A-4

Figures

2-1 Comparison of SPECTROM-32 and SPECTROM-333 results with the analytical solution for the simple shear problem	9
3-1 Benchmark II isothermal room configuration	12
3-2 Stratigraphic details for the Benchmark II problem	14
3-3 Benchmark II heated room configuration	15

Figures (Continued)

3-4	Stratigraphy and boundary conditions for the heated parallel structural calculation	17
4-1	SPECTROM-32 structural mesh and stratigraphy used for the Benchmark II isothermal room calculation	24
4-2	Vertical closure histories for the Benchmark II isothermal room	26
4-3	Midpillar horizontal displacement histories for the Benchmark II isothermal room	27
4-4	SPECTROM-32 Benchmark II isothermal room deformed mesh at 10 years	28
4-5	SPECTROM-333 Benchmark II isothermal room deformed mesh at 10 years	29
4-6	Relative slip across the 642.98-m slide line for the Benchmark II isothermal room	31
4-7	Relative slip across the 650.20-m slide line for the Benchmark II isothermal room	32
4-8	Relative slip across the 661.02-m slide line for the Benchmark II isothermal room	33
4-9	Relative slip across the 669.10-m slide line for the Benchmark II isothermal room	34
4-10	Effective stress profiles through the pillar of the Benchmark II isothermal room	36
4-11	Vertical stress profiles through the pillar of the Benchmark II isothermal room ..	37
4-12	Effective stress profiles along the vertical centerline of the Benchmark II isothermal room	38
4-13	Horizontal stress profiles along the vertical centerline of the Benchmark II isothermal room	39
4-14	Thermal mesh used for the Benchmark II heated room configuration	40
4-15	Temperature histories for the Benchmark II heated room configuration computed with SPECTROM-41	42
4-16	SPECTROM-32 structural mesh and stratigraphy used for the Benchmark II heated room calculation	43
4-17	Vertical closure histories for the Benchmark II heated room	44
4-18	Midpillar displacement histories for the Benchmark II heated room	46
4-19	SPECTROM-32 Benchmark II heated room deformed mesh at 10 years	47
4-20	SPECTROM-333 Benchmark II heated room deformed mesh at 10 years	48
4-21	Relative slip across the 638.86-m slide line for the Benchmark II heated room ...	49
4-22	Relative slip across the 642.98-m slide line for the Benchmark II heated room ...	50

Figures (Continued)

4-23	Relative slip across the 650.20-m slide line for the Benchmark II heated room . . .	51
4-24	Relative slip across the 661.02-m slide line for the Benchmark II heated room . . .	52
4-25	Effective stress profiles through the pillar of the Benchmark II heated room	54
4-26	Vertical stress profiles through the pillar of the Benchmark II heated room	55
4-27	Effective stress profiles along the vertical centerline of the Benchmark II heated room	56
4-28	Horizontal stress profiles along the vertical centerline of the Benchmark II heated room	57
4-29	Thermal mesh used for the simplified heated room configuration	58
4-30	Temperature histories for the simplified heated room configuration computed with SPECTROM-41	59
4-31	SPECTROM-32 structural mesh and stratigraphy used for the simplified heated room configuration	61
4-32	Vertical closure histories for the simplified heated room problem	62
4-33	Midpillar displacement history for the simplified heated room	63
4-34	SPECTROM-32 simplified heated room deformed mesh at 5 years	65
4-35	SPECTROM-333 simplified heated room deformed mesh at 5 years	66
4-36	Effective stress profiles through the pillar of the simplified heated room	67
4-37	Vertical stress profiles through the pillar of the simplified heated room	68
4-38	Effective stress profiles along the vertical centerline of the simplified heated room	69
4-39	Horizontal stress profiles along the vertical centerline of the simplified heated room	70

1.0 INTRODUCTION

This report presents the computational results from **SPECTROM-32** (Callahan et al., 1989) and **SPECTROM-333** obtained by RE/SPEC Inc. for three boundary value problems. **SPECTROM-32** and **SPECTROM-333** were not part of the original nine structural codes used in the comparative analyses described by Morgan et al. (1981) because they were not available at the time. To qualify **SPECTROM-32**, a report was prepared by RE/SPEC and submitted to Sandia containing the **SPECTROM-32** results determined for the Benchmark II problems. After Sandia reviewed the report, RE/SPEC received a formal letter from Sandia stating that **SPECTROM-32** was found qualified to Benchmark II specifications. Since that time, the capabilities of **SPECTROM-32** have been expanded to include finite strain computational capabilities (Version 4.06). **SPECTROM-333** is an undocumented finite element stress analysis computer program developed by RE/SPEC under the auspices of the Office of Civilian Radioactive Waste Management through Battelle Memorial Institute, Project Management Division, Office of Nuclear Waste Isolation. The theoretical basis of the code is given by Chaudhary et al. (1987). This report is intended to demonstrate that **SPECTROM-32** and **SPECTROM-333** are qualified to the Benchmark II specifications and are capable of solving complex problems similar to those commonly analyzed for the Waste Isolation Pilot Plant (WIPP) Program.

The three boundary value problems solved include the isothermal and heated room configurations used for the WIPP Benchmark II study (Krieg et al., 1980) and the simplified heated problem used in the parallel design study for developing quality assurance methodology for nuclear waste repository design calculations (Munson and Morgan, 1986). Munson and Morgan (1986) present results obtained from three boundary value problems that have been referred to as the primary, secondary, and simplified heated problems. The simplified heated problem was used to isolate possible sources of error and to resolve discrepancies encountered during the parallel calculations (in particular, large displacement effects). An analysis of the simplified heated problem was performed to provide an additional validation problem to qualify the codes. These three boundary value problems test a variety of code capabilities and provide a good basis from which to judge the applicability of the codes.

The problems presented in this report emphasize several of the nonlinear deformation features known to influence repository behavior. The three problems were selected because a direct comparison could be made between the results obtained by **SPECTROM-32** and **SPECTROM-333** with those obtained by independent researchers using different codes. Because an analytic solution does not exist for the complex problem of modeling room response, comparison of the

results with those obtained by other codes for an identical problem is an acceptable method for qualifying a code. One objective of the benchmark problem exercise was to compare directly the results and computer codes of a number of different researchers. The fact that several sets of results are in agreement does not mean that they represent the correct solution; it merely indicates the probable correct solution. If results differ significantly, probable reasons for the discrepancies can be identified and investigated.

The remainder of this report is divided into five chapters. Chapter 2.0 provides a brief description of **SPECTROM-32** and **SPECTROM-333** capabilities and includes a section describing how the frictionless slide lines of the Benchmark II problems were modeled. A brief description of the Benchmark II problems and the simplified heated room calculation is given in Chapter 3.0. Detailed results of the three room analyses are presented in Chapter 4.0, and a number of conclusions regarding the results of the large strain **SPECTROM** codes are summarized in Chapter 5.0. References and a detailed discussion of the material characterization for the Benchmark II problems are provided in Chapter 6.0 and Appendix A, respectively.

2.0 CODE DESCRIPTION

SPECTROM-32 and **SPECTROM-333** are updated-Lagrangian, finite-strain computer codes based on the finite element method. Finite-deformation or finite-strain terminology is used to describe the condition when no restrictions are imposed on the magnitude of the deformations or gradients of the deformation. A formulation in terms of the undeformed configuration is usually called the Lagrangian formulation. **SPECTROM-32** was developed as an internal research and development project at RE/SPEC. Since its initial development, **SPECTROM-32** has been enhanced under the auspices of Sandia National Laboratories. These enhancements primarily involve the implementation of constitutive models for crushed salt and damaged intact salt and a finite strain solution option. The theory, user's manual, and example problems for **SPECTROM-32** are described by Callahan et al. (1989). Development of **SPECTROM-333** was initiated by RE/SPEC under the auspices of the Office of Nuclear Waste Isolation (ONWI). The theory upon which the code is based has been described by Chaudhary et al. (1987). The following sections provide details on specific code topics relevant to the current study.

2.1 General Structure and Capabilities

This section provides a brief description of the general structure and capabilities of **SPECTROM-32** and **SPECTROM-333**. Although the two codes are similar in many respects, they contain enough differences to require separate discussion, which is contained in the next two sections.

2.1.1 SPECTROM-32

SPECTROM-32 is a finite element program designed to solve thermomechanical boundary-value problems in two-dimensional planar and axisymmetric geometries. Finite and small strain solution options are included. Surface loading and boundary conditions may be prescribed as functions of time. Construction sequences such as excavation and backfilling may be prescribed at specific times. Several constitutive models may be functions of temperature. The thermal and mechanical problems are assumed to be coupled one way. Thus, temperature histories must be provided by an external heat transfer simulator. **SPECTROM-32** presently contains the following constitutive models:

- Isotropic, linear elastic (Timoshenko and Goodier, 1970)
- Transversely isotropic, linear elastic (Hearmon, 1961; Lekhnitskii, 1963)
- Nonlinear elastic (Owen and Hinton, 1980)
- Norton power law (Norton, 1929; Anderson, 1976)
- Munson-Dawson multimechanism (M-D) model (Munson and Dawson, 1982; Munson et al., 1989)
- MDCF (Munson-Dawson with damage) model (Chan et al., 1992)
- Crushed salt consolidation model (Sjaardema and Krieg, 1987; Callahan and DeVries, 1991)
- TRU waste compaction model (Taylor and Flannagan, 1987; Stone et al., 1988).

A number of additional elastoplastic and viscoplastic material models are available in the code, which are described in the code documentation (Callahan et al., 1989); however, the above list includes those most frequently used for WIPP calculations.

The code uses displacement-based four-node, six-node, eight-node, and nine-node isoparametric elements. Discussion of isoparametric elements can be found in almost any textbook on finite elements (e.g., Cook, 1974; Segerlind, 1976; Zienkiewicz, 1977; Irons and Ahmad, 1980; and Owen and Hinton, 1980). Constitutive relationships use the Green-Naghdi rate of Cauchy stress tensor and the rate of deformation tensor (Malvern, 1969; Dienes, 1979; Pinsky et al., 1983; Roy et al., 1992). The advancement of the material state through the constitutive relations is achieved incrementally with a trial solution corrected by iteration, which is driven by equilibrium. The finite rotation algorithm is based on the simple yet robust polar decomposition scheme of Hoger and Carlson (1984) made available by application of the Cayley-Hamilton theorem.

To solve the system of equations generated through the finite element methodology, the code uses a frontal solver. Options are available for restarting solutions and initiating solutions from a previously established initial stress state. **SPECTROM-32** uses the simple forward method to evaluate inelastic strain increments. The solution performs a complete stiffness matrix update based on a user-prescribed tolerance for change in the effective strain and whenever excavation or backfill operations occur. The geometry and external loads are updated every iteration so that the solution is based on the current configuration.

2.1.2 SPECTROM-333

SPECTROM-333 is a finite element program composed of two separate modules (A and B). Module A is by far the larger module and serves as the preprocessor and postprocessor for the calculational portion (Module B). Both modules can be executed interactively or in batch mode. The program is operational for two-dimensional planar and axisymmetric geometries. Finite and small strain solution options are included. Surface loading and boundary conditions may be prescribed with history functions. Material properties may be prescribed as functions of time and temperature. The thermal and mechanical problems are assumed to be coupled one way. Thus, temperature histories must be provided by an external heat transfer calculator. **SPECTROM-333** presently contains the following constitutive models:

- Isotropic, linear elastic (Timoshenko and Goodier, 1970)
- Orthotropic, linear elastic (Hearmon, 1961; Lekhnitskii, 1963)
- Fully anisotropic, linear elastic (Hearmon, 1961; Lekhnitskii, 1963)
- Norton power law (Norton, 1929; Anderson, 1976)
- Krieg unified creep plasticity (Krieg, 1982)
- Munson-Dawson multimechanism (M-D) model (Munson and Dawson, 1982; Munson et al., 1989).

The code uses a displacement-based, four-node isoparametric element which is presently the only element implemented in the code. Constitutive relationships use the Green-Naghdi rate of Cauchy stress tensor and the rate of deformation tensor. The advancement of the material state through the constitutive relations is considered to be separate from the load steps. With this subincrementation process, flexibility in solution strategy is obtained since the time steps at the constitutive and global levels may be different. Constitutive model integration is accomplished using first through fourth order Runge-Kutta integration schemes. The error tolerance in the constitutive model integration may be specified by the user.

To solve the system of equations generated through the finite element methodology, the code uses a frontal solver. An option is available for performing linear-elastic solutions or for establishing an initial stress state. Various nonlinear solution strategies have been incorporated into **SPECTROM-333** including the full Newton-Raphson (Newton), the Modified Newton-Raphson, and the Broyden-Fletcher-Goldfarb-Shanno (BFGS) update (Matthies and Strang, 1979). The Newton solution performs a complete stiffness matrix (tangent or gradient matrix) update for each iteration within a load/time increment. The Modified Newton-Raphson technique performs a

gradient matrix update only for the first iteration of each increment. The BFGS technique is a quasi-Newton method that essentially performs a rank two update between iterations (see Matthies and Strang, 1979). Each of the above techniques may be supplemented with a line search, which is a linear search in the direction of the current displacement increment. The line search involves locating the zero of the potential energy. Computationally, the line search evaluates the constitutive models for various configurations until the zero of the potential energy is reasonably approximated. The three boundary value problems described in this report were solved using the BFGS solution supplemented with a line search.

2.2 Initial Stresses

The initial stress state for the qualification problems requires input of a lithostatic stress state. In **SPECTROM-333**, a lithostatic stress state is specified by the user with the initial stress option. **SPECTROM-333** uses this initial stress state in conjunction with the prescribed body forces and boundary conditions to determine if the model is in equilibrium. If the model is not in equilibrium, iterations are performed until equilibrium is satisfied based on the convergence tolerances specified. Specification of the initial state of stress in **SPECTROM-32** is identical to **SPECTROM-333** with an added feature. **SPECTROM-32** has a surface initialization option whereby the forces required to make a preexisting surface free of shear and normal forces are computed and used to speed convergence of the solution.

2.3 Slide Lines

Elements with anisotropic properties and very small physical thickness were used as *slide line elements* to model the clay seams. The slide line element width is on the order of 100,000 times its height. For the benchmark problems, slide line elements were given a height of 0.00003 m for the **SPECTROM-333** analyses and 0.0002 m for the **SPECTROM-32** analyses. The bulk modulus of the slide line elements was the same value as that used for halite and the shear modulus was set to zero for **SPECTROM-333** and very close to zero (10^{-15} MPa) for **SPECTROM-32**. By setting the shear modulus at or near zero, the element has no shear strength and the thin interface material (infinitesimal shear modulus) provides for frictionless relative displacement of the adjoining materials. The resulting deformations can result in artificially large normal stress components; however, the stresses are distributed over an infinitesimal area, and the resulting force unbalance is negligible.

2.4 Thermal Structural Modeling

In the Benchmark II heated problem and the simplified heated room calculation, the presence of the heat source requires that the thermal and structural aspects be coupled. The structural calculations are affected in two ways. Temperature changes result in thermal loads from thermal expansion that must be applied to the structure at the appropriate times. Also, the creep strain increments are affected by temperature changes because the creep strain rate is temperature-dependent.

SPECTROM-32 and **SPECTROM-333** use the uncoupled, quasi-static theory of thermoelasticity which assumes that the heat conduction problem can be solved separately. For these two codes, temperature fields are typically supplied by the heat transfer program **SPECTROM-41** (Svalstad, 1989). Different meshes were used for the thermal and structural analyses because the thermal problem requires that the boundaries be further removed than the structural problem to eliminate the boundary influence on the computed temperatures. Interpolation of temperatures from the thermal mesh to the structural mesh was accomplished with the data transfer program **MERLIN** (Gartling, 1981). **MERLIN** produces a data file containing the interpolated temperatures at the nodes for the structural mesh at the supplied times. Thus, the nodal temperatures and corresponding times are simply read by **SPECTROM-32** and **SPECTROM-333** from a peripheral storage device. **SPECTROM-333** uses linear interpolation for times that are not in the temperature data file, and **SPECTROM-32** uses a three-point Lagrangian interpolation scheme for times not available in the temperature data file.

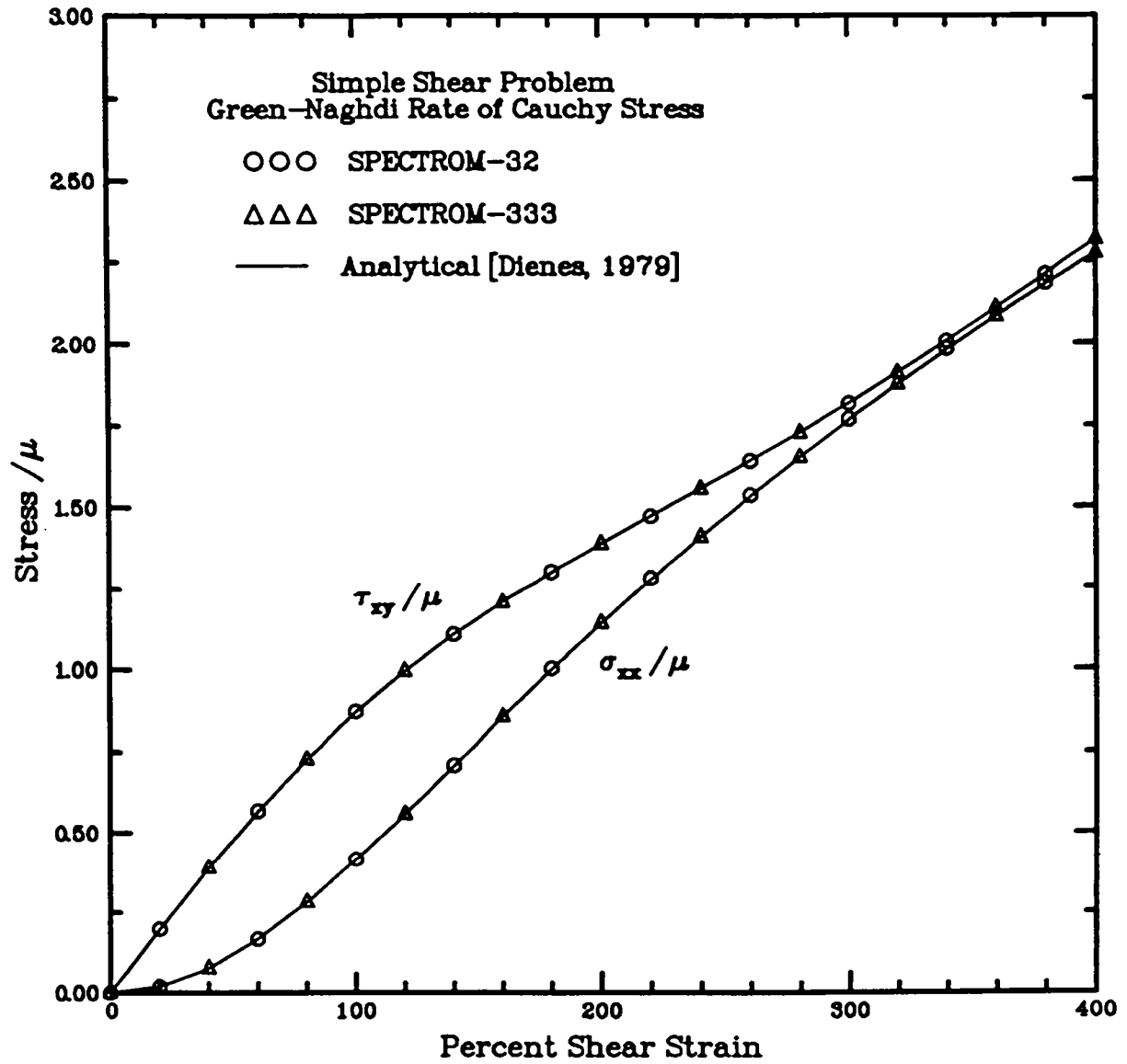
2.5 Verification Problem

As a finite-strain verification problem for **SPECTROM-32** and **SPECTROM-333**, a simple shear problem presented by Taylor and Flanagan (1987) was selected, which was originally presented by Dienes (1979). This problem was selected for presentation because it serves to point out the symptoms that can occur because of a deficiency in the Jaumann stress rate (Dienes, 1979; Taylor and Flanagan, 1987; Roy et al., 1992) and presents the solution using the Green-Naghdi rate of Cauchy stress. Therefore, the problem provides an excellent check of the finite-strain capability and the implementation of the Green-Naghdi rate of Cauchy stress in the programs.

One four-noded element measuring 1 m by 1 m was selected for the **SPECTROM-32** and **SPECTROM-333** solutions to this problem. The element was pinned along the bottom edge. Kinematic displacements in the x-direction were specified for the top two nodes with no normal

displacement specified in the y-direction. Thus, the unit block was placed in simple shear. The block was deformed a total of 400 percent engineering shear strain in the final configuration. The material was specified as elastic with Young's modulus and Poisson's ratio equal to 1.2 MPa and 0.2, respectively, which yields a shear modulus of 0.5 MPa.

The analytical solution given by Dienes (1979) using the Green-Naghdi rate of Cauchy stress is shown in Figure 2-1 as the solid lines. Curves for the shear (upper curve) and normal stress (lower curve, $\sigma_{xx} = -\sigma_{yy}$) are given with the **SPECTROM-32** results plotted as circles and the **SPECTROM-333** results plotted as diamonds. The **SPECTROM-32** and **SPECTROM-333** results are plotted at different shear strains for clarity. Excellent agreement exists between the analytical and finite element codes' solutions with results from both codes within 0.3 percent of the analytical solution.



RSI-262-94-051

Figure 2-1. Comparison of SPECTROM-32 and SPECTROM-333 results with the analytical solution for the simple shear problem.

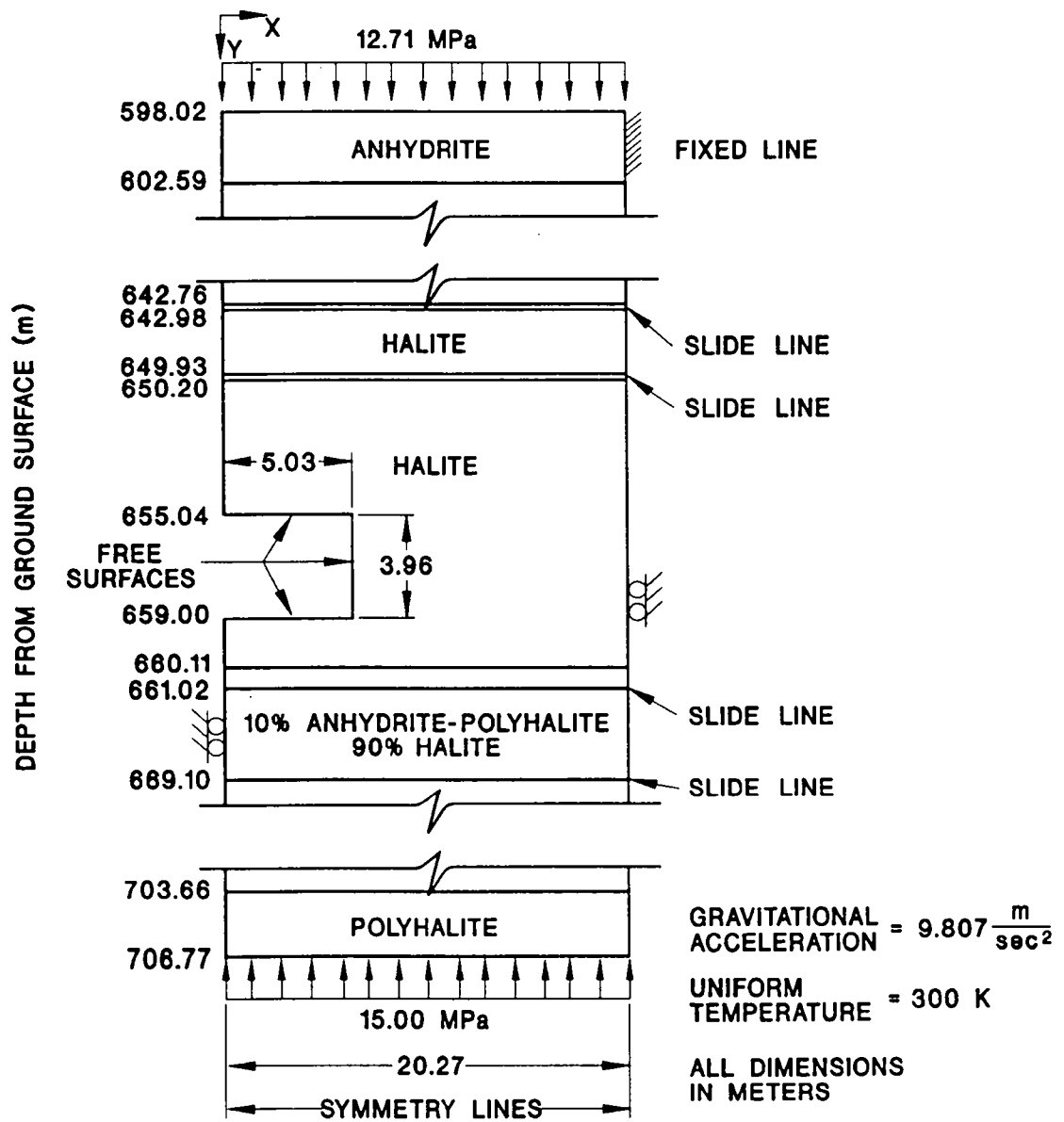
3.0 PROBLEM DESCRIPTIONS

Analyses of three well-defined boundary value problems were performed using **SPECTROM-32** and **SPECTROM-333**. For the three problems, plane strain and symmetry assumptions are made to model the regular arrays of long drifts using a single half-room. Two of the problems are described by Krieg et al. (1980) and were used in the WIPP Benchmark II study. Benchmark II involves two room configurations, an isothermal room and a heated room. The two rooms have different dimensions and are located at different depths in the stratigraphy. Both rooms are excavated instantaneously at time = 0, and the time-dependent deformation of the surrounding medium is analyzed for a period of 10 years. The third problem (simplified heated room) is described by Munson and Morgan (1986) and was used in developing quality assurance methodology for nuclear waste repository design calculations. The room is excavated instantaneously at time = 0 and deforms unheated for 6 months. At 6 months, a thermal load is applied to simulate the emplacement of heat-producing waste canisters beneath the floor of the room. The time-dependent deformation of the surrounding medium is analyzed for an additional 4.5-year period after application of the thermal load. Descriptions of the three boundary value problems are repeated below for completeness.

3.1 Benchmark II Isothermal Room Configuration

The two-dimensional, isothermal room configuration used in the benchmark calculations is shown in Figure 3-1. The temperature of the rock mass was assumed to be uniform and to remain at a constant 300 K. The vertical extremities of the configuration extend from a depth of 598.02 m to 706.77 m below the ground surface. The left and right boundaries are symmetry planes through the center of the room and through the center of the pillar between adjacent rooms, respectively. Mixed boundary conditions were imposed on these planes of symmetry permitting vertical motion but preventing horizontal motion. The horizontal distance between the left and right boundaries is 20.27 m. To prevent vertical motion, the top anhydrite layer was fixed along the line $598.02 \leq y \leq 602.59$ on the pillar centerline. The room is rectangular with a half-width of 5.03 m and a height of 3.96 m. The floor of the room is positioned at the 659.00-m level.

A lithostatic initial stress was assumed; i.e., $\sigma_{xx} = \sigma_{yy} = \sigma_{zz} = -0.021252y$, where y is depth in meters and stresses are in MPa. The rock above 598.02 m was replaced by a traction of 12.71 MPa acting downward on the top of the medium. The rock below 706.77 m was replaced by a traction of 15.00 MPa acting upward.



RSI-262-04-048

Figure 3-1. Benchmark II isothermal room configuration.

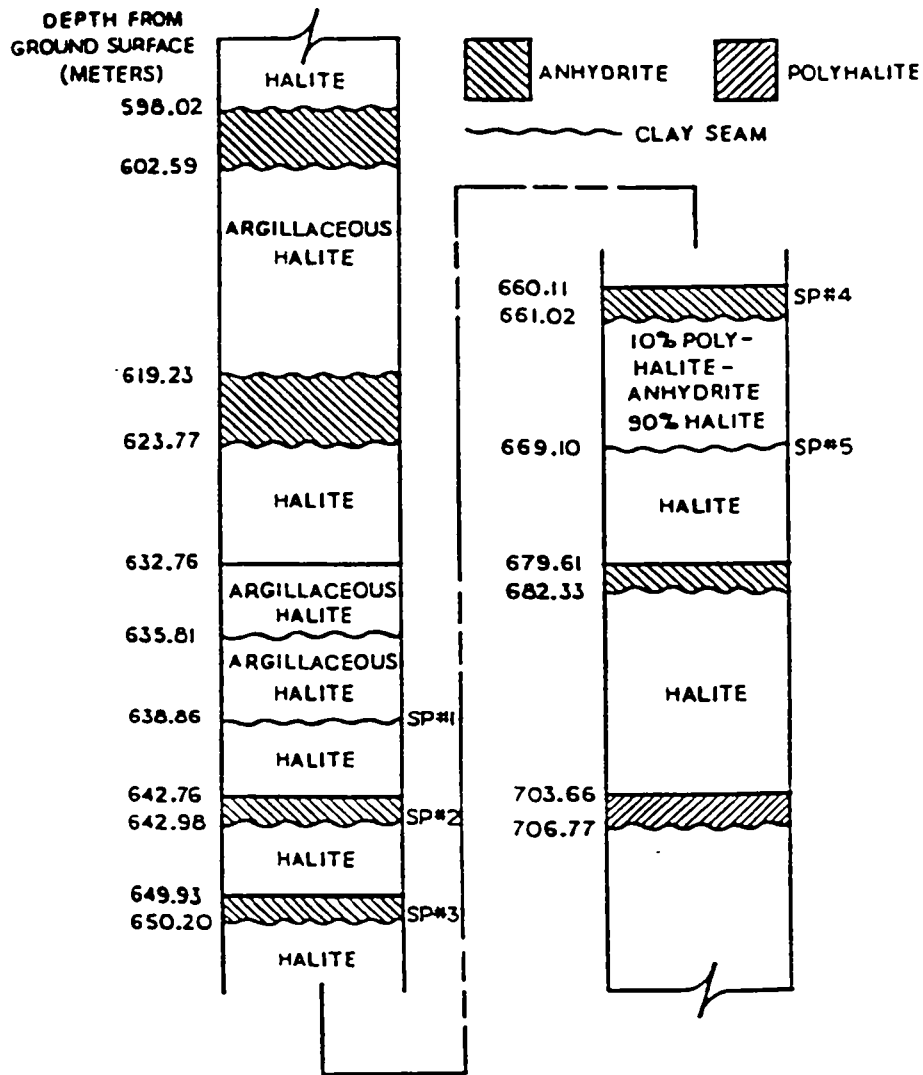
The WIPP stratigraphy shown in Figure 3-2 was simplified so that only four of the 10 clay seams were taken as active slide planes. The four active clay seams include the two clay seams immediately above the room and the two clay seams immediately below the room. The clay seams are located at depths of 642.98, 650.20, 661.02, and 669.10 m and are identified as SP #2 through SP #5 in Figure 3-2. Perfect slip was assumed for the clay seam; i.e., the coefficient of friction on the slide planes is zero. The WIPP stratigraphy shown in Figure 3-2 consists of layers of halite, argillaceous halite, anhydrite, polyhalite, and a layer consisting of 10 percent polyhalite and anhydrite mixed with 90 percent halite. This stratigraphy was proposed for the WIPP site and was established by Sandia and the WIPP Project Office Contractors in November 1979 (Morgan et al., 1981). Each of the layers was assumed to have an elastic deformation component. In addition, the halite, 10 percent polyhalite and anhydrite mixed with 90 percent halite, and argillaceous layers were assumed to have inelastic deformation components that obey a secondary creep law (Norton power law). A summary of the complete material characterization is given in Appendix A.

3.2 Benchmark II Heated Room Configuration

The two-dimensional, heated room configuration used in the benchmark calculations is shown in Figure 3-3. All boundary conditions, initial stresses, and body forces were the same as those for the isothermal room except for the bottom traction, which was 15.01 MPa instead of 15.00 MPa. This slight difference in the two cases is a result of the slightly larger extraction ratio for the isothermal room. The horizontal distance between the left and right boundaries is 22.86 m. The room is rectangular with a half-width of 2.29 m and a height of 4.57 m. The floor is positioned at the 652.00-m level. The heat source extends from a depth of 655.00 m to a depth of 656.83 m along the vertical centerline of the heated room. This heat source simulates canisters positioned at regular intervals beneath the floor. The waste was idealized as a plane source with no x -direction dimension. The source was modeled as one continuously distributed below the floor along the room centerline with a time-dependent output of

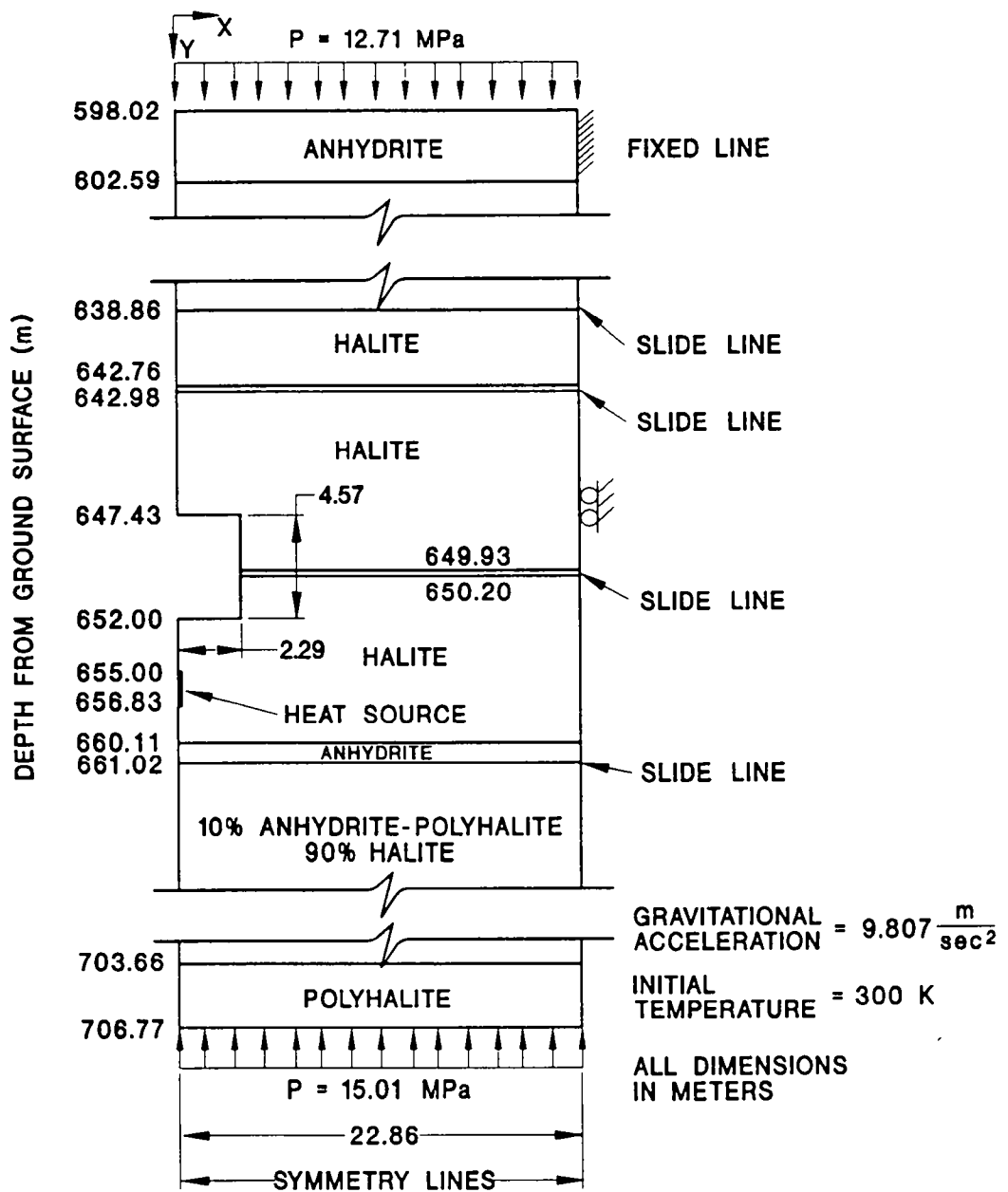
$$q = 169.5 \exp(-t/1.365 \times 10^9) \text{ [W/m]} \quad (3-1)$$

where t is in seconds. This heat flux was uniformly distributed over the 1.83-m height of the source. This is approximately equal to an initial thermal power density of 30 kW/acre. The initial temperature of the rock mass was 300 K. Thermal radiation between the surfaces of the heated room was simulated by an artificial thermal material. The conductivity of this material was chosen such that a thermal calculation with conduction heat transfer in the room would produce the same temperatures around the room as a thermal calculation with radiation heat



RSI-024-61-24

Figure 3-2. Stratigraphic details for the Benchmark II problem.



RSI-262-64-049

Figure 3-3. Benchmark II heated room configuration.

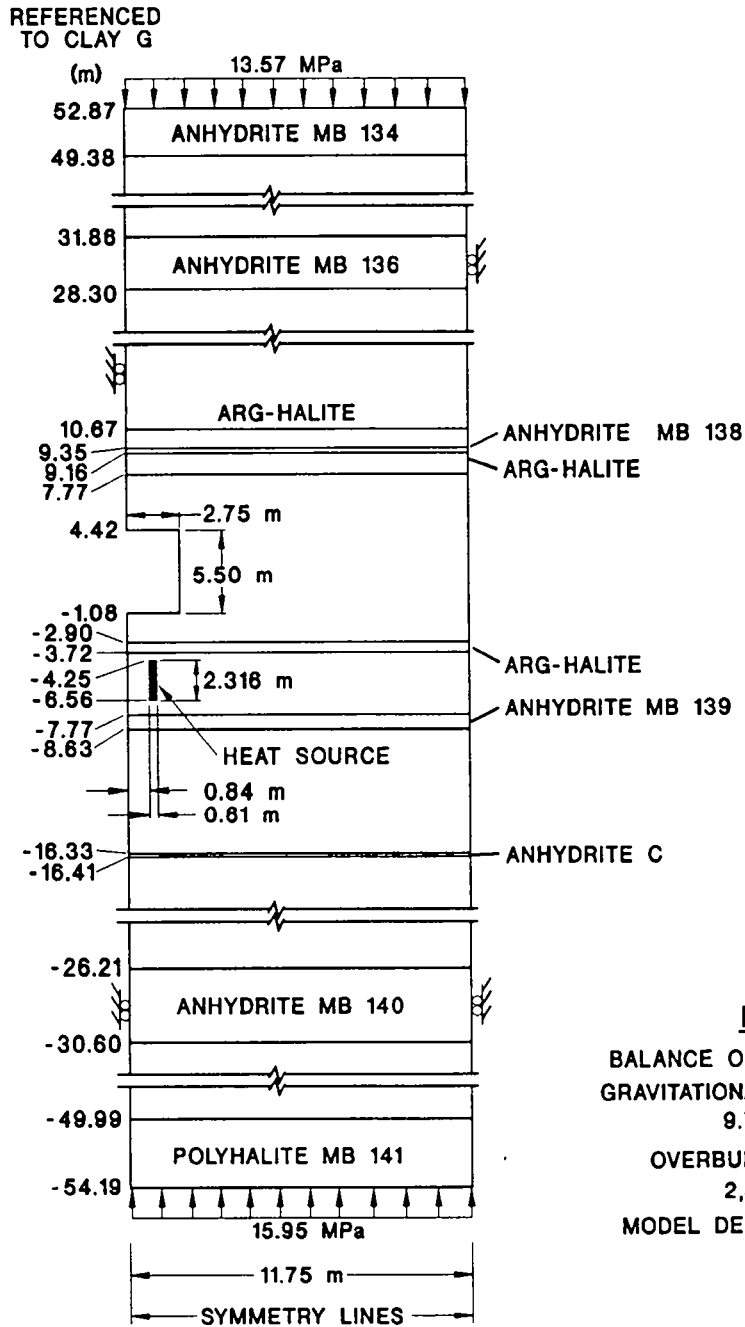
transfer. This thermal material has no structural properties. The thermal and mechanical properties of the different materials required for the Benchmark II heated problem are provided in Appendix A.

The same stratigraphy as that used in the isothermal problem was used in the heated problem. The stratigraphy was again simplified so that only four of the ten clay seams were taken as active slide planes. The four active clay seams include the two clay seams immediately above the heated room, the clay seam located at the center of the heated room, and the clay seam immediately below the heated room. The clay seams are located at depths of 638.86, 642.98, 650.20, and 661.02 m and are identified as SP #1 through SP #4 in Figure 3-2. Perfect slip was assumed for the clay seam; i.e., the coefficient of friction on the slide planes was taken to be zero. A summary of the complete material characterization is given in Appendix A.

3.3 Simplified Heated Parallel Problem Configuration

The two-dimensional, heated room configuration used in the secondary parallel calculation (Munson and Morgan, 1986) is shown in Figure 3-4. For the simplified heated parallel calculation, the stratigraphy shown in Figure 3-4 was simplified by replacing the anhydrite in the pillar with halite and by allowing no slip at the clay seam locations. The vertical extremities of the configuration extend 52.87 m above and 54.19 m below Clay G, the reference from which all vertical distances are measured. The left and right boundaries are symmetry planes through the center of the room and through the center of the pillar between adjacent rooms, respectively. Mixed boundary conditions were imposed on these planes of symmetry, permitting vertical motion but preventing horizontal motion. The horizontal distance between the left and right boundaries is 11.75 m. To prevent vertical motion, the top anhydrite layer was fixed along the line $52.87 \leq y \leq 49.38$ on the pillar centerline. The room is square with a half-width of 2.75 m and a height of 5.50 m. The floor is positioned 1.08 m below Clay G.

A traction of 13.57 MPa, which represents the weight of the overburden above the configuration, was applied to the top boundary. An average overburden density of $2,320 \text{ kg/m}^3$ and a gravitational acceleration of 9.79 m/s^2 were used to compute the weight of the overburden. An average density of $2,300 \text{ kg/m}^3$ was used for all stratigraphic layers within the configuration to compute the bottom traction of 15.95 MPa. An initial hydrostatic stress state was specified that varied linearly with depth (i.e., $\sigma_{xx} = \sigma_{yy} = \sigma_{zz} = -0.022517y$ MPa plus the overburden pressure of -13.57 MPa, where y is depth in meters from the upper boundary of the model). Each of the layers was assumed to have an elastic deformation component. In addition, the halite



NOTES

BALANCE OF MODEL - HALITE

GRAVITATIONAL ACCELERATION = 9.79 m/sec^2

OVERBURDEN DENSITY = $2,320 \text{ kg/m}^3$

MODEL DENSITY = $2,300 \text{ kg/m}^3$

RSI-068-84-01

Figure 3-4. Stratigraphy and boundary conditions for the heated parallel structural calculation.

and argillaceous halite layers were assumed to have inelastic deformation components that obey the secondary creep law (Norton power law). The material models have the same form as those used for the Benchmark II problems; however, some of the material constants are different. The elastic and creep constants are given in Table 3-1.

Table 3-1. Mechanical properties for the simplified heated parallel calculation^a

Material	Elastic Constants ^b			Creep Constants ^c		
	ν	E (Pa)	α K ⁻¹	D (Pa ^{-4.9} - s ⁻¹)	n	Q (kcal/mole)
Halite	0.25	3.10×10^{10}	45.0×10^{-6}	5.79×10^{-36}	4.9	12.0
Argillaceous Salt	0.25	3.10×10^{10}	40.0×10^{-6}	1.74×10^{-35}	4.9	12.0
Anhydrite	0.35	7.51×10^{10}	20.0×10^{-6}	—	—	—
Polyhalite	0.36	5.53×10^{10}	24.0×10^{-6}	—	—	—

^a From Munson and Morgan (1986).

^b Poisson's ratio, ν ; Young's modulus, E ; and coefficient of linear thermal expansion, α .

^c See Appendix A for creep law description.

The initial temperature of the configuration was 300 K. The configuration includes an infinite volumetric heat source equivalent to the thermal power output of canister heaters placed below the floor. The canisters were assumed to exist in a square array about the centerline of the room with a 2.29-m spacing. The source is 2.316 m high and 0.61 m wide. The top of the heat source is 4.25 m below Clay G. The heater power was 0.470 kW per canister and had an assumed half-life of 30 years. The resulting thermal load is

$$q = 145.3 \exp(-7.327 \times 10^{-10} t) \quad (3-2)$$

where q is the volumetric heat-generation rate in W/m³ and t is time in seconds. The configuration remained at 300 K for 6 months, at which time the thermal load was applied.

The thermal properties of the various stratigraphic materials used in the thermal calculation of the simplified parallel problem are the same as those for halite. Heat transfer through the halite was modeled with a nonlinear thermal conductivity of the form

$$k = \lambda_o (300/\theta)^\Gamma \quad (3-3)$$

where k is the conductivity in W/m-K, θ is the absolute temperature in Kelvin, and λ_o and Γ are material constants for halite. Thermal radiation between the surfaces of the heated room were simulated by an artificial thermal material. The conductivity of this material was chosen such that a thermal calculation with conduction heat transfer in the room produces the same temperatures around the room as a thermal calculation with radiation heat transfer. The thermal properties for halite and the “equivalent thermal material” are given in Table 3-2.

Table 3-2. Thermal properties for the simplified heated parallel calculation^a

Material	Density ρ kg/m ³	Specific Heat C_p J/kg-K	Thermal Conductivity ^b Parameters	
			λ_o W/m-K	Γ
Halite	2,300	860	5.0	1.14
“Equivalent Thermal Material”	1	1,000	50.0	0.00

^a From Munson and Morgan (1986).

^b $k = \lambda_o(300/\theta)^\Gamma$, where θ is temperature in Kelvin, was used in the simplified heated parallel calculation. $k = \lambda_o(\theta/300)^\Gamma$, which is incorrect, was used in the heated benchmark calculation because the incorrect form was specified in the initial benchmark problems.

4.0 COMPUTATIONAL RESULTS

The results for the Benchmark II isothermal and heated room problems and the simplified heated parallel problem are presented in this section. Comparison of the results predicted by **SPECTROM-32** and **SPECTROM-333** with results predicted by other independent researchers who participated in the Benchmark II exercise is provided. Because data are not readily available for all of the codes that participated in the Benchmark II exercise, a few selected results were digitized to provide a sample comparison. Specifically, the range in responses reported at 10 years by Morgan et al. (1981) for seven of the nine codes that participated in the Benchmark II exercise is presented in each of the figures provided. The results predicted by two of the nine codes (**REM** and **STEALTH**) were not used to determine the range of the responses in this report. The predicted results of these two codes were not used because they frequently predicted results which were not “typical” of the responses predicted by the seven other codes. The selected range of the responses reported by Morgan et al. (1981) are identified by the brackets (---) in the figures provided for the Benchmark II problems.

Vertical closure and horizontal displacement results predicted by two other codes are also provided for the Benchmark II problems. Namely, the results predicted by Biffle (1981) and Branstetter et al. (1981) using the finite-element codes **JAC** (Biffle and Blanford, 1994) and **SANCHO** (Stone et al., 1988), respectively, were selected for comparison. These codes were selected because they provide finite-strain solutions and have been used extensively to solve boundary value problems for the WIPP. For the simplified heated room calculation, the vertical closure history predicted by the **SPECTROM** codes are compared with the **JAC** and **SANCHO** predictions, which were digitized from the figures reported by Munson and Morgan (1986).

Even though the boundary value problems are well defined, the finite element mesh used and certain features of a finite element code can account for significant differences in the predicted responses. Table 4-1 identifies a few features of the finite element codes **JAC**, **SANCHO**, **SPECTROM-32**, and **SPECTROM-333**. As shown in Table 4-1, a direct integration solution method is used by **SPECTROM-32**, and **SPECTROM-333** used the BFGS solution method. **JAC** and **SANCHO** use conjugate gradient and dynamic relaxation solution methods, respectively. The **SPECTROM** codes use a thin element with no shear strength to simulate a frictionless interface material while **JAC** and **SANCHO** use a master/slave algorithm. The number of nodes, type and number of elements, and degrees of freedom used for the Benchmark II problems and the simplified heated parallel problem are also given in Table 4-1. The meshes used by the **SPECTROM-32** code contain significantly more degrees of freedom than the meshes used by the other codes.

Table 4-1. Features of finite element codes and mesh statistics

Code	Nodes/ Element	Int. Pts./ Element	Solution Method	Slip Algorithm	Large Deformation	Large Strain	Mesh Statistics ^a (Number of)		
							Nodes	Elements	Degrees of Freedom
JAC	9	9	Conjugate Gradient	Master/ Slave	Yes	Yes	I-889	I-160	I-1,494
							H-940	H-175	H-1,475
							P-NA	P-NA	P-NA
SANCHO	4	4	Dynamic Relaxation	Master/ Slave	Yes	Yes	I-718	I-586	I-1,311
							H-777	H-644	H-1,432
							P-NA	P-NA	P-NA
SPECTROM-32	8	4	Direct Integration	Thin Element	Yes	Yes	I-2,437	I-764	I-4,700
							H-2,875	H-906	H-5,550
							P-2,886	P-909	P-5,568
SPECTROM-333	4	4/1 ^b	BFGS	Thin Element	Yes	Yes	I-837	I-764	I-1,585
							H-985	H-906	H-1,868
							P-989	P-909	P-1,874

^a I – Isothermal Benchmark II Problem, H – Heated Benchmark II Problem, P – Simplified Heated Parallel Problem.

^b Four integration points are used for the stiffness and one integration point for the constitutive models.

4.1 Benchmark II Isothermal Room Results

4.1.1 Structural Mesh Statistics

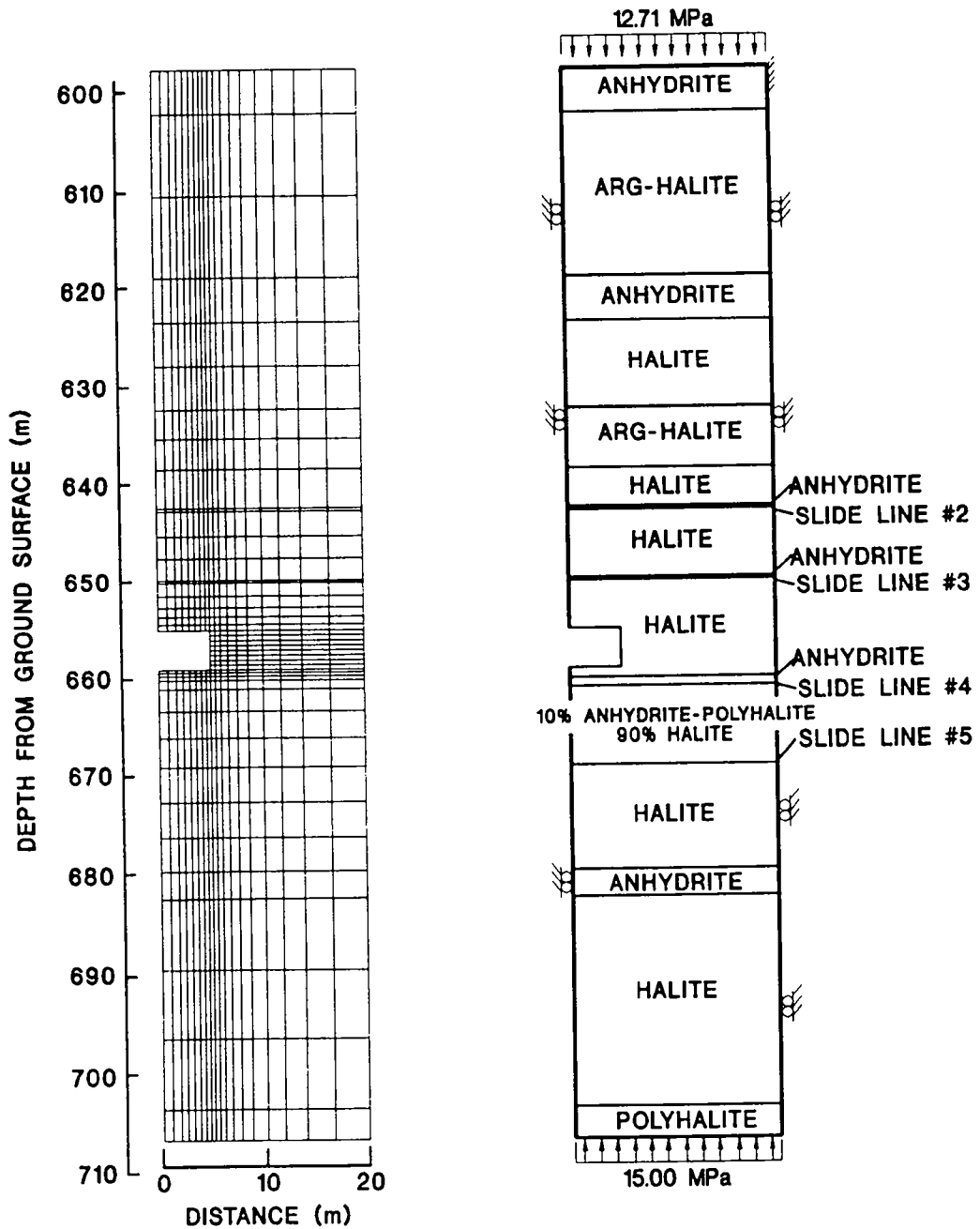
The required mesh statistics include a figure showing the undeformed mesh, the number of nodes in the mesh, the number and type of elements, the number of degrees of freedom, and the minimum and maximum node spacing. The number of nodes, the number and type of elements, and the number of degrees of freedom for the two meshes are given in Table 4-1. The undeformed mesh used by **SPECTROM-32** is shown in Figure 4-1. The **SPECTROM-333** mesh is identical to the **SPECTROM-32** mesh except that it contains four-node elements and has thinner slide line elements. Eighteen 0.00003-m-thick slide line elements were used to model each clay seam in the **SPECTROM-333** mesh, while 0.0002-m-thick slide line elements were used in the **SPECTROM-32** mesh. The minimum thickness which could be obtained by the mesh generation program used to create the **SPECTROM-32** mesh was 0.0002 m. The thickness of the slide line elements is excluded from the following discussion on node spacing.

The mesh spacing in the horizontal direction was determined by the room location. The smallest horizontal node spacing in the **SPECTROM-333** mesh was 0.47 m between the nodes on the rib boundary ($x = 5.03$ m) and the adjacent nodes in the pillar. The largest horizontal node spacing in the **SPECTROM-333** mesh was 3.03 m between nodes on the vertical centerline of the pillar and the adjacent nodes. Similarly, the minimum and maximum horizontal spacing between any two nodes in the **SPECTROM-32** mesh were 0.24 and 1.52 m, respectively.

The mesh spacing in the vertical direction was determined by the room location and the WIPP stratigraphy. Because each anhydrite layer was modeled with one element vertically, the minimum spacing of 0.22 m in the **SPECTROM-333** mesh occurred in the anhydrite layer located from 642.76 m to 642.98 m beneath the ground surface. The minimum vertical node spacing around the room was 0.31 m immediately below the room. The maximum vertical node spacing was 8.32 m in the argillaceous halite below the top anhydrite layer modeled. Similarly, the minimum and maximum vertical spacing between any two nodes in the **SPECTROM-32** mesh were 0.11 m and 4.16 m, respectively.

4.1.2 Displacement Histories and Deformed Mesh

The benchmark comparisons call for two displacement histories: (1) vertical closure history of the room and (2) horizontal displacement history of the rib midpoint. Vertical closure is the



RSI-262-94-047

Figure 4-1. SPECTROM-32 structural mesh and stratigraphy used for the Benchmark II isothermal room calculation.

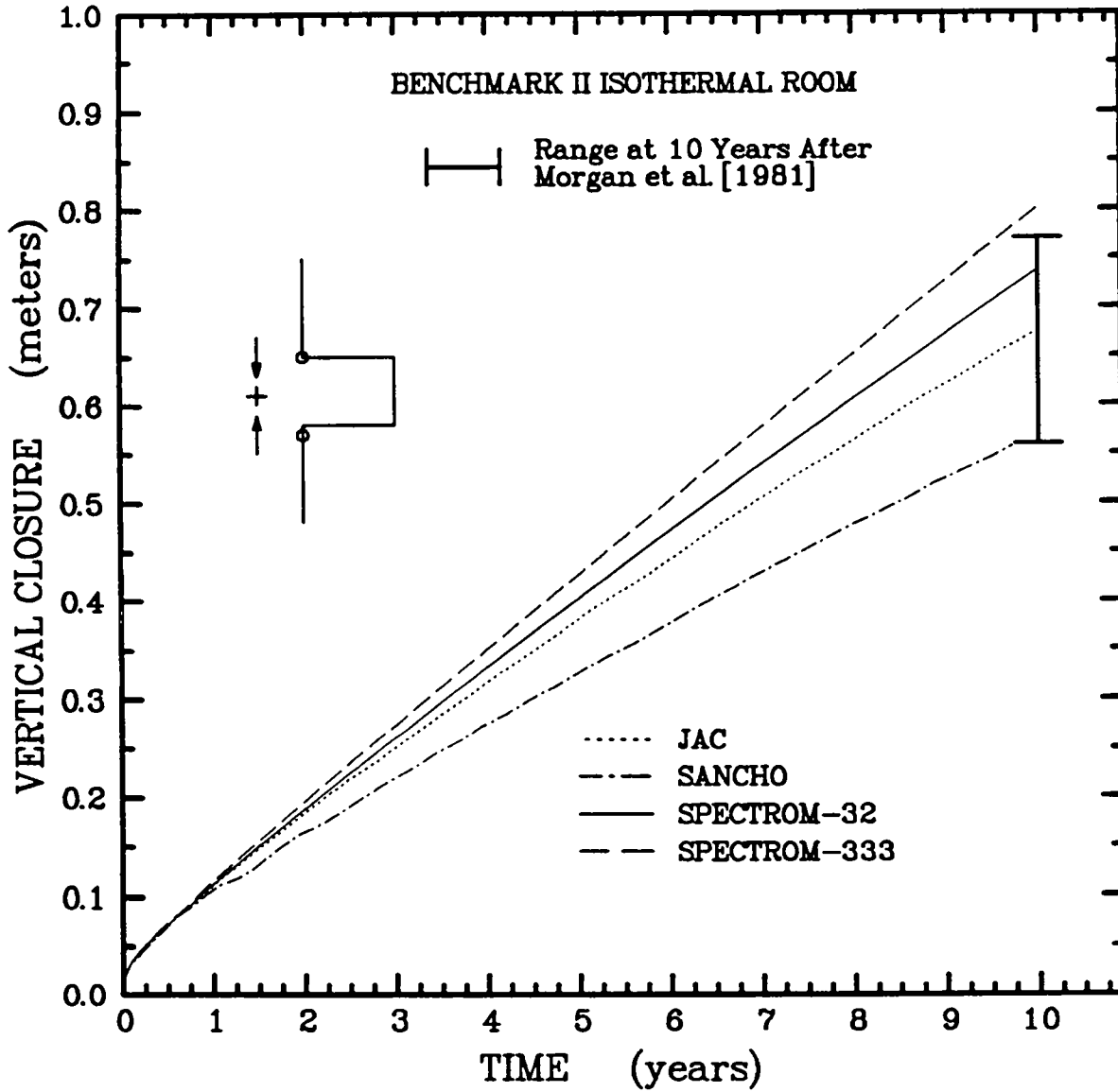
relative vertical displacement of the point initially located at (0,655.04) with respect to the point initially located at (0,659.00). Figure 4-2 shows the room vertical closure history predicted by **SPECTROM-32** and **SPECTROM-333**. The vertical closure after 10 years predicted by **SPECTROM-32** is 0.738 m. The vertical closure after 10 years predicted by **SPECTROM-333** is 0.802 m. As indicated by the vertical bar at 10 years, the vertical closures predicted by **SPECTROM-32** fall within the range predicted by the other codes; however, the **SPECTROM-333** results are slightly greater than the upper range at 10 years. The range bar includes seven of the nine code results examined in the Benchmark II study (Morgan et al., 1981) where the two codes that were clearly giving unrepresentative results were eliminated.

Horizontal displacement histories at the center of the rib are shown in Figure 4-3. The negative values indicate that the ribs are moving inward toward the center of the room. The rib horizontal displacements predicted by **SPECTROM-32** and **SPECTROM-333** at 10 years are -0.385 m and -0.387 m, respectively. The horizontal displacement predicted by **SPECTROM-32** and **SPECTROM-333** fall within the range of displacements predicted by the codes used by other independent researchers, as shown by the vertical bar at 10 years.

The **SPECTROM-32** and **SPECTROM-333** deformed meshes (deformation to geometry ratio of 1:1) at 10 years are shown in Figures 4-4 and 4-5, respectively. Each eight-node element used in the **SPECTROM-32** structural mesh was subdivided (for postprocessing purposes) into 4 four-node elements in Figure 4-4. The mesh distortion is greatest in the corners of the room and the roof sag is noticeably larger than the floor heave. This unsymmetric vertical closure is mainly caused by the stiff anhydrite layer beneath the room, which restricts the vertical movement of the floor.

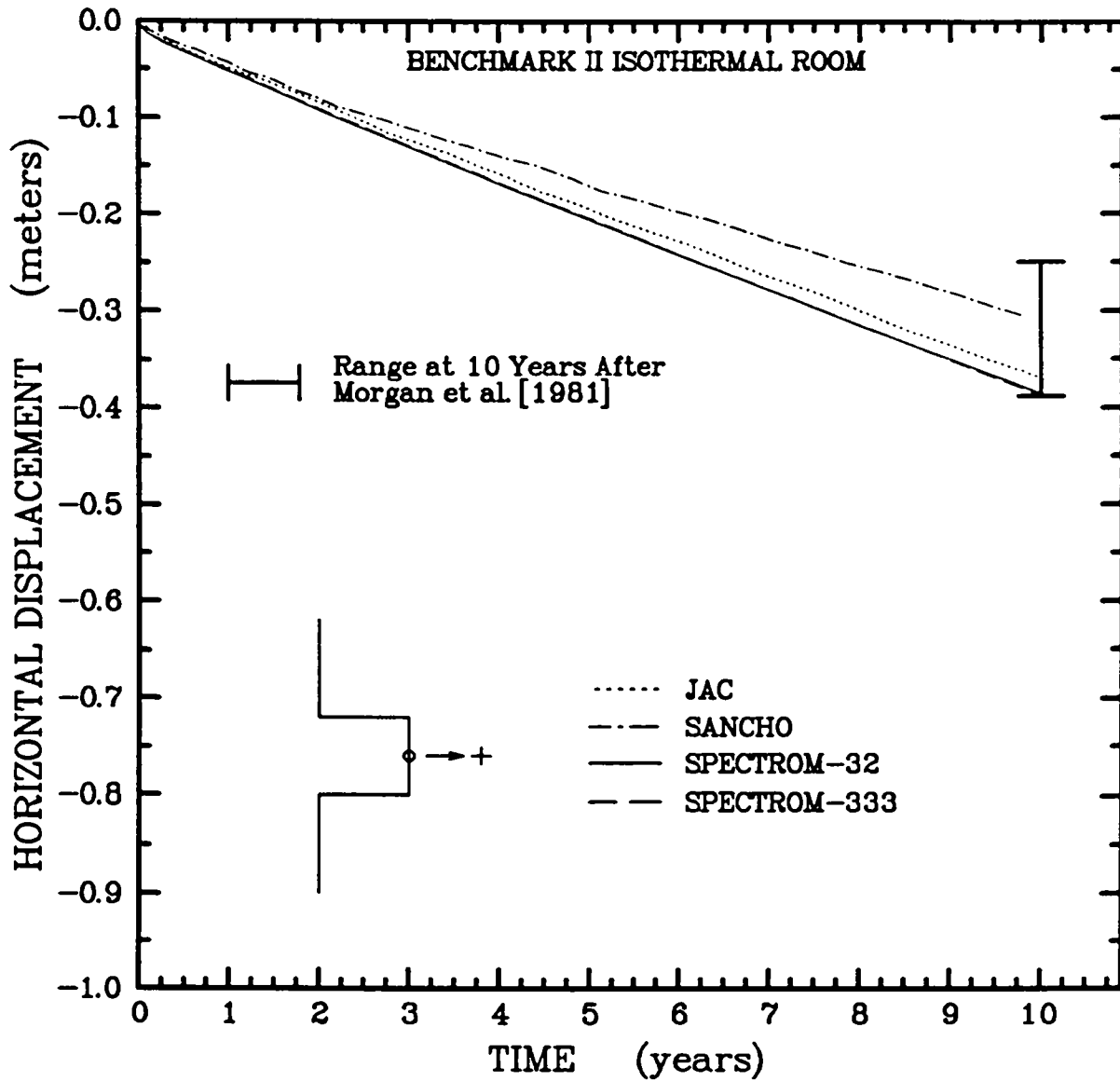
While no attempt is made here to directly compare the deformed meshes from the various calculations, the following observations can be made based on published results. Morgan et al. (1981) presented the deformed mesh resulting from the preliminary **MARC** analysis performed by Sandia National Laboratories referred to as **MARC(S)**. The **MARC(S)** deformed mesh was selected as the representative deformed mesh for presentation because the **MARC(S)** closure histories were located near the middle of the clustering of results. Comparison of Figures 4-4 and 4-5 to the **MARC(S)** deformed mesh and the **JAC** and **SANCHO** deformed meshes presented by Biffle (1981) and Branstetter et al. (1981), respectively, shows that qualitatively similar deformation patterns are produced by all of the codes.

Perhaps the most important comparison in the benchmark problems is the predicted closure of the room. The **SPECTROM-32** room closure results fall within the range of results predicted by the other representative participants of the benchmark exercise. The **SPECTROM-333** vertical



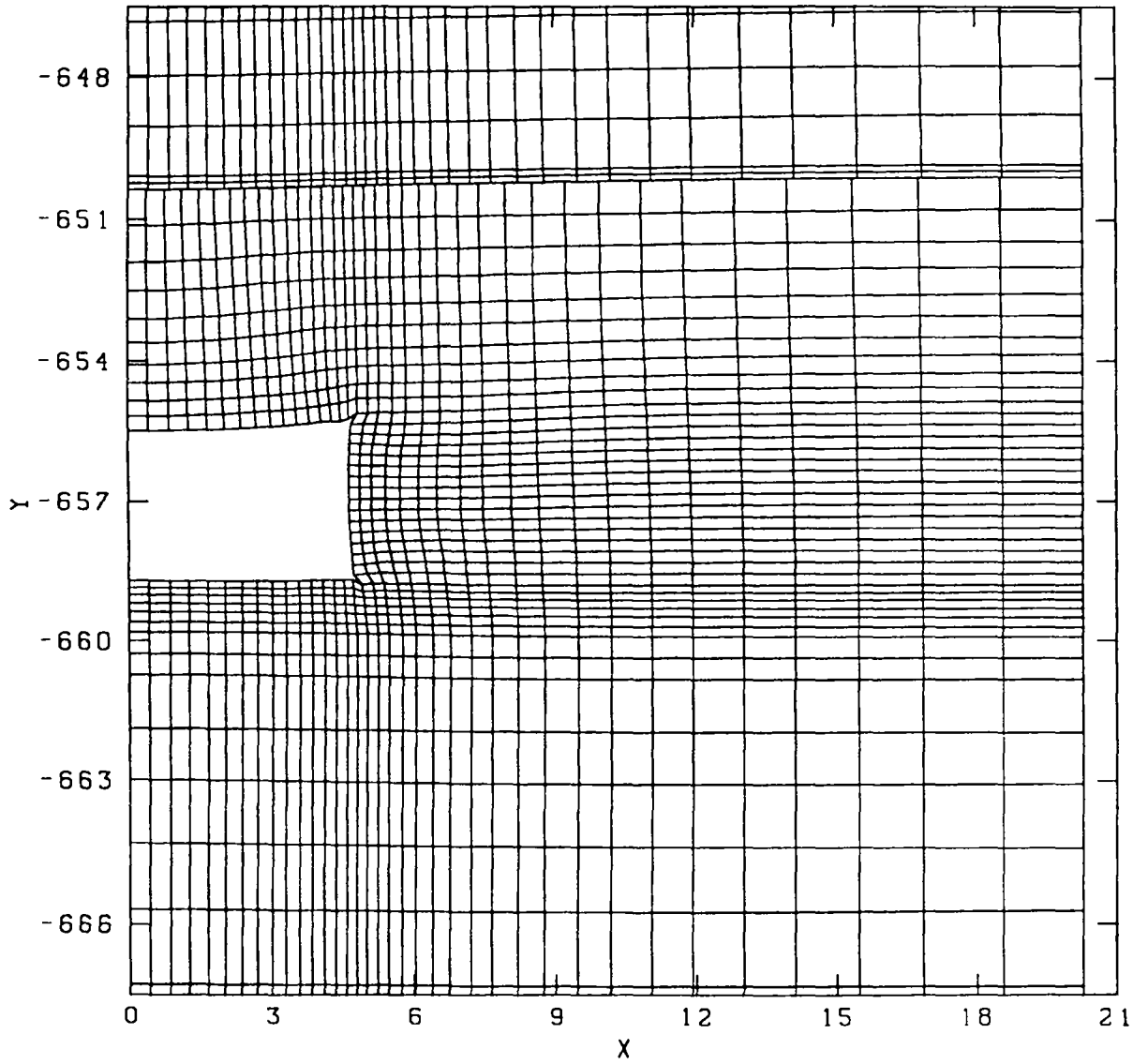
RSI-262-94-052

Figure 4-2. Vertical closure histories for the Benchmark II isothermal room.



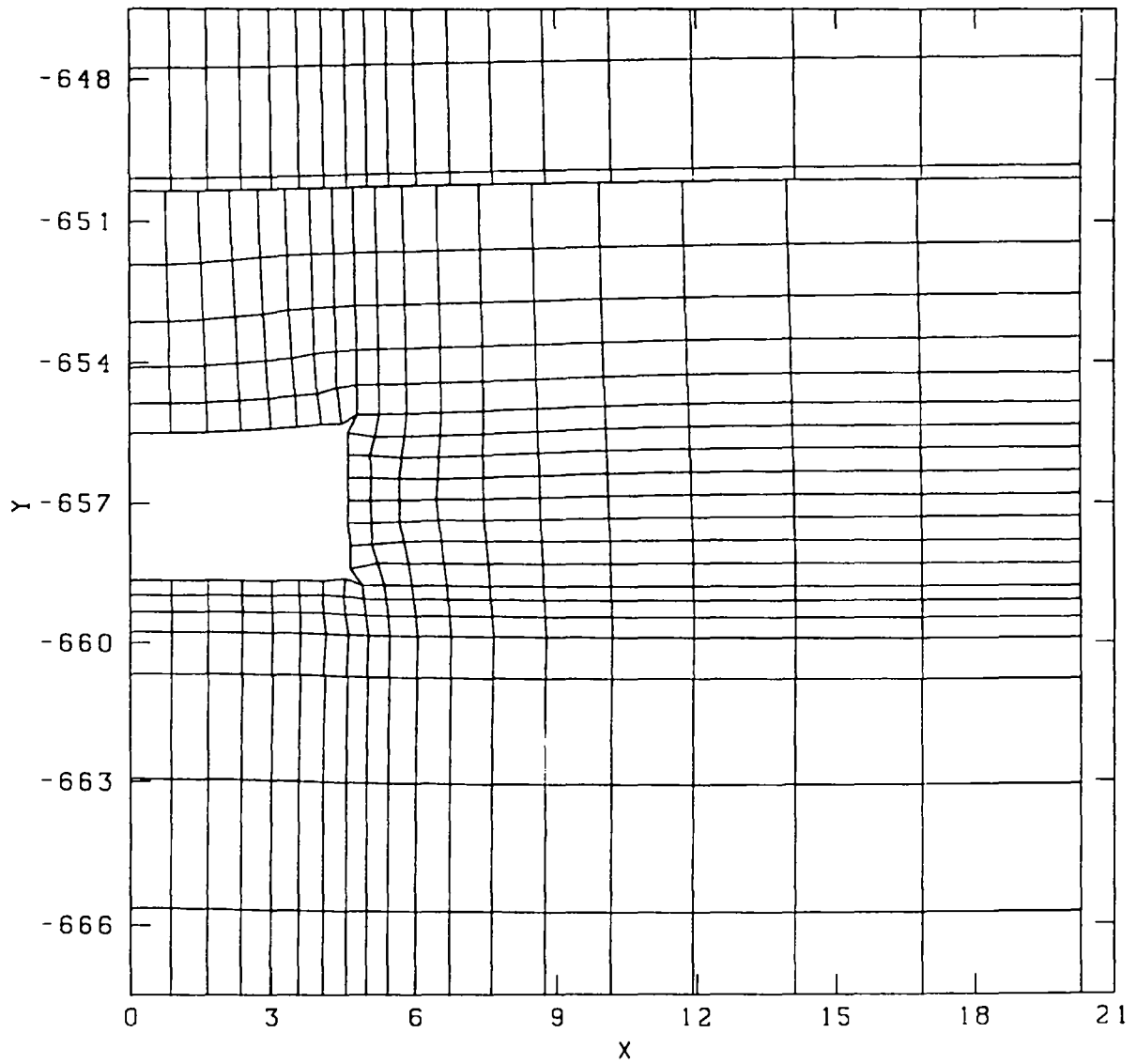
RSI-262-94-053

Figure 4-3. Midpillar horizontal displacement histories for the Benchmark II isothermal room.



RSI-262-94-054

Figure 4-4. SPECTROM-32 Benchmark II isothermal room deformed mesh at 10 years.



RSI-262-94-055

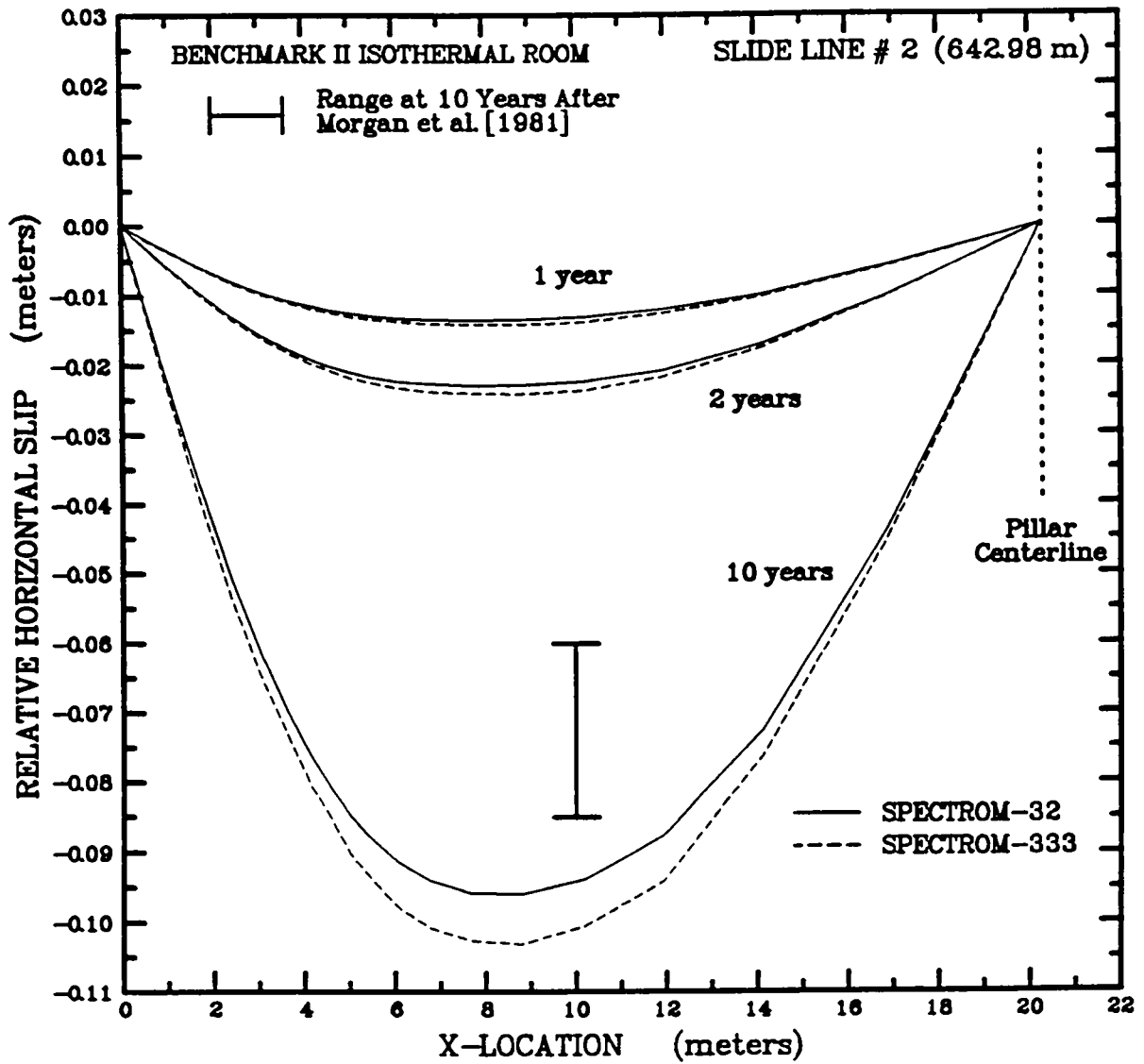
Figure 4-5. SPECTROM-333 Benchmark II isothermal room deformed mesh at 10 years.

closure results are 4 percent greater at 10 years than the maximum vertical closure result predicted by the representative codes that participated in the benchmark exercise. The most probable cause for this discrepancy is mesh refinement and the fact that **SPECTROM-333** uses only one integration point for the constitutive models. In general, the difference in the closure response between **SPECTROM-32** and **SPECTROM-333** is less than the predicted differences between **SANCHO** and **JAC** or **SANCHO** and **SPECTROM-32**. The **SPECTROM-333** predicted midpillar horizontal displacement of the isothermal room is virtually the same as **SPECTROM-32**, which is less than 5 percent greater than **JAC**.

4.1.3 Relative Displacements Across the Slide Lines

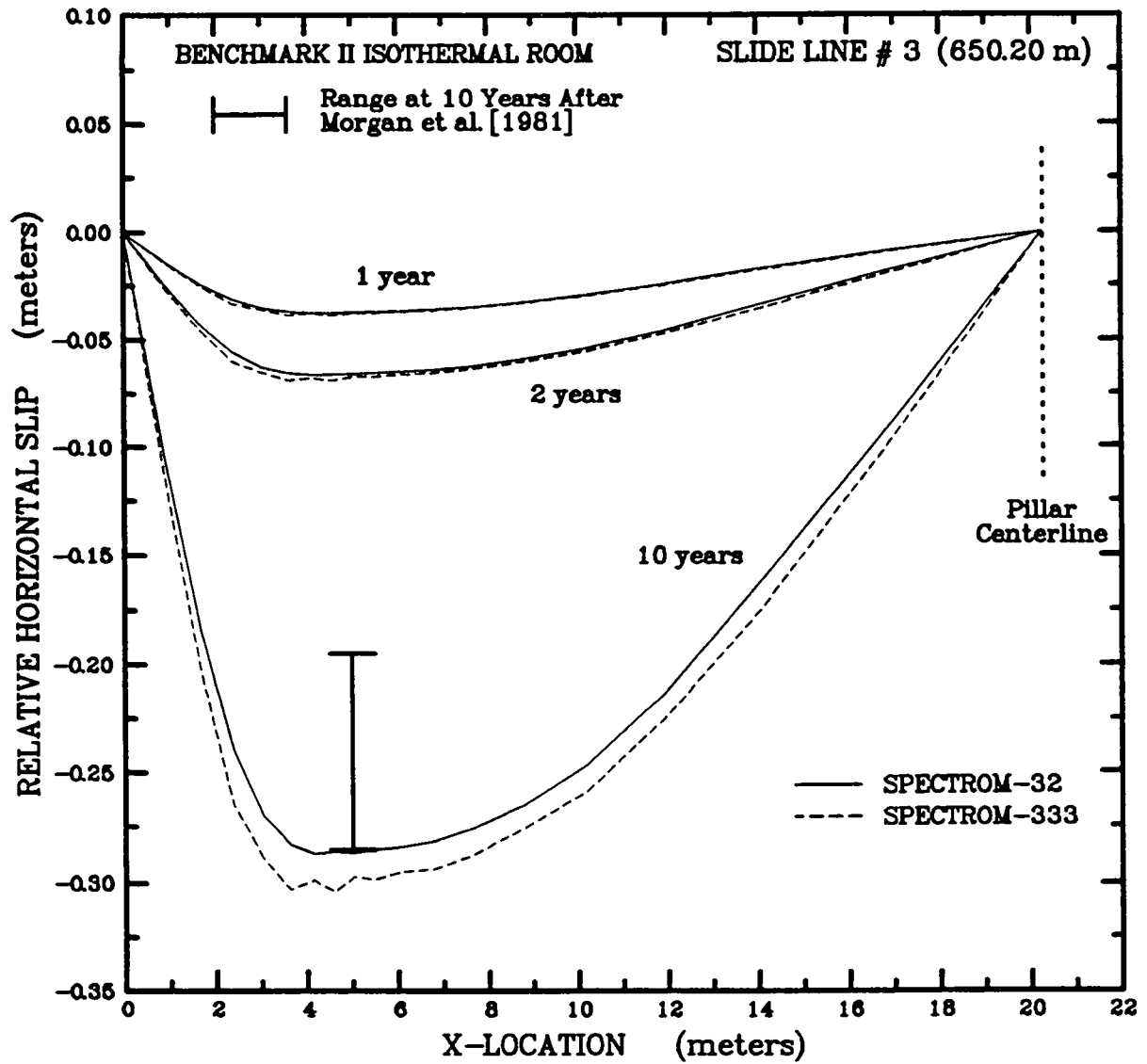
Relative horizontal displacements across the four active slide lines are plotted as a function of horizontal position in Figures 4-6 through 4-9. Relative displacements across the slide lines are provided at 1, 2, and 10 years. Relative displacement was calculated as the displacement of the node on the bottom surface of the slide line interface minus the displacement of the corresponding node on the top surface. A positive value for relative displacement implies that the bottom surface moves horizontally to the right with respect to the top surface. The motion is reversed for negative values of relative horizontal displacement.

In general, **SPECTROM-32** and **SPECTROM-333** predicted more displacement across the four slide lines than most of the other representative codes that participated in the benchmark, as shown by the vertical bars for 10 years in the figures. The variation in results reflects the different methods used by the participants in the benchmark exercise to model the active slide lines. The **SPECTROM** codes employ a special property element to model frictionless slip. The slightly larger displacements predicted across the slide lines by the **SPECTROM** codes compared to the other codes, which participated in the benchmark exercise, can be attributed to the different slide line algorithm. The relative slip predicted by **SPECTROM-333** across the two slide lines below the room resulted in curves which are not smooth at 10 years (see Figures 4-7 and 4-8). The relative displacement across these two slide lines is much less than the relative displacement across the slide lines above the room. A mesh with greater refinement would probably result in a smoother curve; however, this irregularity was not investigated further.



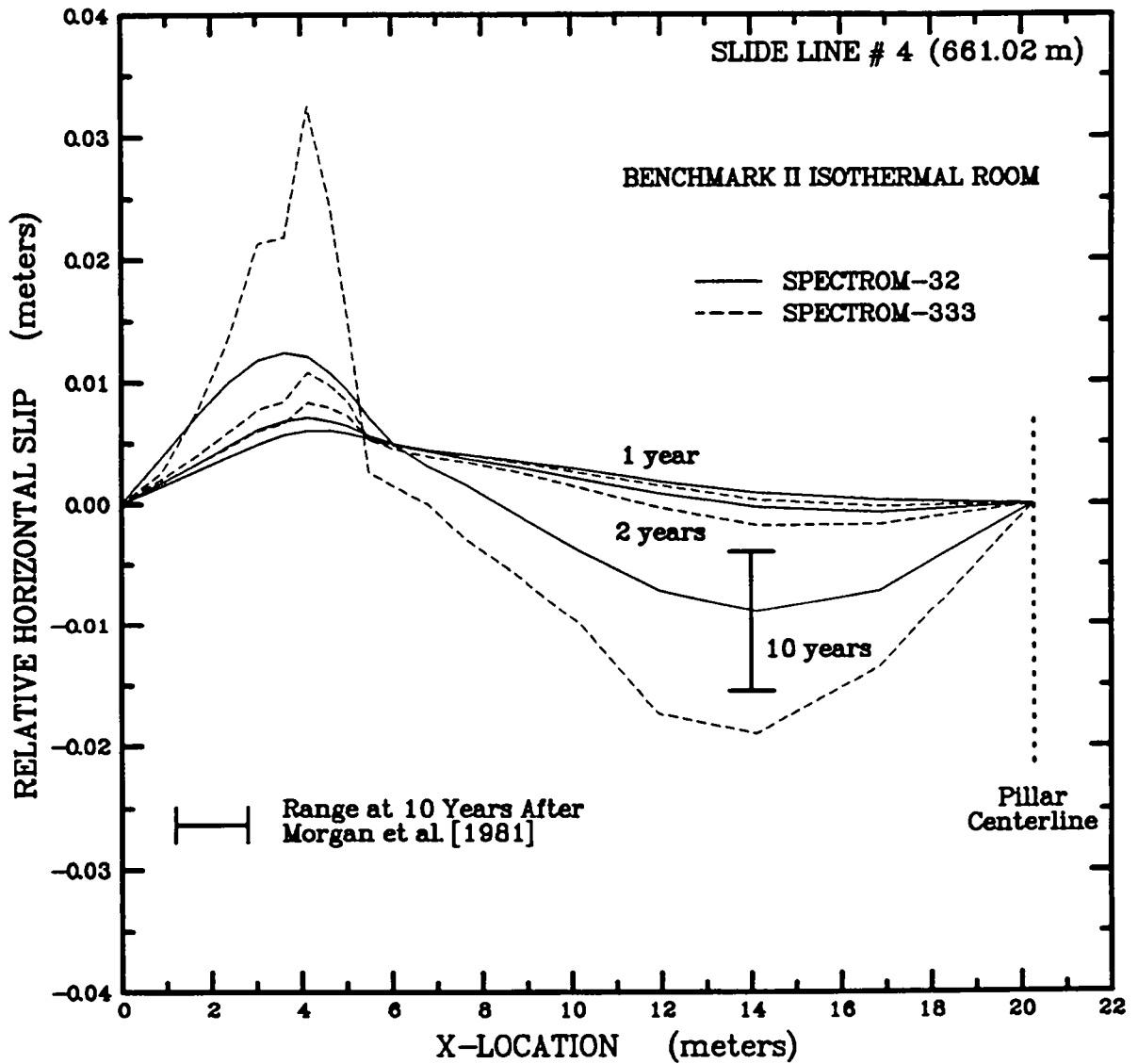
RSI-262-94-056

Figure 4-6. Relative slip across the 642.98-m slide line for the Benchmark II isothermal room.



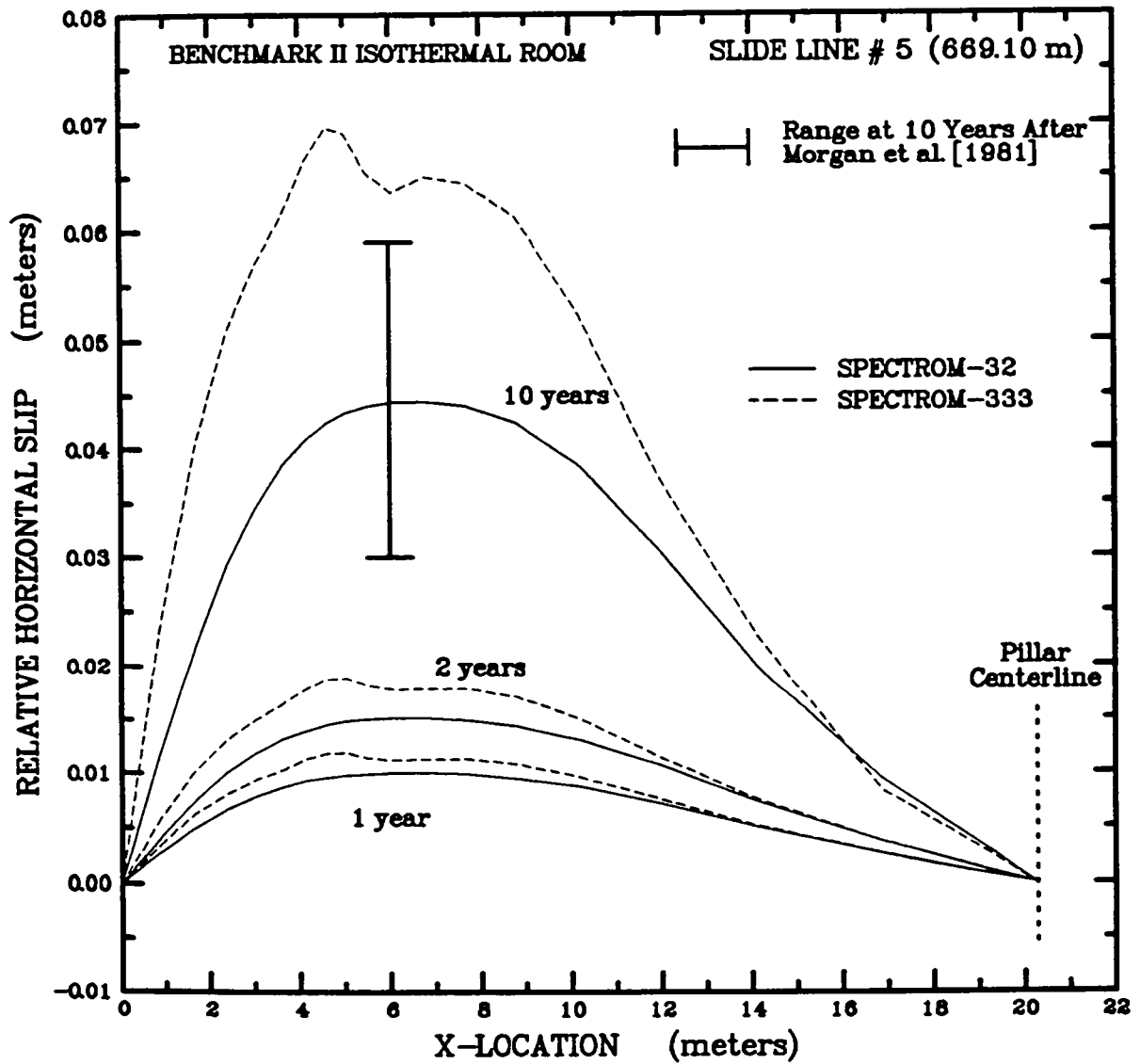
RSI-262-94-057

Figure 4-7. Relative slip across the 650.20-m slide line for the Benchmark II isothermal room.



RSI-262-94-058

Figure 4-8. Relative slip across the 661.02-m slide line for the Benchmark II isothermal room.



RSI-262-94-069

Figure 4-9. Relative slip across the 669.10-m slide line for the Benchmark II isothermal room.

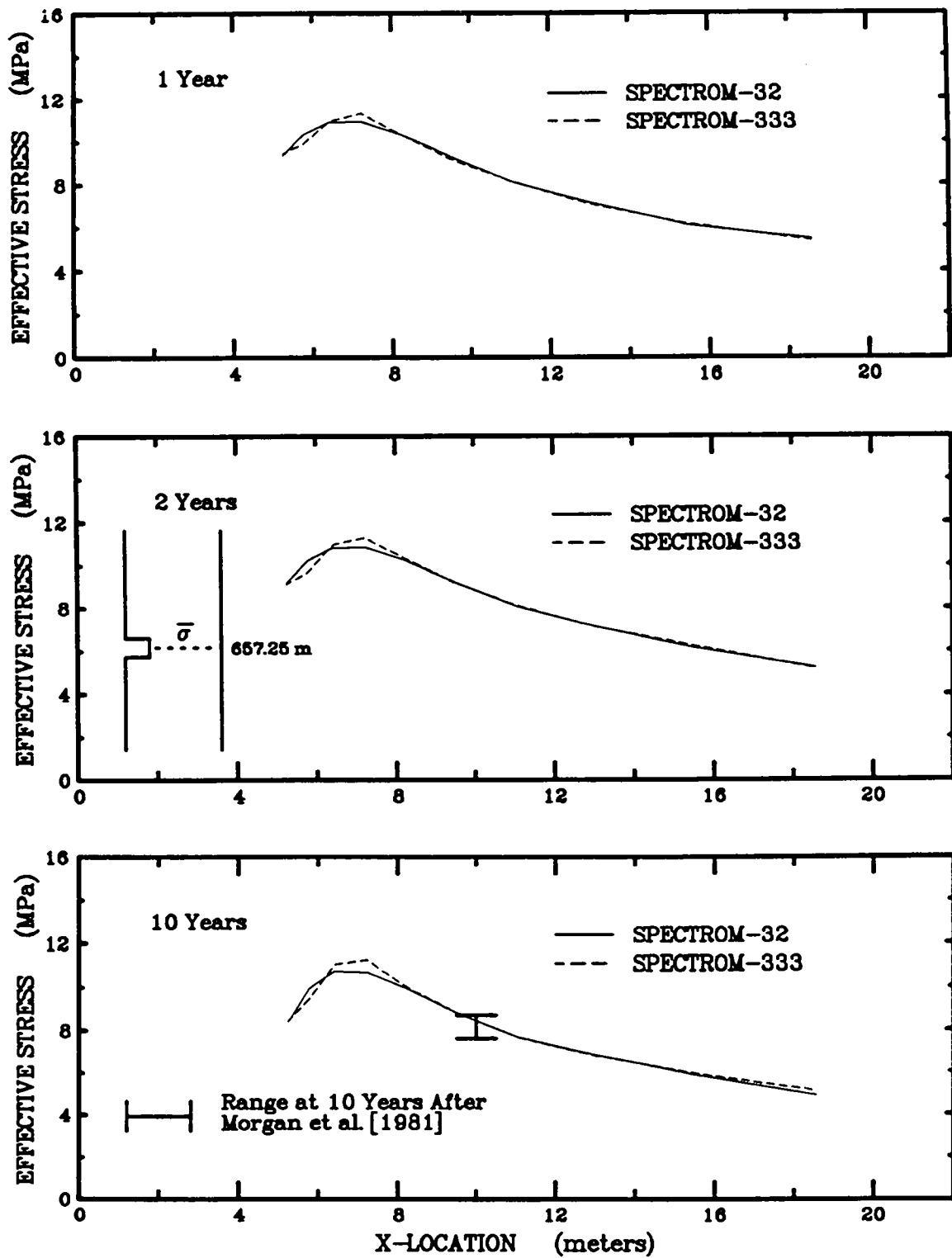
4.1.4 Stress Profiles

Four stress profiles are provided for the isothermal room. Figure 4-10 is a plot of the effective stress near the pillar midheight along the line $y = 657.25$ m, as a function of horizontal position at 1, 2, and 10 years. The pillar midheight is located at $y = 657.02$ m; however, no stress data were available at that location. Therefore, the element immediately below the pillar midheight was used to provide the stress information from both the **SPECTROM-32** and **SPECTROM-333** calculations. The stress results at the four integration points in the **SPECTROM-32** elements were averaged to compare with the stresses at the single integration point in the **SPECTROM-333** elements. Effective stress is defined in terms of the deviatoric stress as given in Appendix A (Equation A-5). Figure 4-11 is similar to Figure 4-10 except vertical stress is plotted as a function of horizontal position. Figure 4-12 is a plot of the effective stress along the vertical centerline of the room ($x = 0$) for values of y between 648.2 m and 667.5 m at 1, 2, and 10 years. Figure 4-13 is the same as Figure 4-12 except that the horizontal stress is presented instead of the effective stress. In general, the stress measures predicted by **SPECTROM-32** and **SPECTROM-333** fall within the range of stresses predicted by other codes that participated in the benchmark exercise (Morgan et al., 1981). The **SPECTROM-333** predictions of stress in the anhydrite beds are less than those predicted by the other codes. This discrepancy may be caused by the single integration point used for the constitutive models by **SPECTROM-333**. However, this discrepancy was not investigated further.

4.2 Benchmark II Heated Room Results

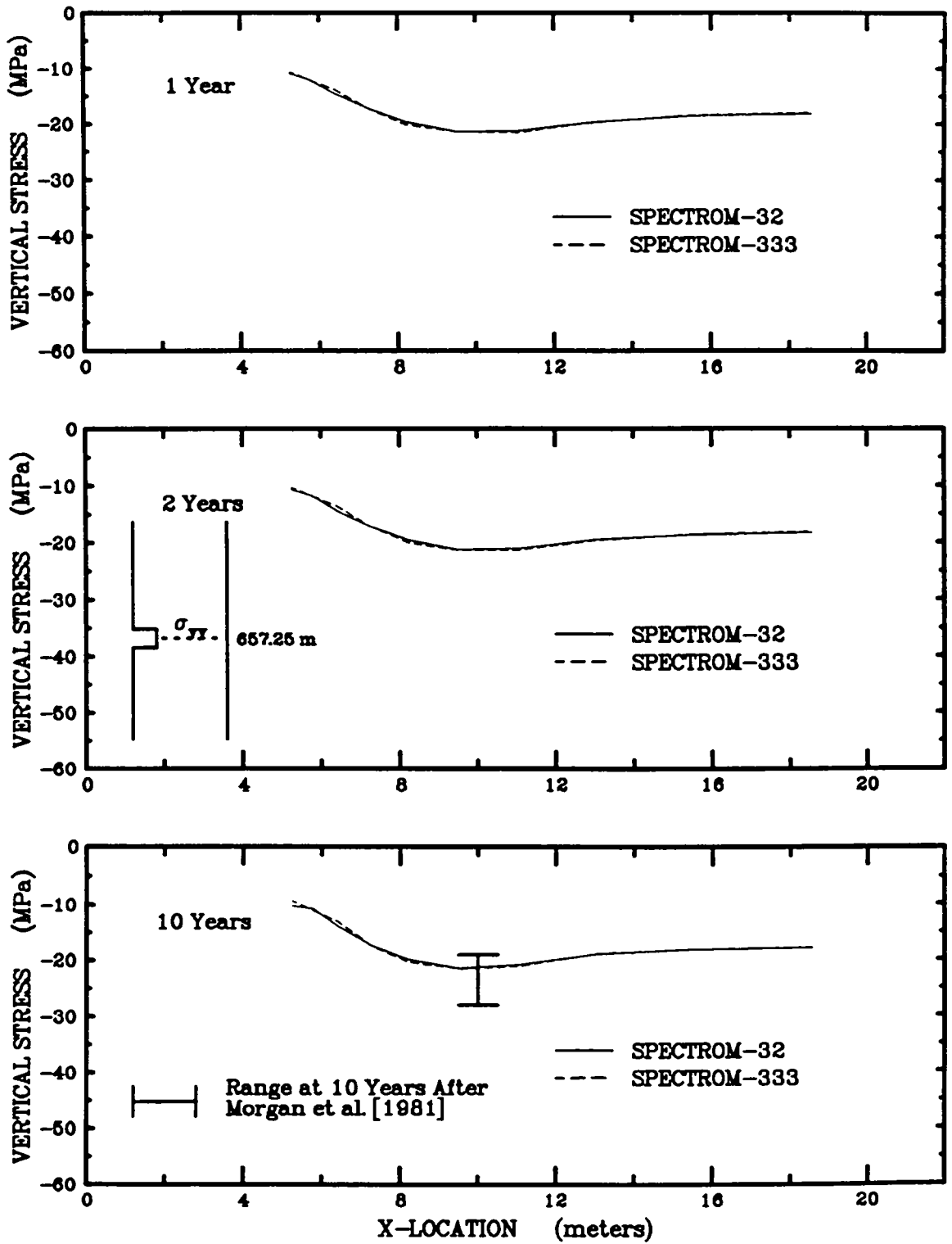
4.2.1 Temperature Calculations

The temperature calculation was performed using the finite element code **SPECTROM-41** (Svalstad, 1989). The finite element mesh used for the thermal calculation is shown in Figure 4-14. The horizontal extremities are the same as those used for the structural analysis; however, the vertical extremities of the thermal mesh extend from 523.00 m to 806.77 m below the ground surface. The vertical extent of the model was extended to assure that the temperatures at these boundaries would remain constant during the analysis and, therefore, would not affect the solution. The mesh contains 1,301 nodes and 400 eight-node quadrilateral elements. The initial temperature was prescribed as 300 K, and all boundaries were specified as adiabatic. The thermal load was modeled as a very thin volumetric heat generating source. The initial heat output (see Equation 3-1) was approximately equal to a thermal power density of 7.5 W/m^2 (30 kW/acre) and was uniformly distributed over the 1.83-m height of the source. The thermal



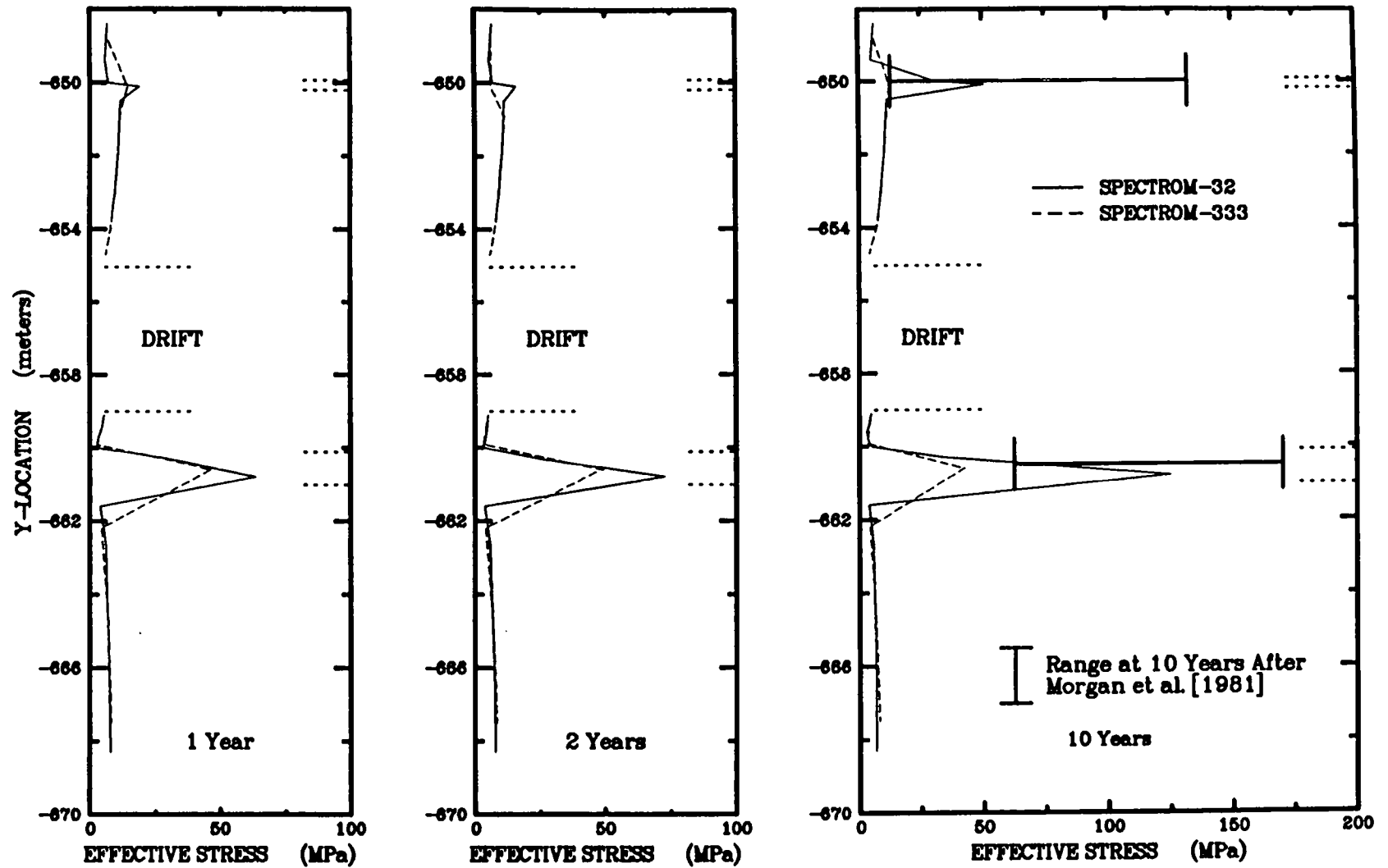
RSI-262-94-060

Figure 4-10. Effective stress profiles through the pillar of the Benchmark II isothermal room.



RSI-262-94-061

Figure 4-11. Vertical stress profiles through the pillar of the Benchmark II isothermal room.



RSI-262-94-062

Figure 4-12. Effective stress profiles along the vertical centerline of the Benchmark II isothermal room.

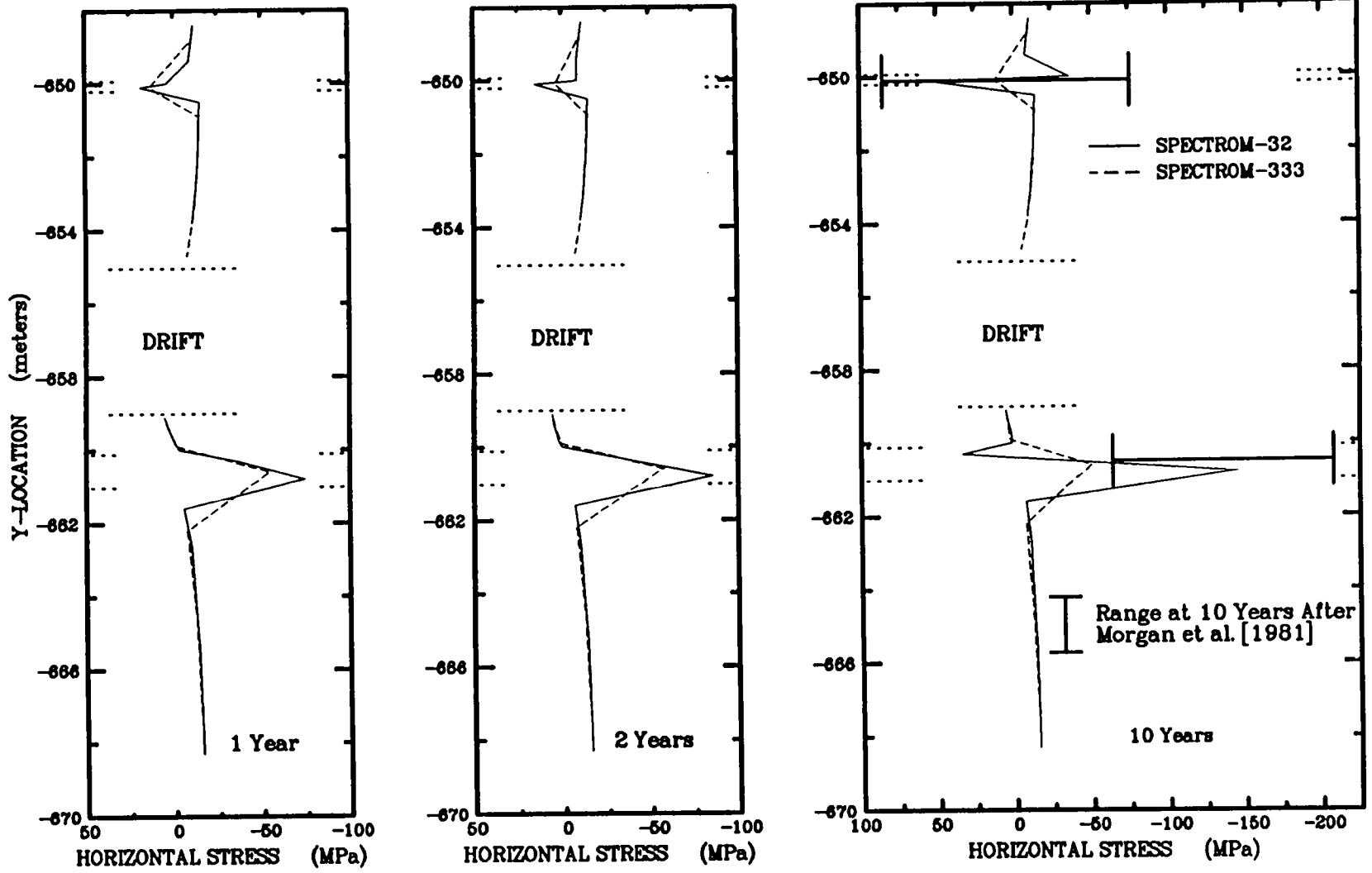
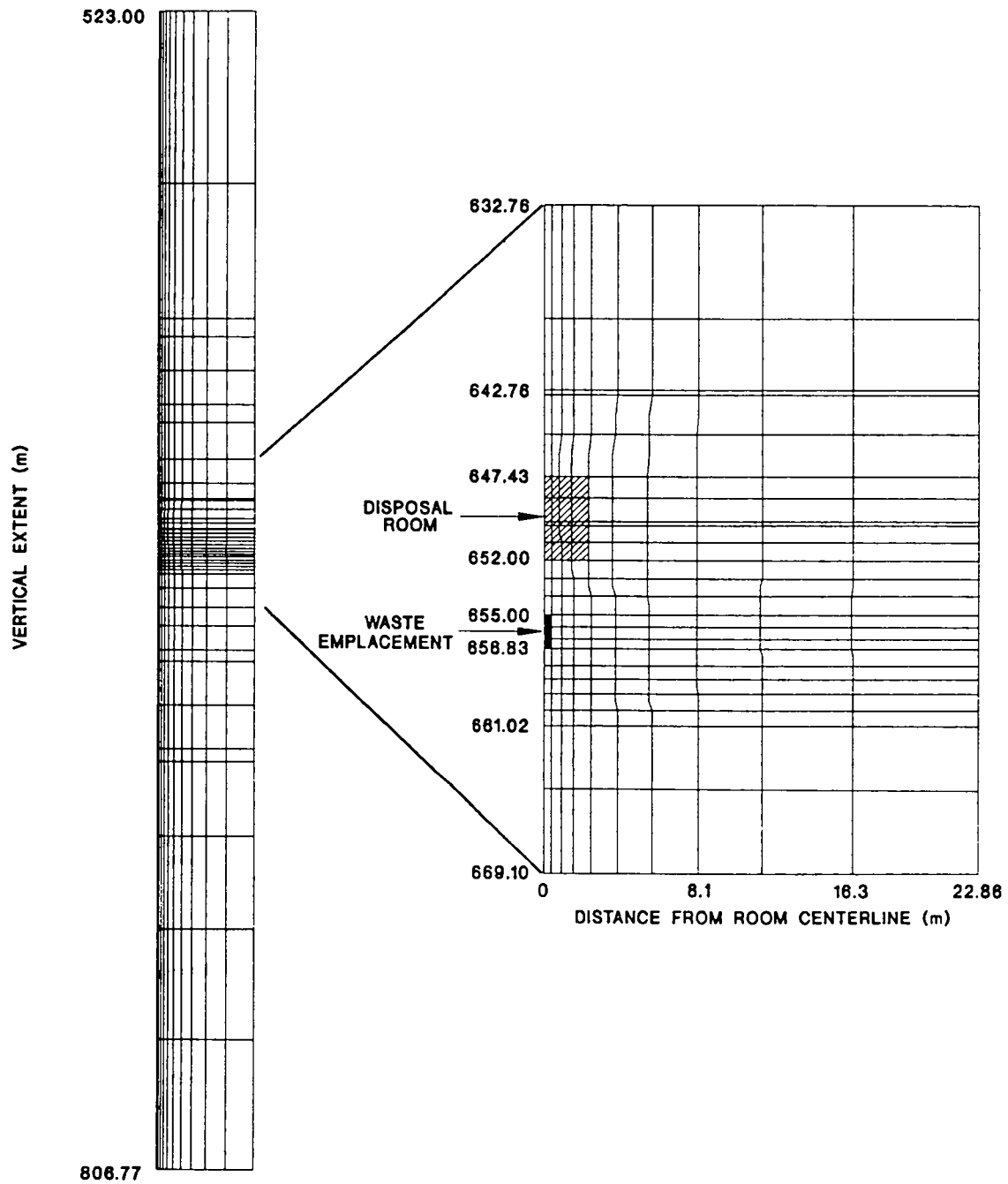


Figure 4-13. Horizontal stress profiles along the vertical centerline of the Benchmark II isothermal room.



RSI-115-89-035

Figure 4-14. Thermal mesh used for the Benchmark II heated room configuration.

response was computed for a 10-year simulation period. Temperatures from the thermal calculation were interpolated for the structural meshes using **MERLIN** (see Section 2.4). The interpolated temperatures were used as input to the **SPECTROM-32** and **SPECTROM-333** structural calculations.

Temperature histories are specified in the benchmark problem formulation for the floor midpoint, midpoint of the heat source, and for the point where the horizontal centerline of the heated room intersects the pillar vertical centerline. These temperature histories are shown in Figure 4-15.

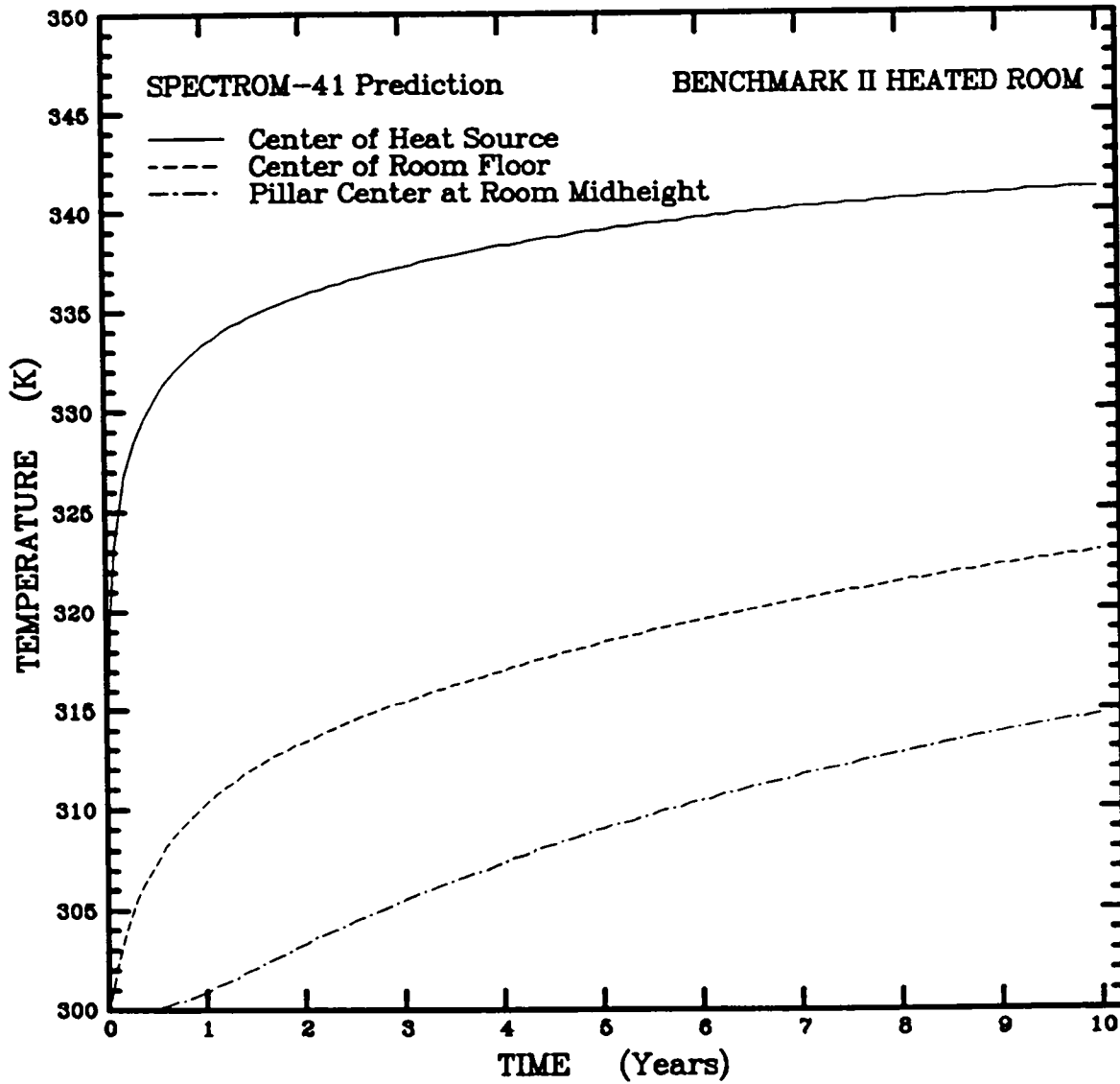
4.2.2 Structural Mesh Statistics

Mesh statistics of the heated benchmark problem are given in Table 4-1. The **SPECTROM-32** undeformed structural mesh is shown in Figure 4-16. The **SPECTROM-333** mesh is identical to the **SPECTROM-32** mesh shown in Figure 4-16 except for the thickness specified for the slide line elements and element type specified. The **SPECTROM-333** mesh consists of 985 nodes, 840 four-node plane strain quadrilaterals, 66 slide line elements, and 1,868 degrees of freedom. The **SPECTROM-32** mesh consists of 2,875 nodes, 840 eight-node plane strain quadrilaterals, 66 slide line elements, and 5,550 degrees of freedom.

The minimum horizontal node spacing was 0.29 m and the maximum horizontal spacing was 3.86 m in the **SPECTROM-333** structural mesh. Excluding the slide lines, a minimum vertical node spacing of 0.22 m and a maximum node spacing of 5.54 m were used for the mesh. Similarly, the minimum spacing of the nodes for the **SPECTROM-32** mesh is 0.11 m vertically and 0.145 m horizontally with a maximum node spacing of 2.77 m vertically and 1.93 m horizontally.

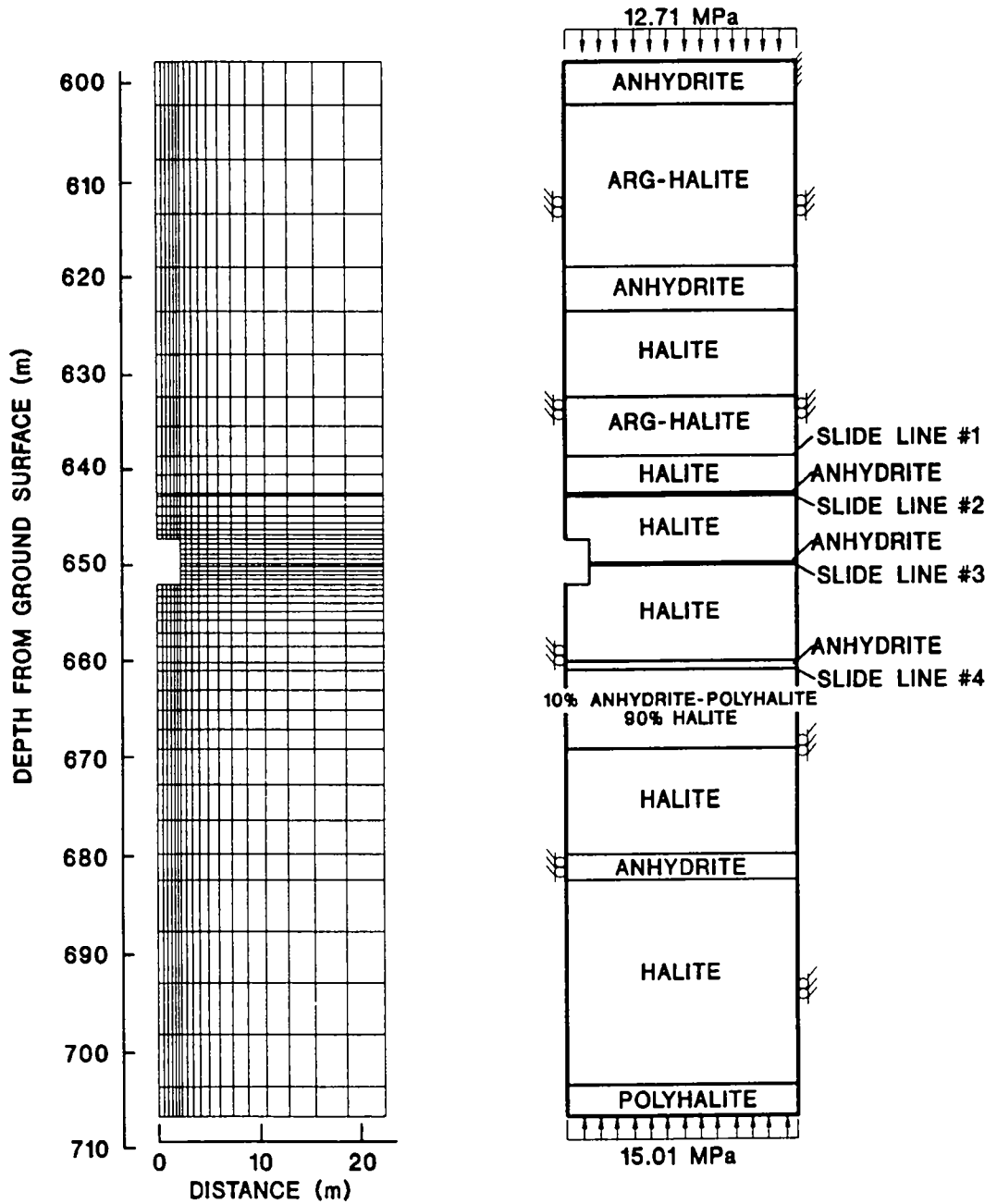
4.2.3 Displacement Histories and Deformed Mesh

Figure 4-17 shows the vertical room closure history for the heated room. After 10 years, the vertical closures predicted by **SPECTROM-32** and **SPECTROM-333** are 0.493 m and 0.495 m, respectively. The vertical closures predicted by **SPECTROM-32** and **SPECTROM-333** fall within the range of displacements predicted by other codes that participated in the benchmark exercise. In the heated Benchmark II problem, results from six codes are presented by Morgan et al. (1981), and one of these codes (**STEALTH**) was unrepresentative and eliminated.



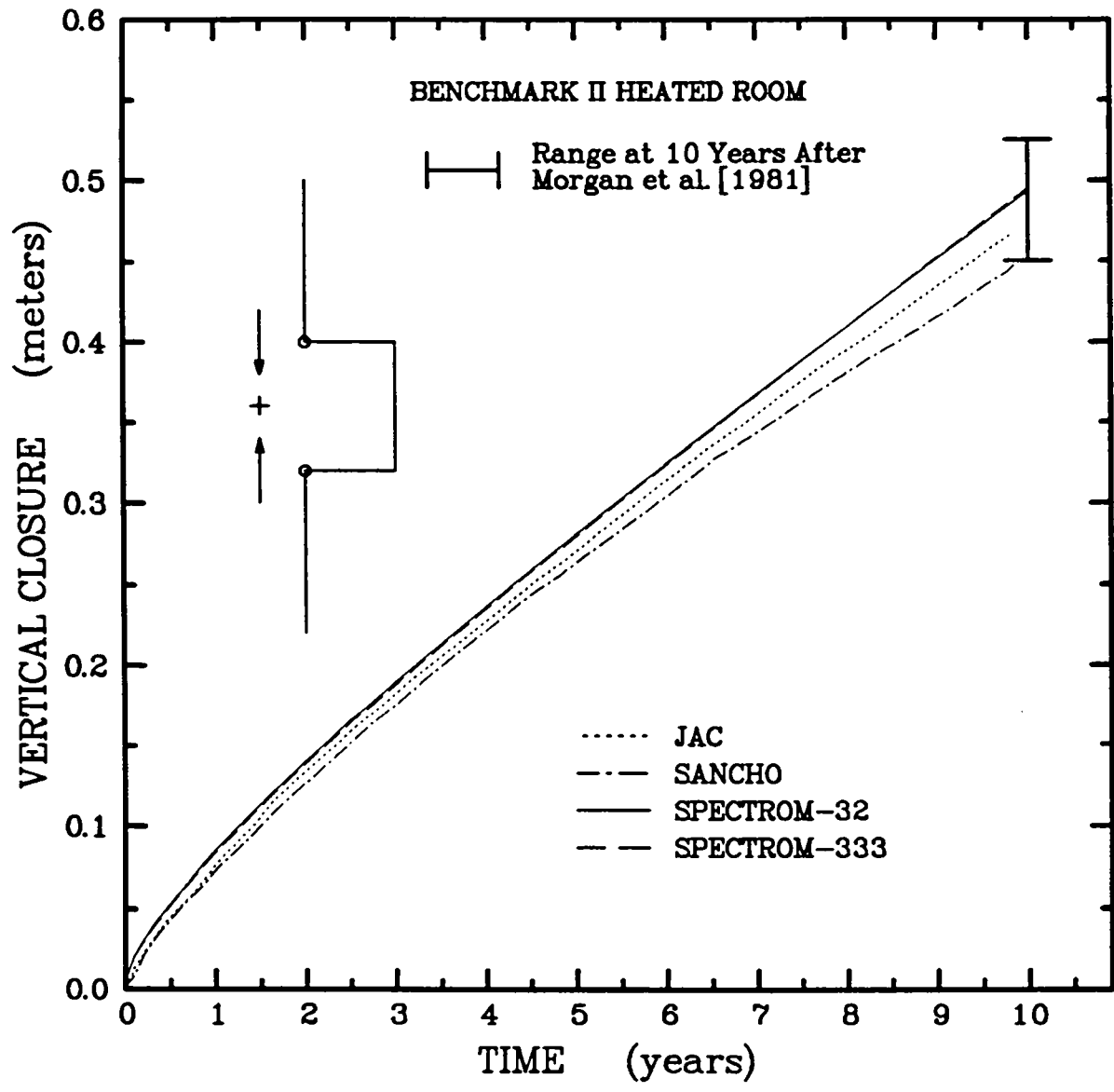
RSI-262-94-064

Figure 4-15. Temperature histories for the Benchmark II heated room configuration computed with SPECTROM-41.



RSI-262-94-046

Figure 4-16. SPECTROM-32 structural mesh and stratigraphy used for the Benchmark II heated room calculation.



RSI-282-94-065

Figure 4-17. Vertical closure histories for the Benchmark II heated room.

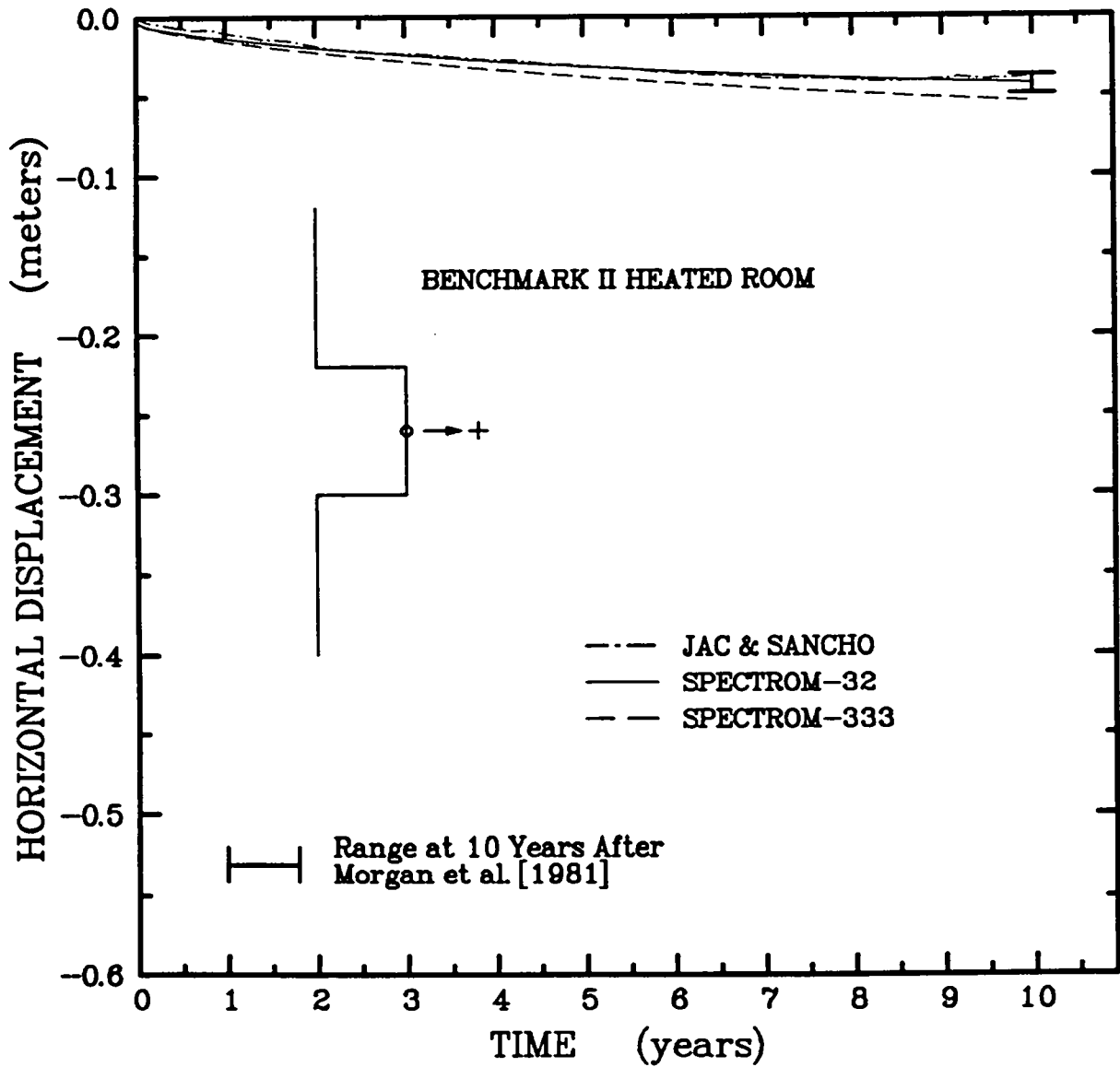
Figure 4-18 shows the horizontal displacement at the top of the anhydrite layer where it intersects the room. After 10 years, the horizontal displacements predicted by **SPECTROM-32** and **SPECTROM-333** are -0.043 m and -0.054 m, respectively. The **SPECTROM-32** results fall within the range predicted by other representative codes; however, the **SPECTROM-333** displacements are slightly greater than the results reported by Morgan et al. (1981). This small discrepancy may be caused by the single integration point used for the constitutive models by **SPECTROM-333**; however, this discrepancy was not investigated.

The **SPECTROM-32** and **SPECTROM-333** deformed meshes (deformation to geometry ratio of 1:1) at 10 years are shown in Figures 4-19 and 4-20, respectively. Each eight-node element used in the **SPECTROM-32** structural mesh was subdivided (for postprocessing purposes) into 4 four-node elements in Figure 4-20. The presence of the slide line and anhydrite in the center of the room is reflected in the displacement discontinuity in the room rib. The anhydrite layer restricts the horizontal displacement of the halite layer above the slide line; however, the halite below the slide line is free to flow into the room.

While no attempt is made here to directly compare the deformed meshes from the various calculations, the following observations can be made based on published results. As was done for the isothermal room problem, Morgan et al. (1981) presented the deformed mesh resulting from the preliminary **MARC** analysis for the heated room problem performed by Sandia National Laboratories. Comparison of Figures 4-19 and 4-20 to the **MARC(S)** deformed mesh and the **JAC** and **SANCHO** deformed meshes presented by Biffle (1981) and Branstetter et al. (1981), respectively, shows that qualitatively similar deformation patterns are produced by all of the codes.

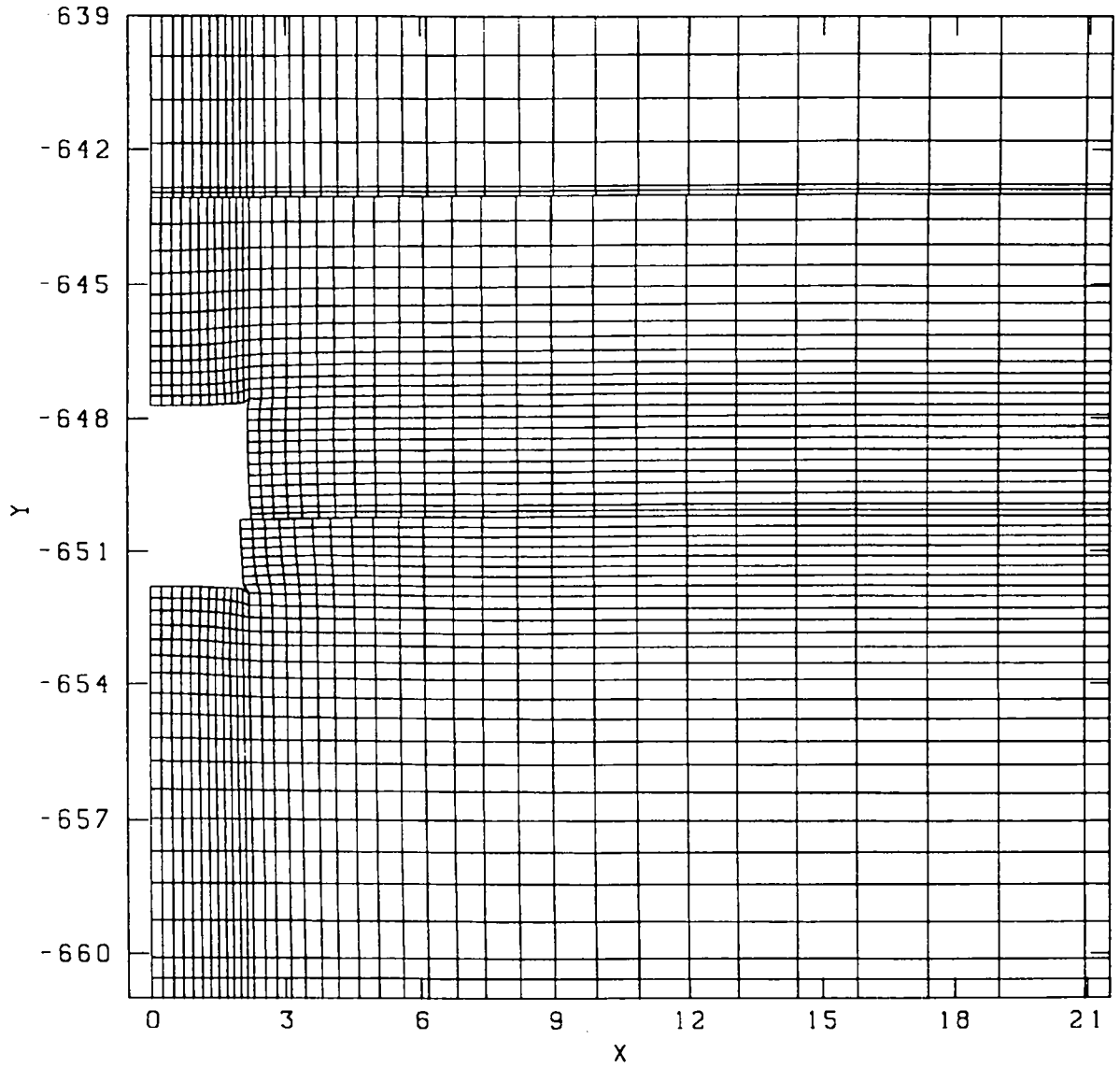
4.2.4 Relative Displacements Across the Slide Lines

Relative horizontal displacements across the four active slide lines are plotted as a function of horizontal position in Figures 4-21 through 4-24. Relative displacements across the slide lines are provided at 1, 2, and 10 years. These displacements were calculated in the same manner as the relative displacements for the isothermal room. In general, the results predicted by **SPECTROM-32** fall within the range of displacements predicted by other participants in the benchmark exercise. However, the relative horizontal displacements across the slide lines predicted by **SPECTROM-333** tend to be slightly greater than those predicted by most of the other participants in the benchmark exercise.



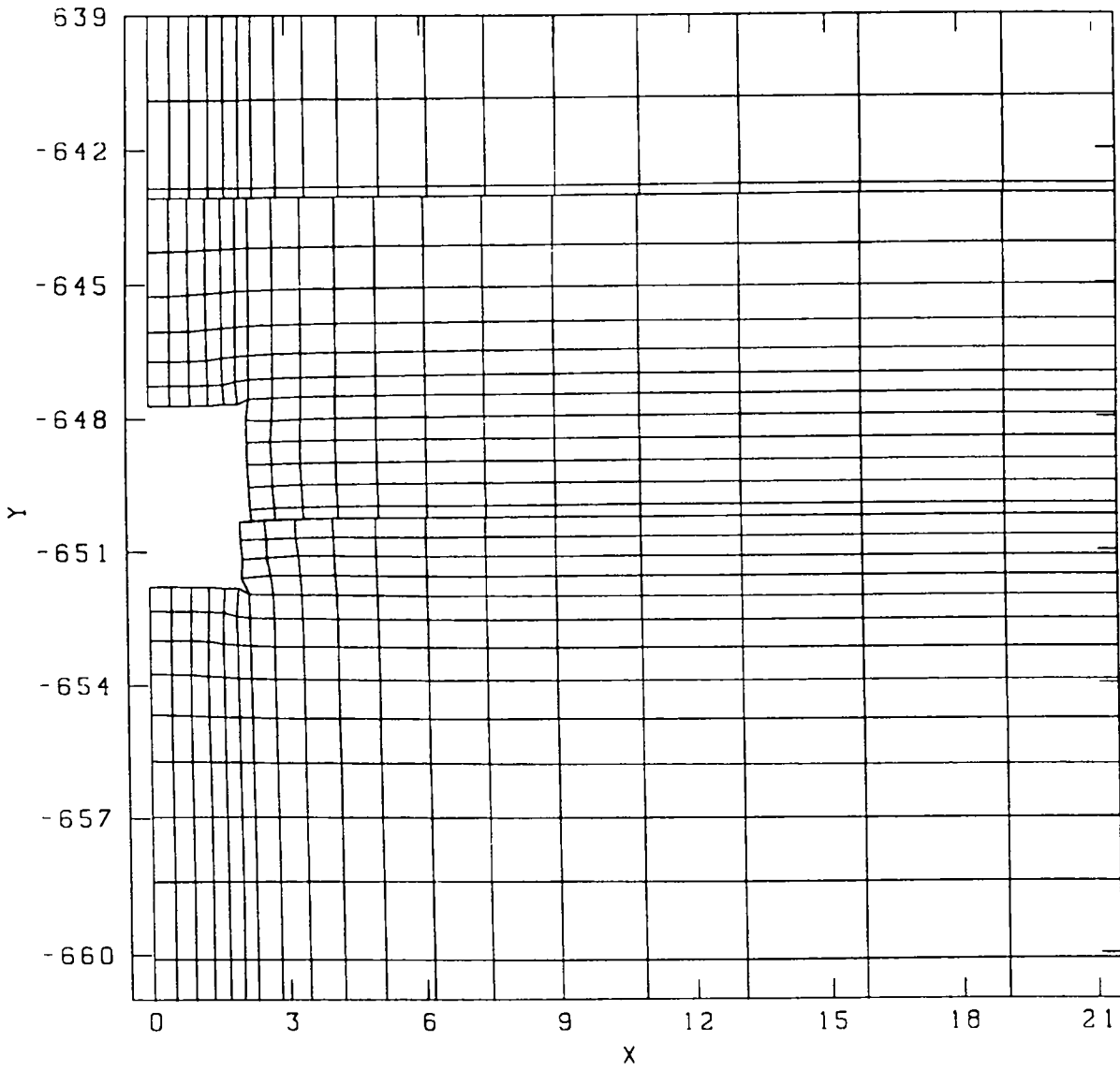
RSI-282-94-066

Figure 4-18. Midpillar displacement histories for the Benchmark II heated room.



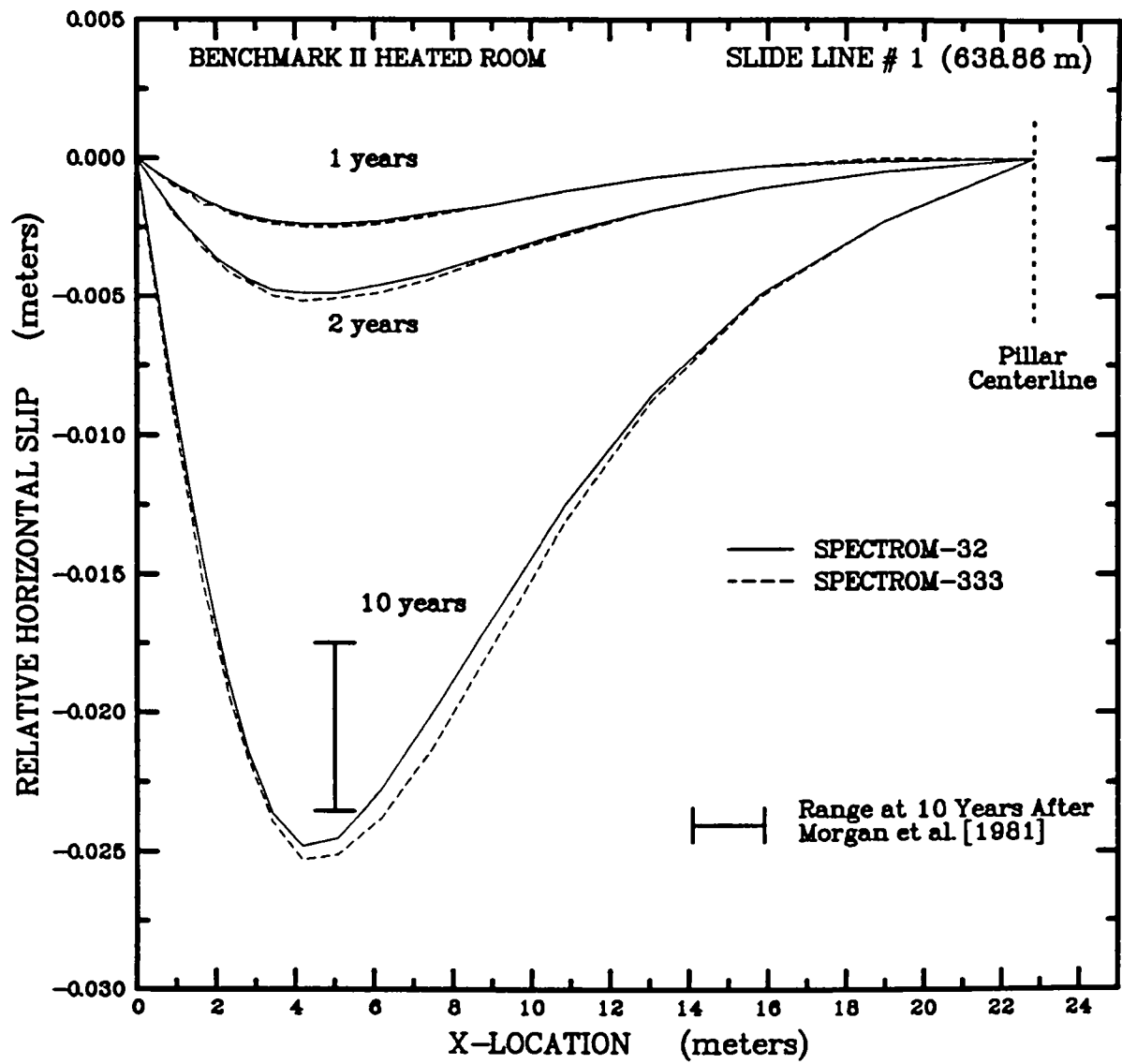
RSI-262-94-067

Figure 4-19. SPECTROM-32 Benchmark II heated room deformed mesh at 10 years.



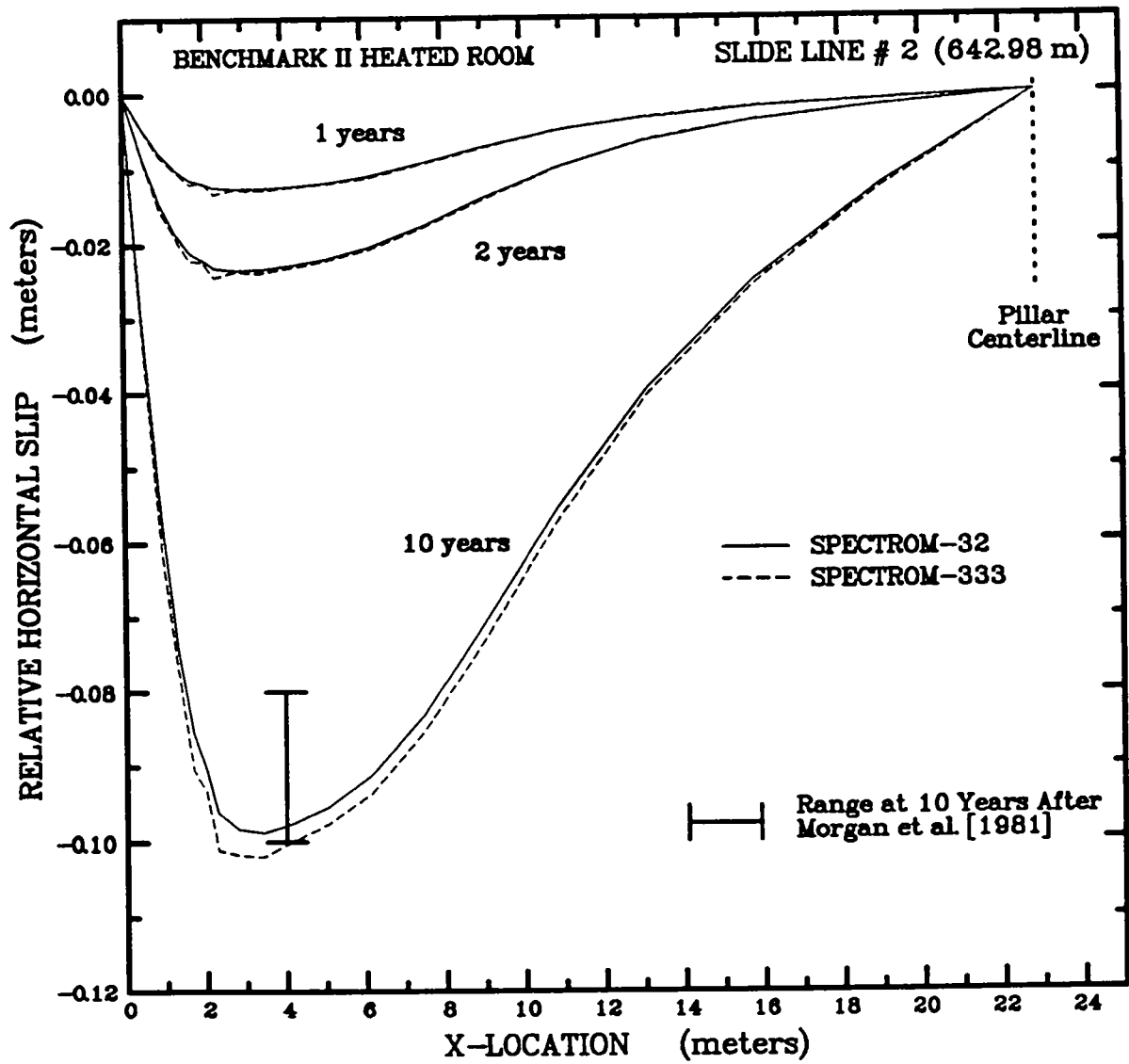
RSI-262-94-068

Figure 4-20. SPECTROM-333 Benchmark II heated room deformed mesh at 10 years.



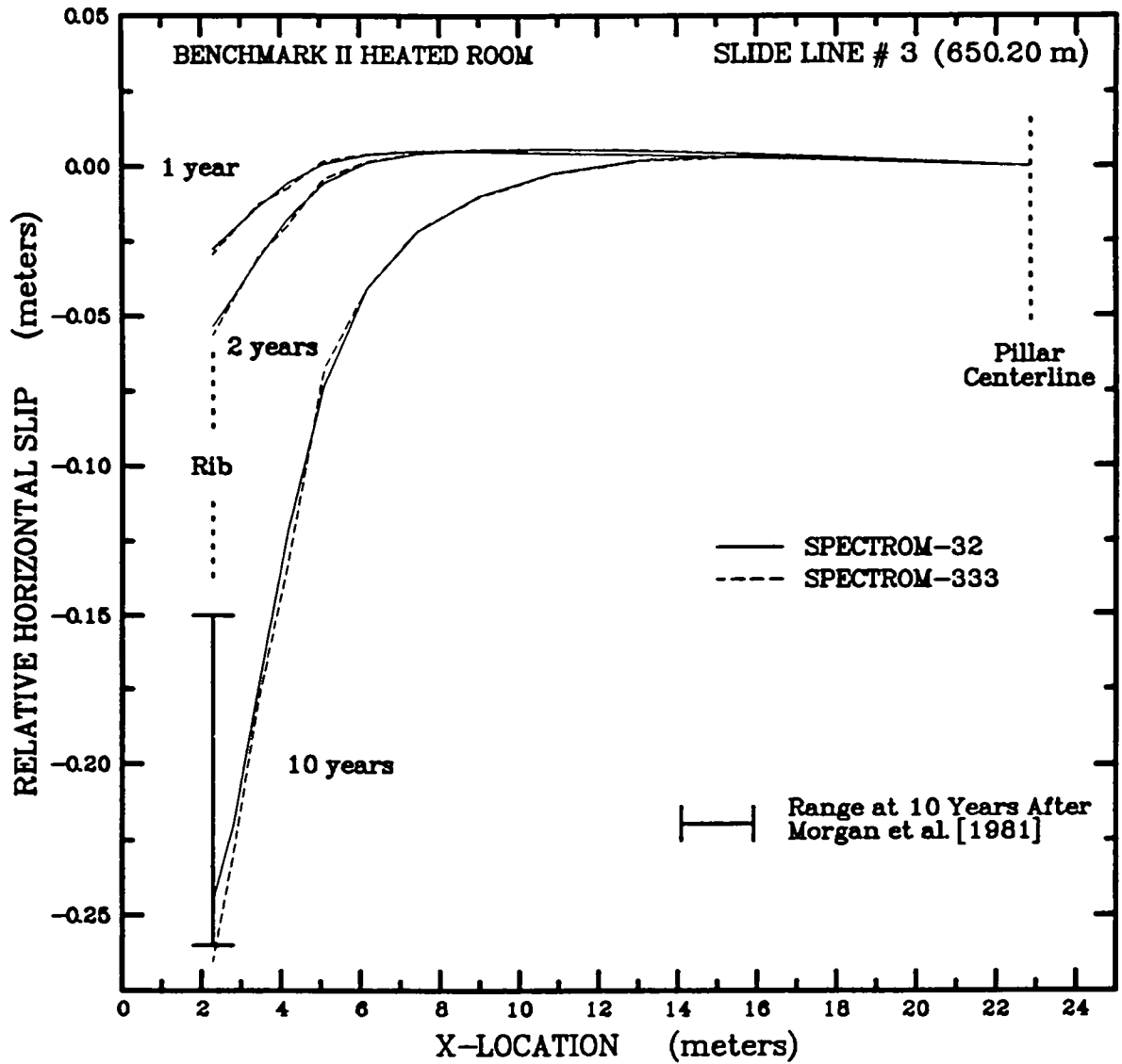
RSI-262-94-069

Figure 4-21. Relative slip across the 638.86-m slide line for the Benchmark II heated room.



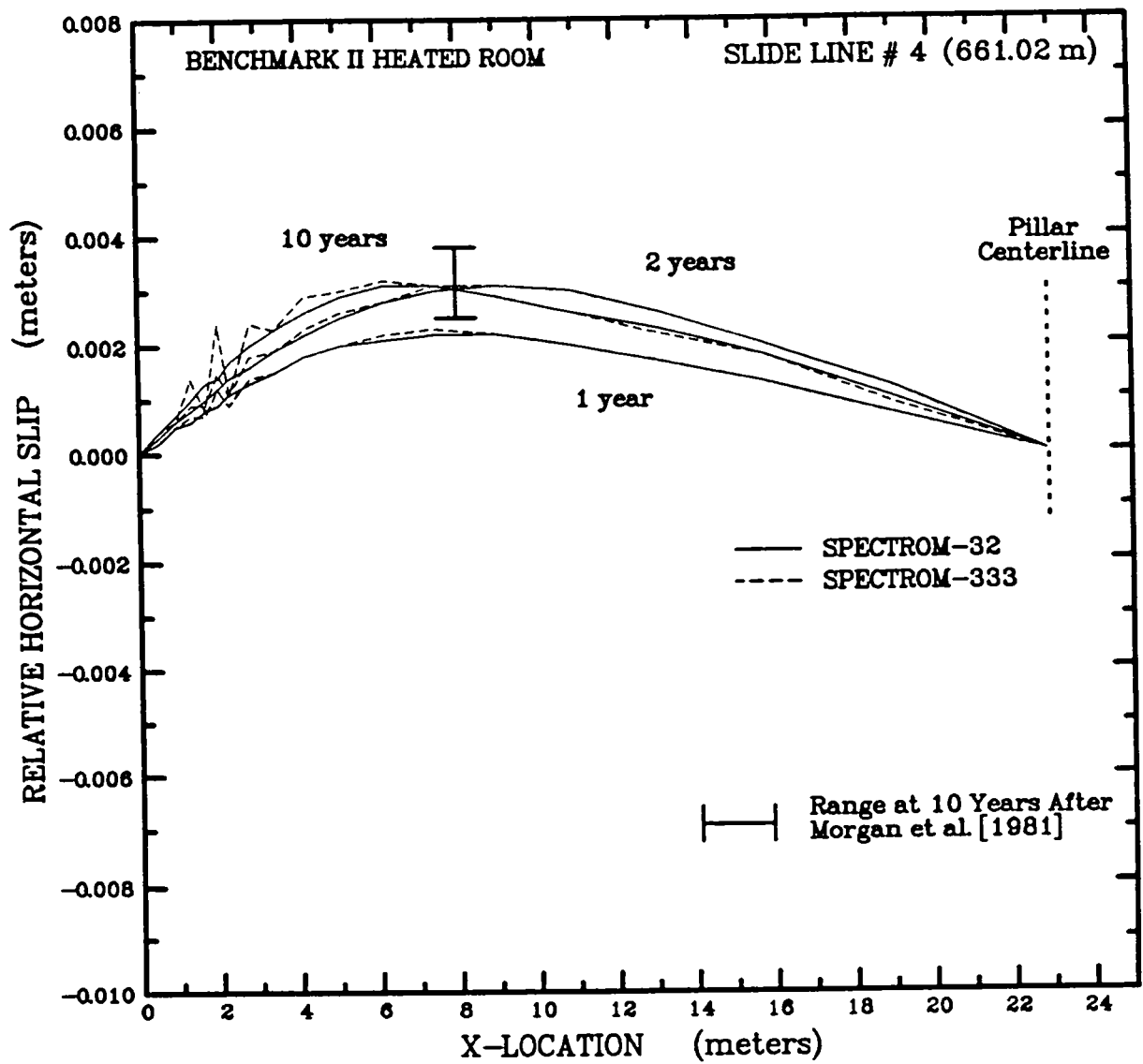
RSI-282-94-070

Figure 4-22. Relative slip across the 642.98-m slide line for the Benchmark II heated room.



RSI-262-94-071

Figure 4-23. Relative slip across the 650.20-m slide line for the Benchmark II heated room.



RSI-262-94-072

Figure 4-24. Relative slip across the 661.02-m slide line for the Benchmark II heated room.

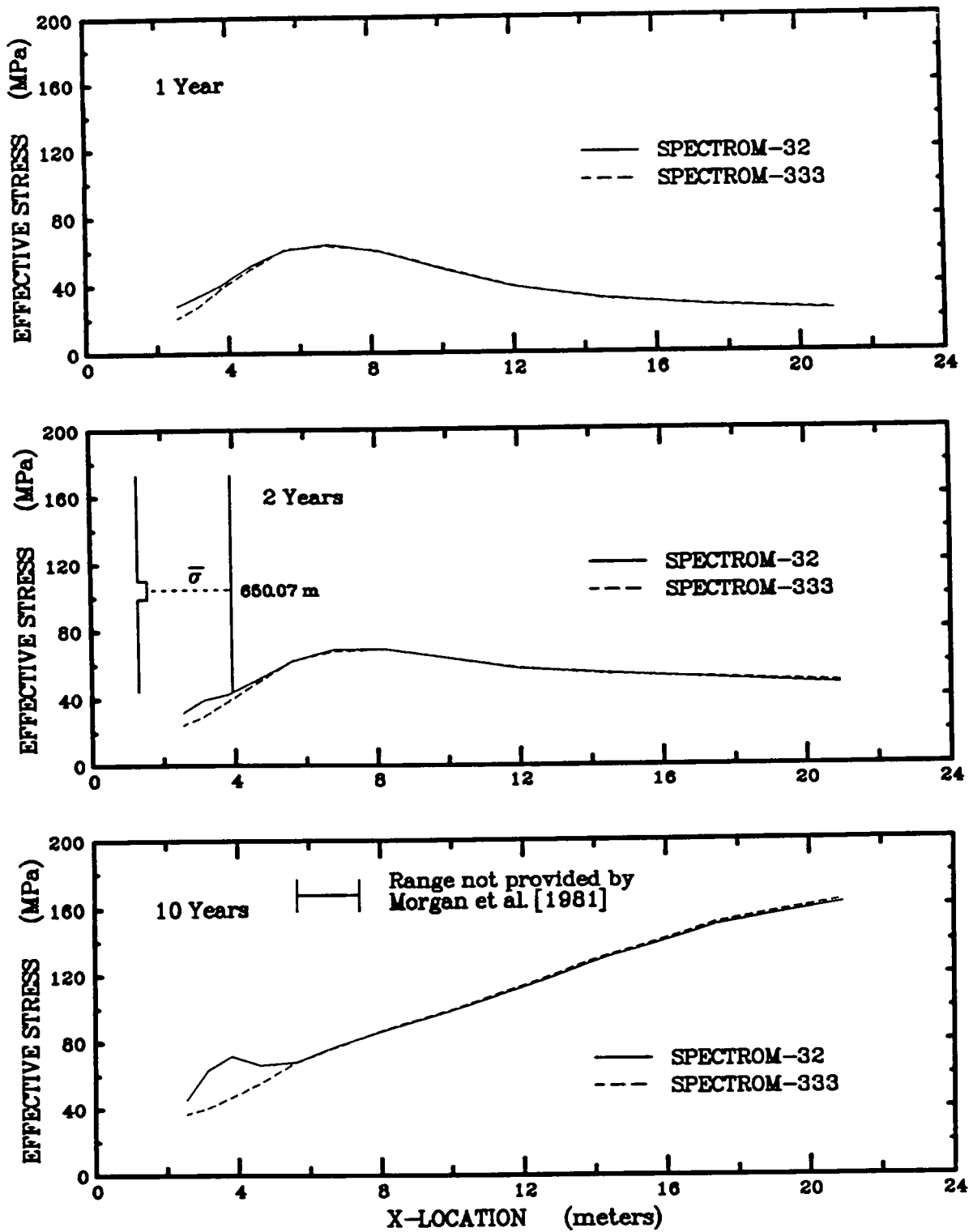
4.2.5 Stress Profiles

Four stress profiles are provided for the heated room. Figure 4-25 is a plot of the effective stress in the anhydrite layer along the line $y = 650.07$ m as a function of horizontal position at 1, 2, and 10 years. The pillar midheight is located at $y = 649.72$ m. The stresses at the four integration points in the **SPECTROM-32** elements were averaged to compare with the stresses at the single integration point in the **SPECTROM-333** elements. Figure 4-26 is similar to Figure 4-25 except vertical stress is plotted as a function of horizontal position. Figure 4-27 is a plot of the effective stress along the vertical centerline of the room ($x = 0$) for values of y between 635.81 m and 661.02 m at 1, 2, and 10 years. Figure 4-28 is the same as Figure 4-27 except that the horizontal stress is presented instead of the effective stress. The stresses predicted by **SPECTROM-32** and **SPECTROM-333** appear to follow the same trend and generally fall within the range of stresses predicted by other participants for the benchmark problem. Similar to the isothermal calculation, the stresses predicted by **SPECTROM-333** in the anhydrite are less than those predicted by the other representative codes.

4.3 Simplified Heated Room Calculation Results

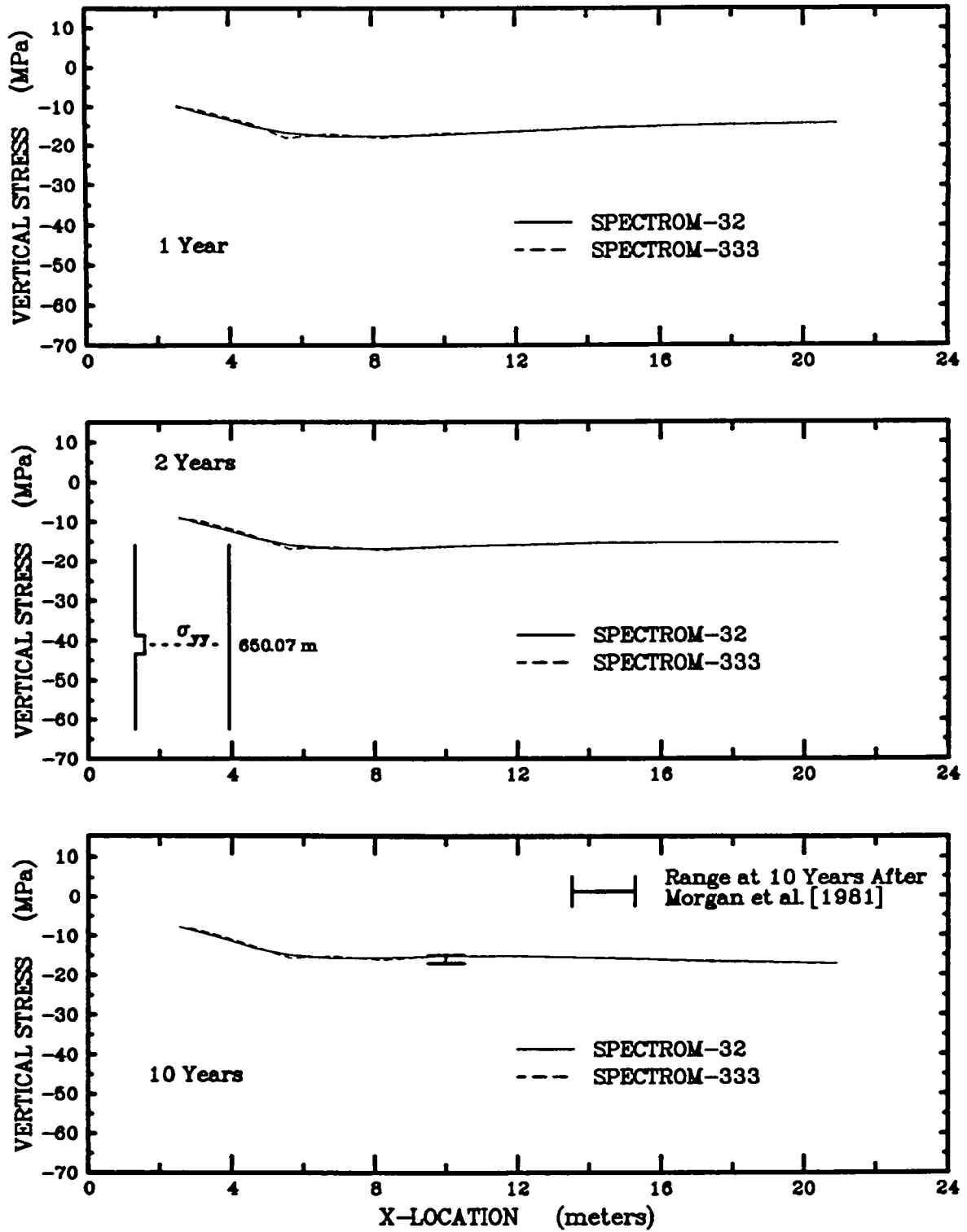
4.3.1 Thermal Calculations

The temperature calculation for the simplified heated room calculation problem was performed using the finite element code **SPECTROM-41** (Svalstad, 1989). The finite element mesh used for the thermal calculation is shown in Figure 4-29. The horizontal mesh extremities are the same as those used for the structural analysis; however, the vertical extremities of the thermal mesh extend 100 m above and below the vertical boundaries specified for the structural analysis. The thermal mesh was extended to assure that the temperature at these boundaries would remain constant during the analysis and, therefore, would not affect the solution. The mesh contains 1,301 nodes and 400 eight-node quadrilateral elements. The initial temperature was prescribed as 300 K and all boundaries were specified as adiabatic. The model was to remain at this temperature for 6 months, at which time the thermal load was applied. The thermal response was computed for a 4.5-year simulation period after application of the thermal load. Temperatures from the thermal calculation were interpolated for the structural mesh using **MERLIN** (see Section 2.4). The interpolated temperature distributions were used as input to the **SPECTROM-32** and **SPECTROM-333** structural calculations. Temperature histories are provided in Figure 4-30 at the floor midpoint, roof midpoint, midheight of the rib, and center of the heat source. Previous



RSI-262-94-073

Figure 4-25. Effective stress profiles through the pillar of the Benchmark II heated room.



RSI-262-94-074

Figure 4-26. Vertical stress profiles through the pillar of the Benchmark II heated room.

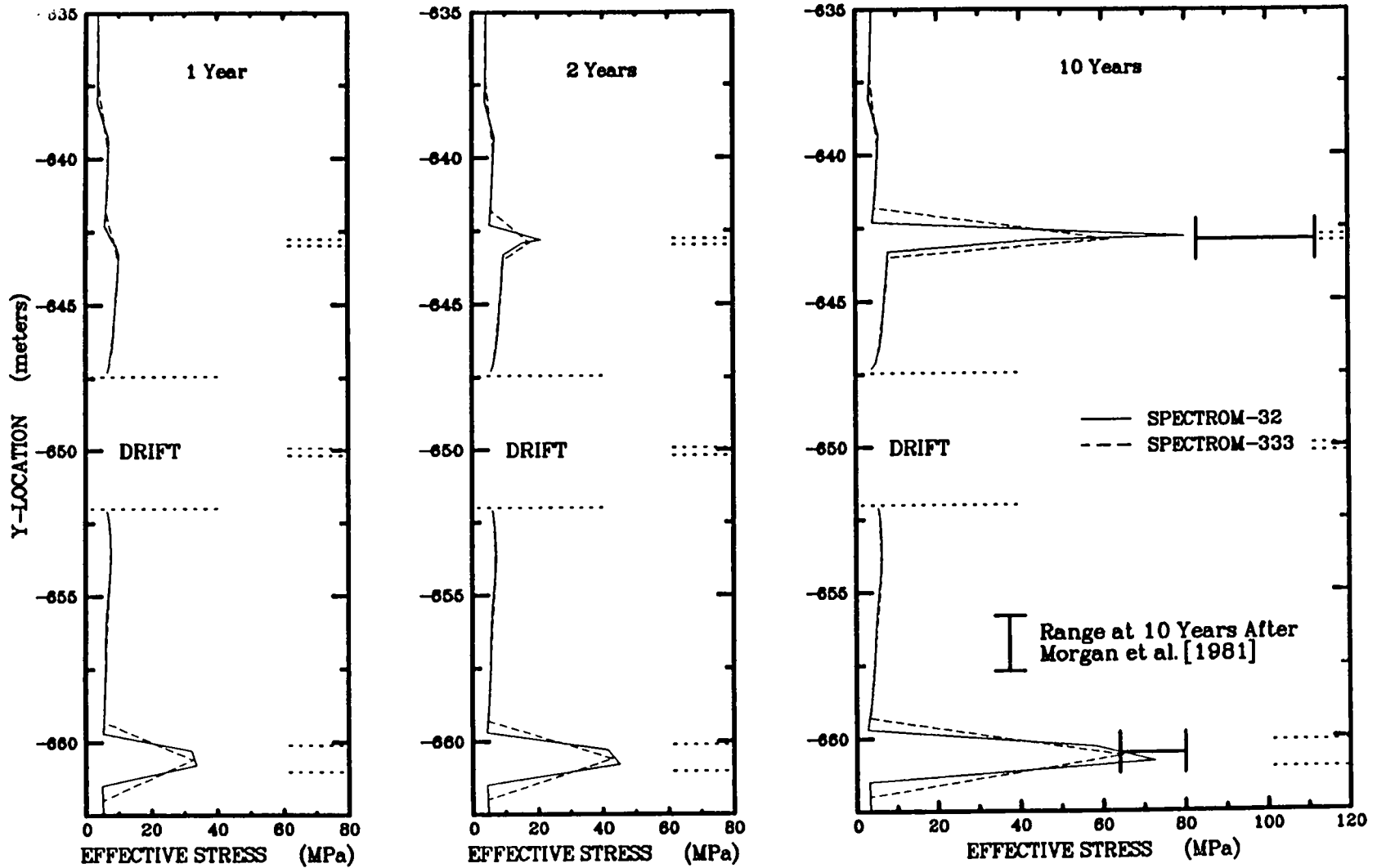


Figure 4-27. Effective stress profiles along the vertical centerline of the Benchmark II heated room.

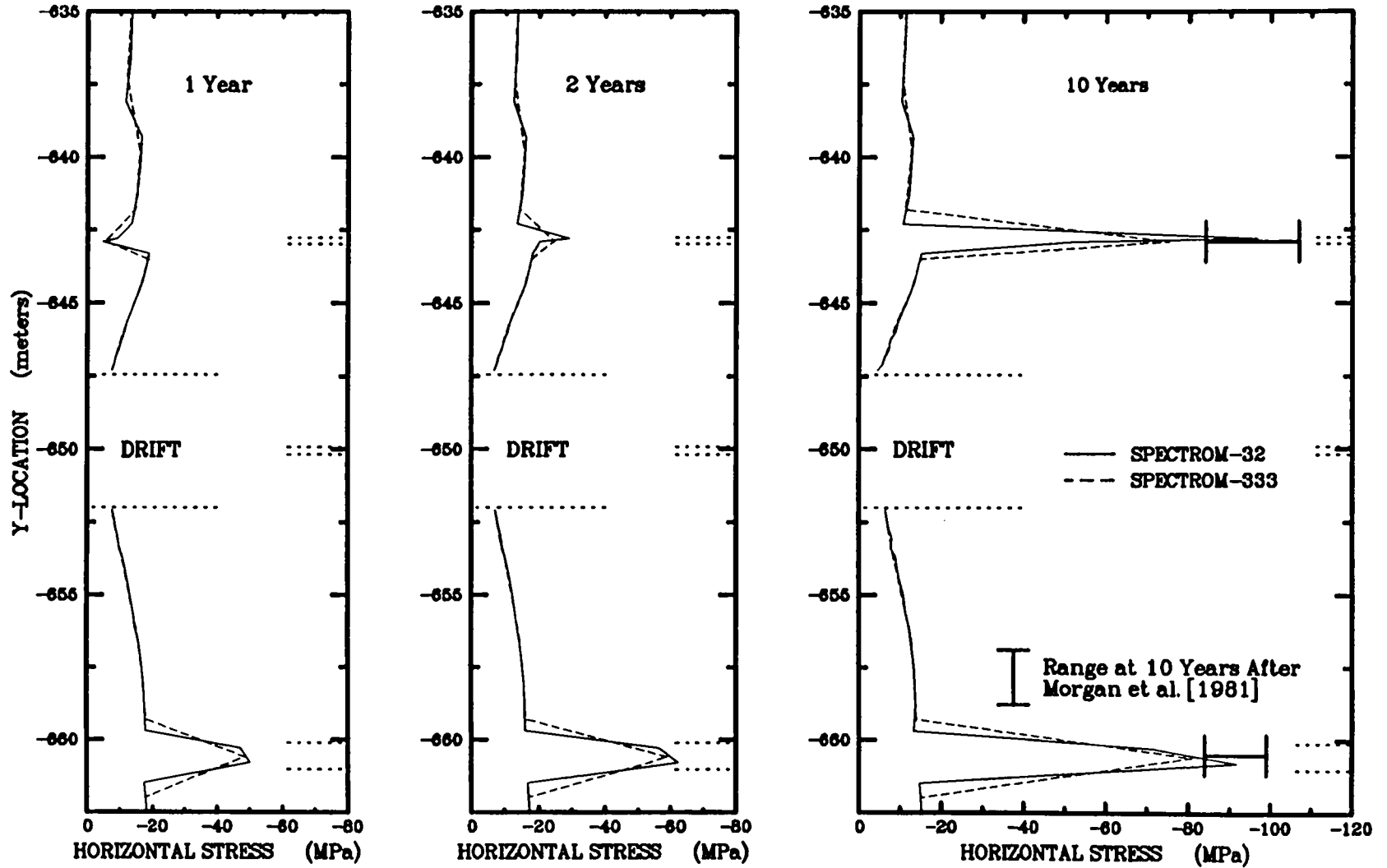
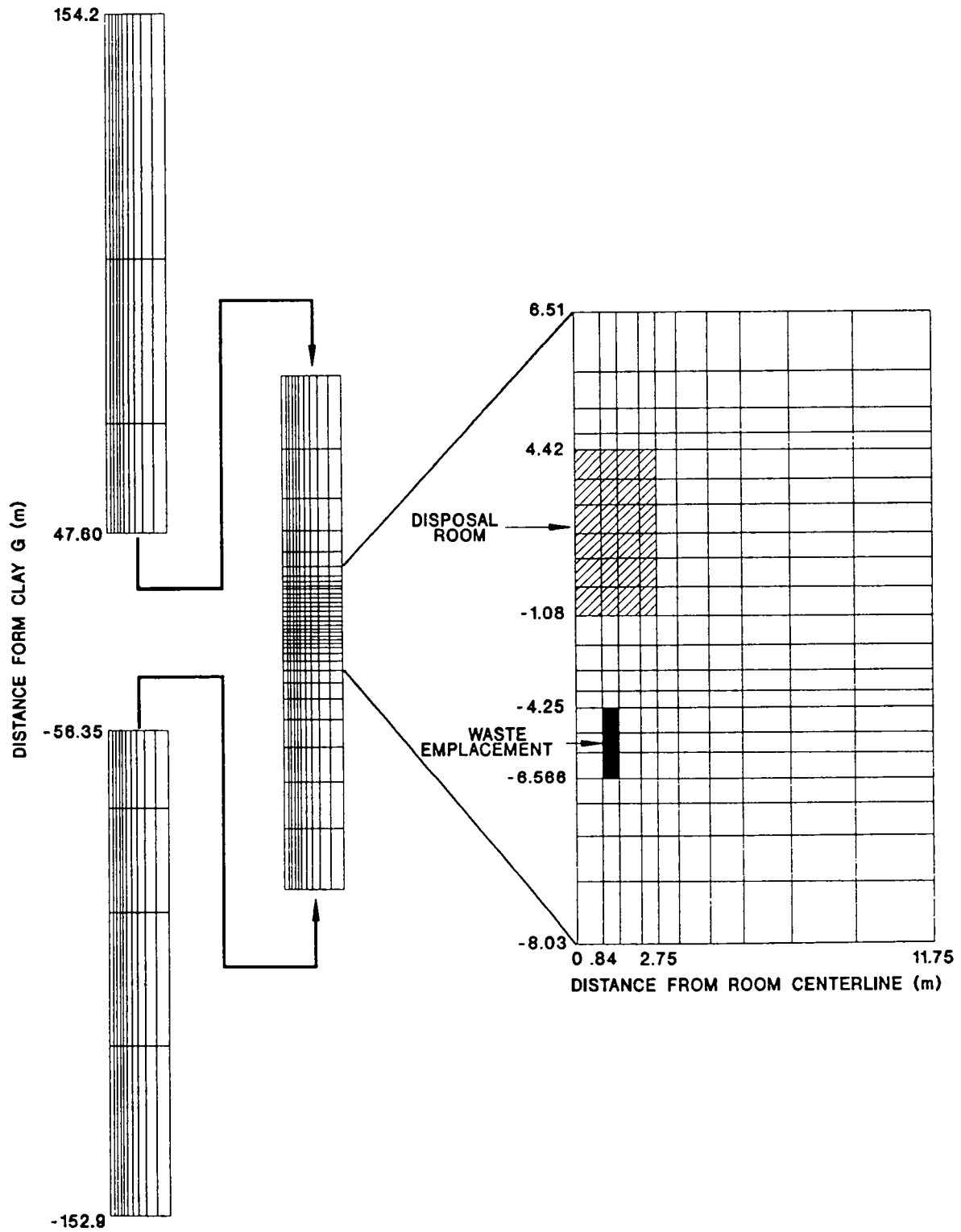
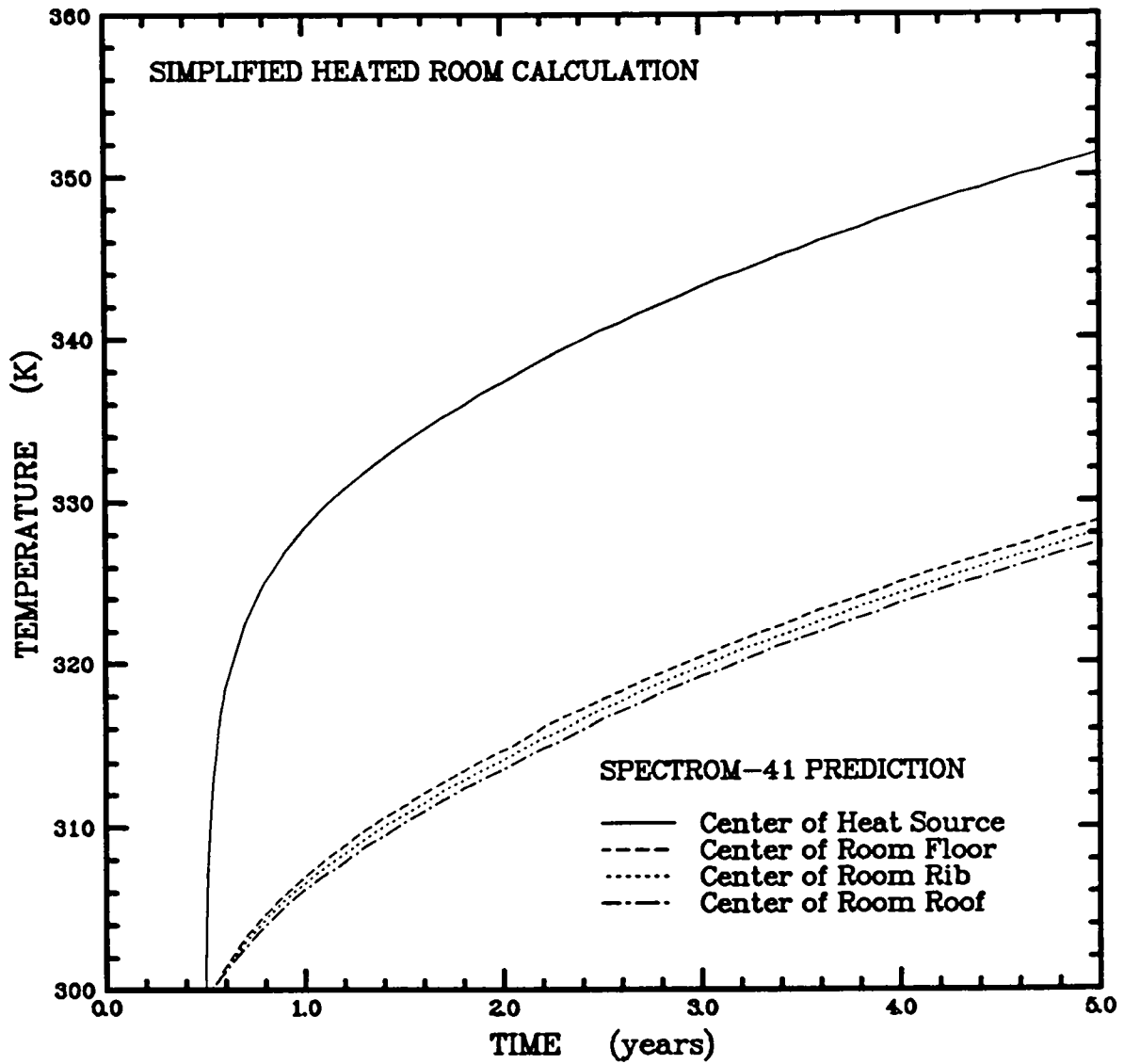


Figure 4-28. Horizontal stress profiles along the vertical centerline of the Benchmark II heated room.



RSI-115-89-036

Figure 4-29. Thermal mesh used for the simplified heated room configuration.



RSI-262-94-077

Figure 4-30. Temperature histories for the simplified heated room configuration computed with SPECTROM-41.

comparisons of the **SPECTROM-41** and **COYOTE** (Munson and Morgan, 1986) temperature results show that the computed temperatures were within 1 percent of each other.

4.3.2 Structural Mesh Statistics

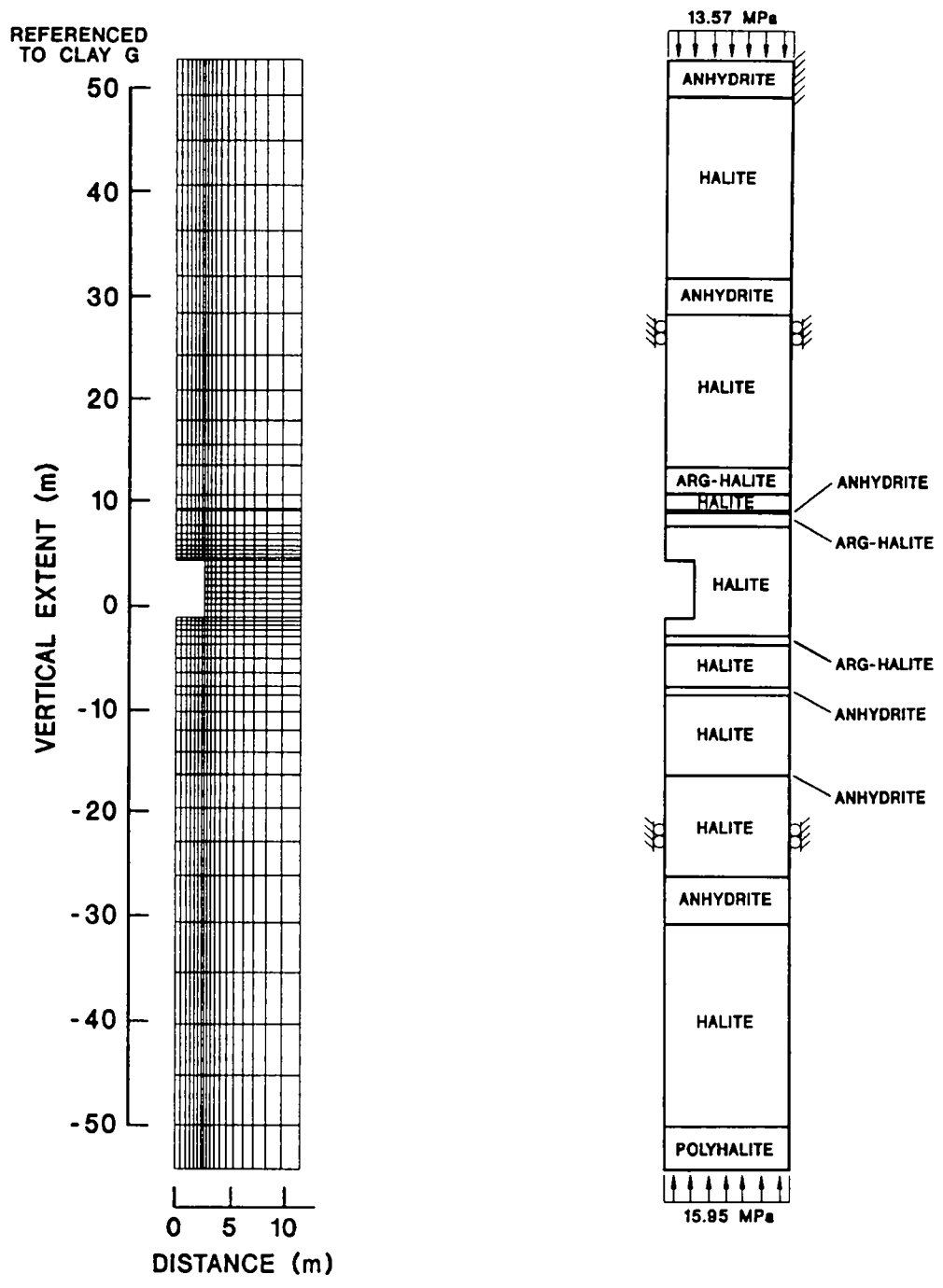
The **SPECTROM-32** undeformed mesh used for the simplified heated room calculation is shown in Figure 4-31. The **SPECTROM-333** mesh is identical to the **SPECTROM-32** mesh except that it is comprised of four-node elements whereas the **SPECTROM-32** mesh contains eight-node elements. The **SPECTROM-333** mesh consists of 989 nodes, 909 four-node plane strain quadrilaterals, and 1,874 degrees of freedom. The **SPECTROM-32** mesh consists of 2,886 nodes, 909 eight-node plane strain quadrilateral elements, and 5,568 degrees of freedom. None of the clay seams were modeled as slide lines for this analysis.

The minimum horizontal node spacing in the **SPECTROM-333** mesh was 0.28 m, and the maximum horizontal spacing was 1.74 m. Because each anhydrite layer was modeled with one element vertically, the minimum vertical node spacing of 0.08 m occurred in the anhydrite layer located from 16.33 m to 16.41 m beneath Clay G. The maximum vertical node spacing was 4.84 m. Similarly, the minimum node spacing in the **SPECTROM-32** mesh is 0.04 m vertically and 0.14 m horizontally with a maximum node spacing of 2.42 m vertically and 0.87 m horizontally.

4.3.3 Displacement Histories and Deformed Mesh

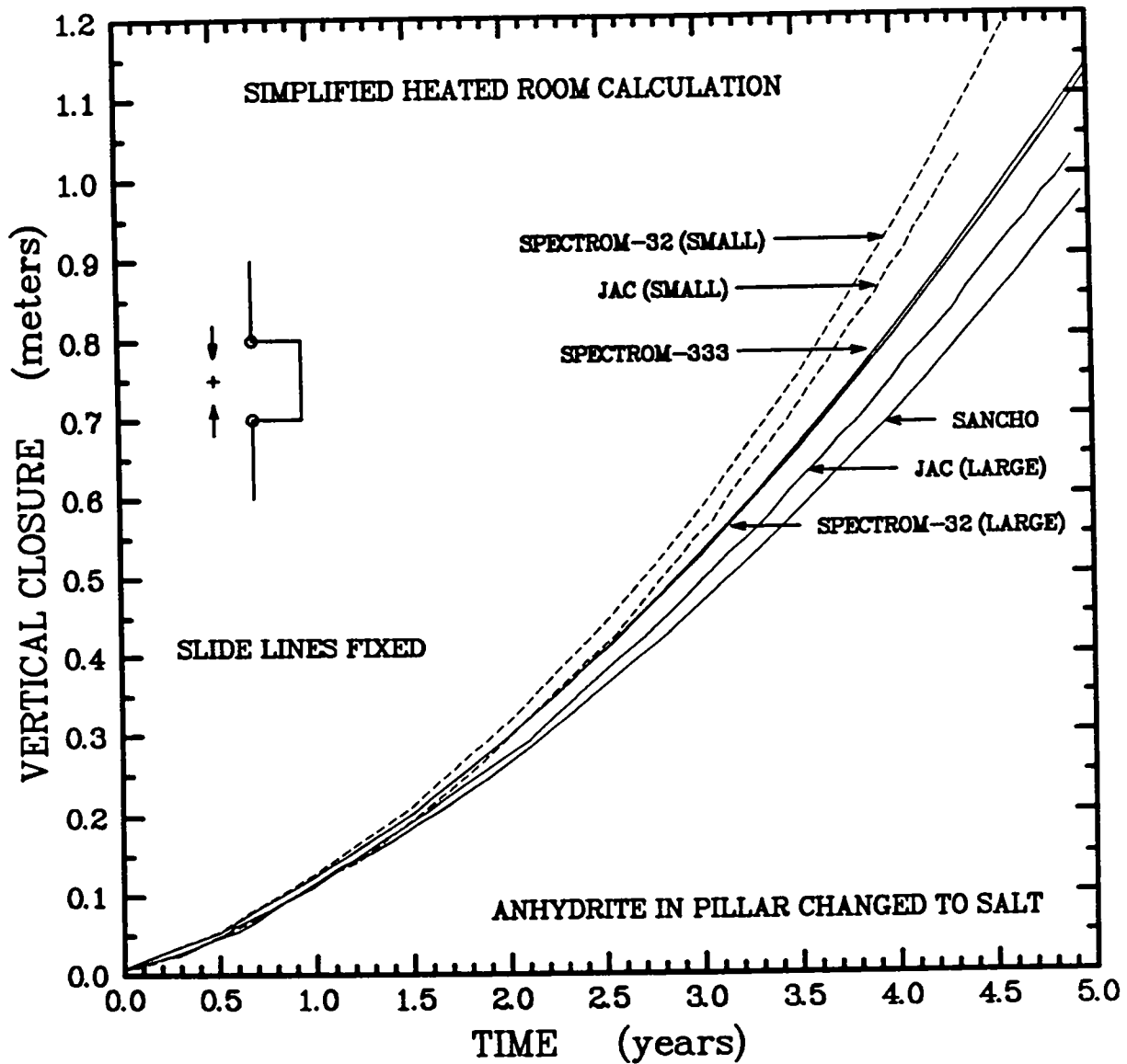
Figure 4-32 shows the predicted vertical room closure history for the simplified heated room calculation. After 5 years, the vertical closures predicted by **SPECTROM-32** and **SPECTROM-333** are 1.13 and 1.14 m, respectively. The **JAC**, **SANCHO**, and **SPECTROM-32** (small strain) predictions of vertical closure reported by Munson and Morgan (1986) were digitized and included in Figure 4-32 for comparative purposes. The **JAC** computer code has both large deformation and small deformation capabilities and was used to verify that large deformation effects were important for the heated parallel calculation. The **JAC**, **SANCHO**, **SPECTROM-32**, and **SPECTROM-333** large deformation solutions resulted in less vertical closure than the **JAC** and **SPECTROM-32** small deformation solutions, which is typical for compressional-type problems with large deformations.

Figure 4-33 shows the horizontal displacement history predicted at the pillar midheight for the simplified heated room calculation. **SPECTROM-32** predicted a midpillar displacement of -0.671 m compared to -0.670 m predicted by **SPECTROM-333** at 5 years. Results were not



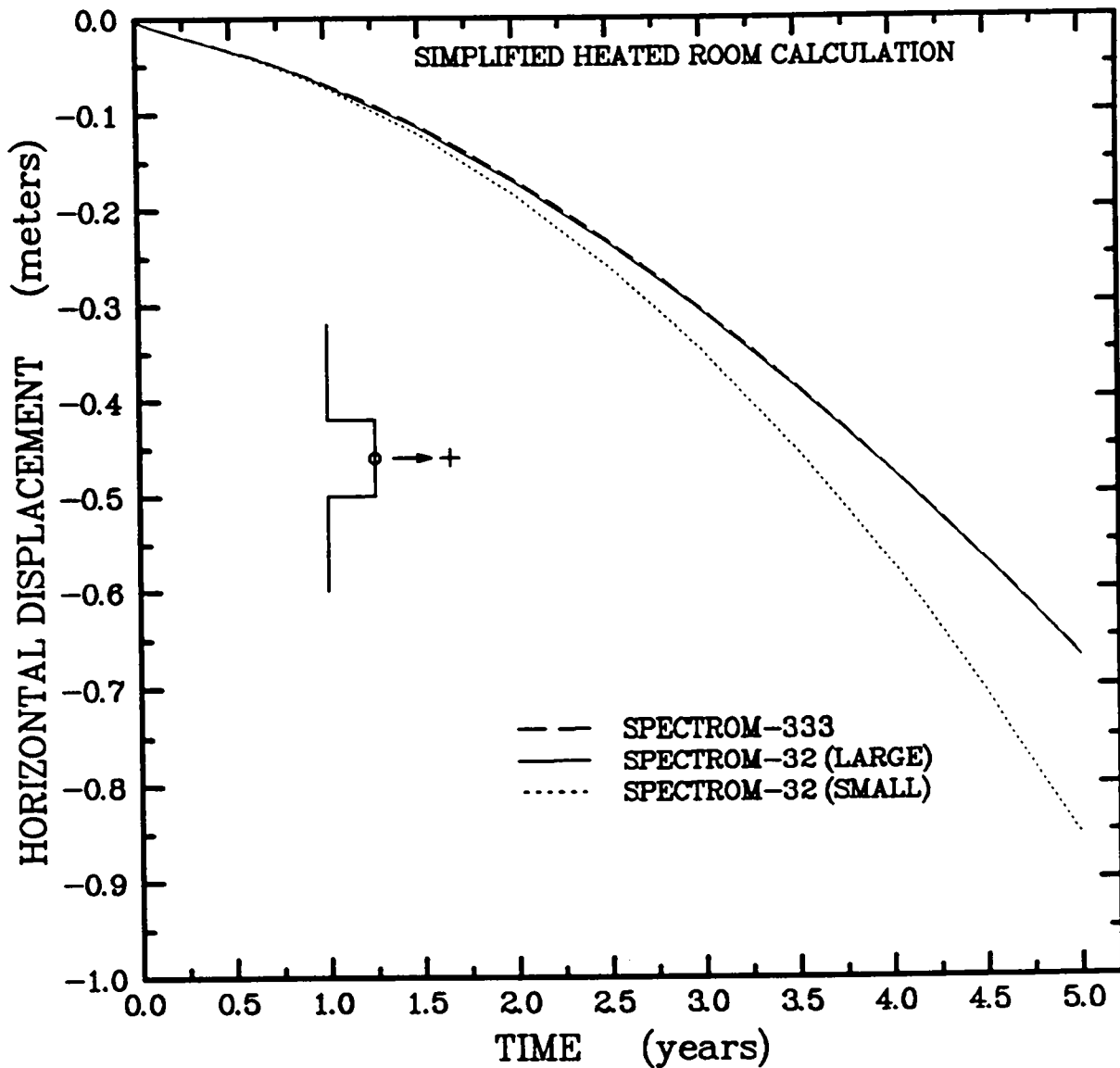
RSI-262-94-050

Figure 4-31. SPECTROM-32 structural mesh and stratigraphy used for the simplified heated room configuration.



RSI-262-94-078

Figure 4-32. Vertical closure histories for the simplified heated room problem.



RSI-282-94-079

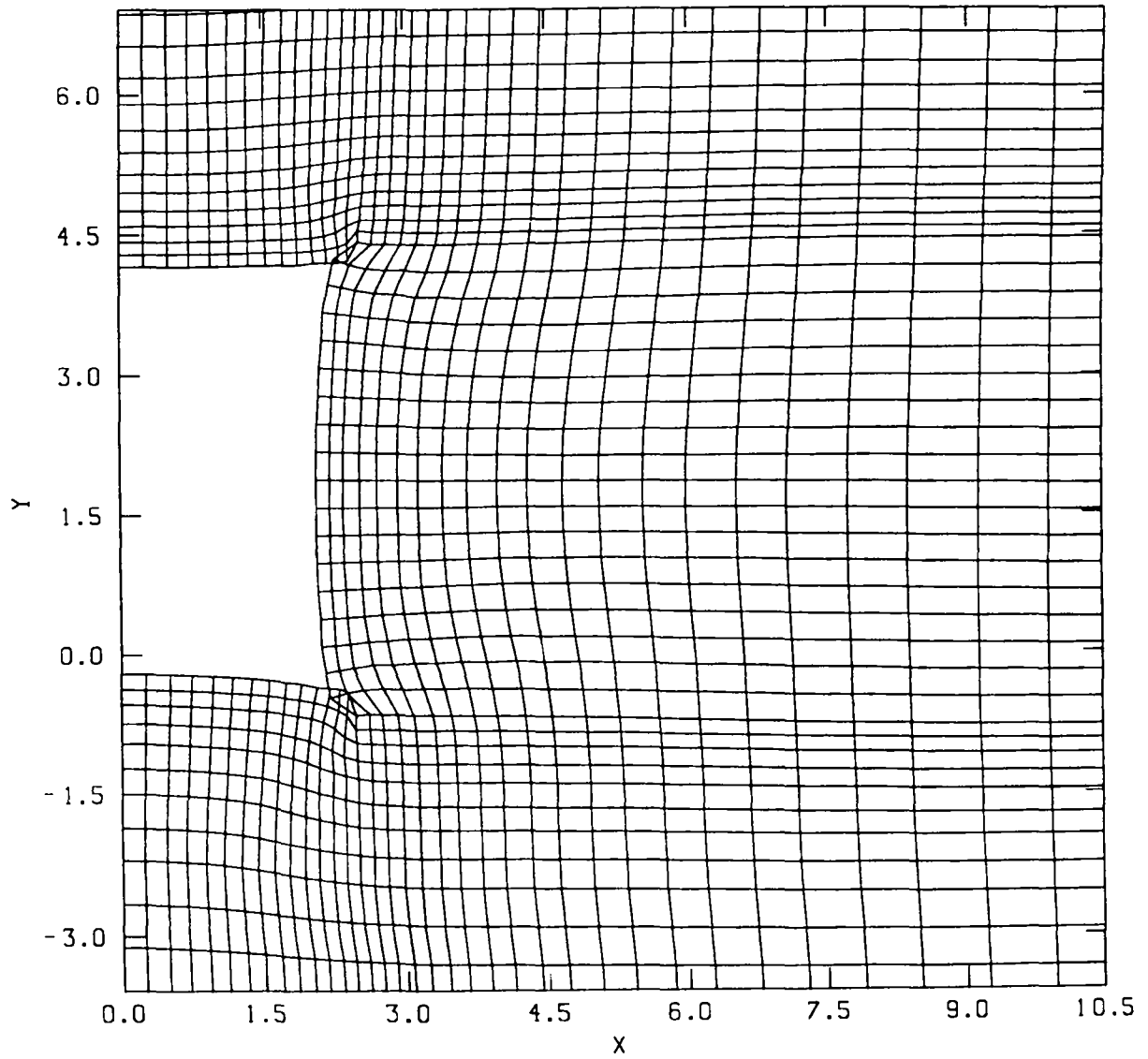
Figure 4-33. Midpillar displacement history for the simplified heated room.

reported by Munson and Morgan (1986) for the midpillar horizontal displacement. However, the **SPECTROM-32** small deformation solution was obtained from a supplemental calculation and included in Figure 4-33. Similar to the vertical closure history, the large deformation solutions predicted less displacement than the small deformation solution.

The **SPECTROM-32** and **SPECTROM-333** deformed meshes at 5 years are shown in Figures 4-34 and 4-35, respectively. Because of the large deformation occurring in this problem, both the **SPECTROM-32** and **SPECTROM-333** deformed meshes show material overlap in the corners of the room. The **SANCHO** and **JAC** codes contain surface contact algorithms that prevent surface penetrations; whereas, neither **SPECTROM-32** nor **SPECTROM-333** contain algorithms of this type. Although Munson and Morgan (1986) do not provide deformed meshes or discussion of the contacting surfaces, neither the **SANCHO** nor the **JAC** calculations are believed to have had the contact algorithms activated for the simplified heated room calculation, which could have reduced the magnitude of their computed deformations.

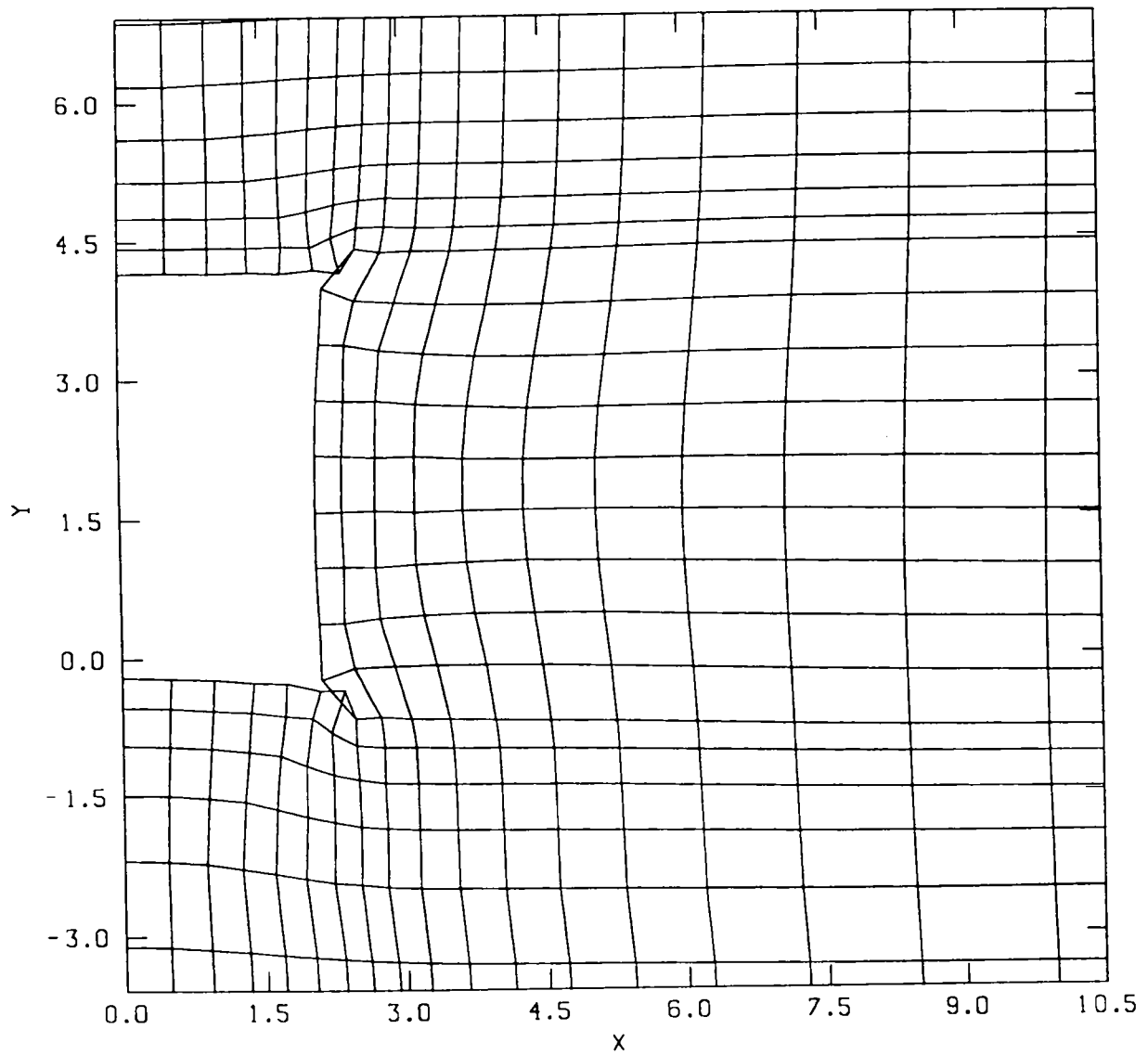
4.3.4 Stress Profiles

Four stress profiles are provided for the simplified heated room calculation. Figure 4-36 is a plot of the effective stress as a function of horizontal position along pillar midheight ($y = 1.67$ m) at 1, 2, and 5 years. The stress results at the four integration points in the **SPECTROM-32** elements were averaged to compare with the stresses at the single integration point in the **SPECTROM-333** elements. Figure 4-37 is similar to Figure 4-36 except vertical stress is plotted as a function of horizontal position. Figure 4-38 is a plot of the effective stress along the vertical centerline of the room ($x = 0$) for values of y between -10.00 and 15.00 m at 1, 2, and 5 years. Figure 4-39 is the same as Figure 4-38 except that the horizontal stress is presented instead of the effective stress. Stress history results from other codes are not available for comparative purposes for this problem.



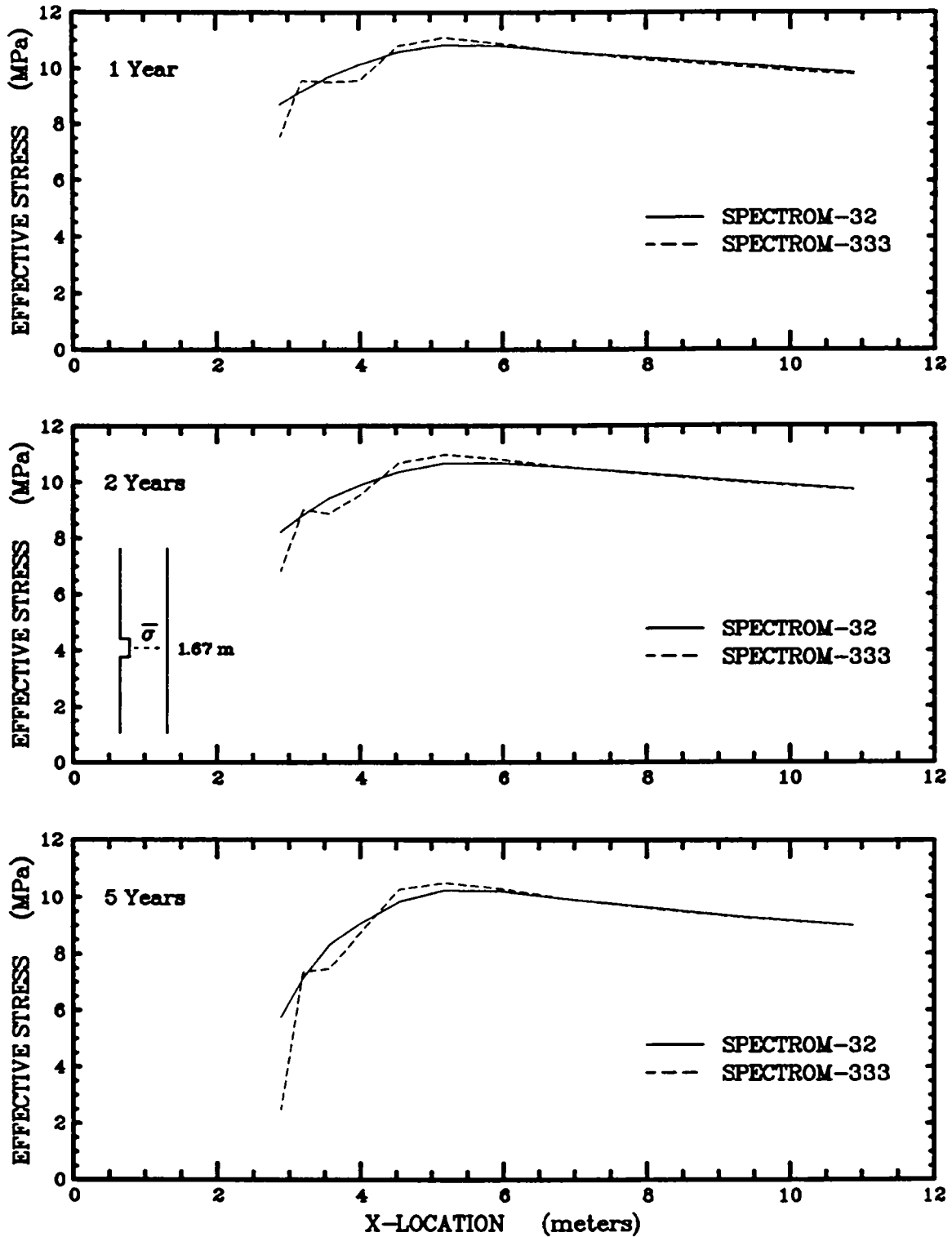
RSI-282-94-080

Figure 4-34. SPECTROM-32 simplified heated room deformed mesh at 5 years.



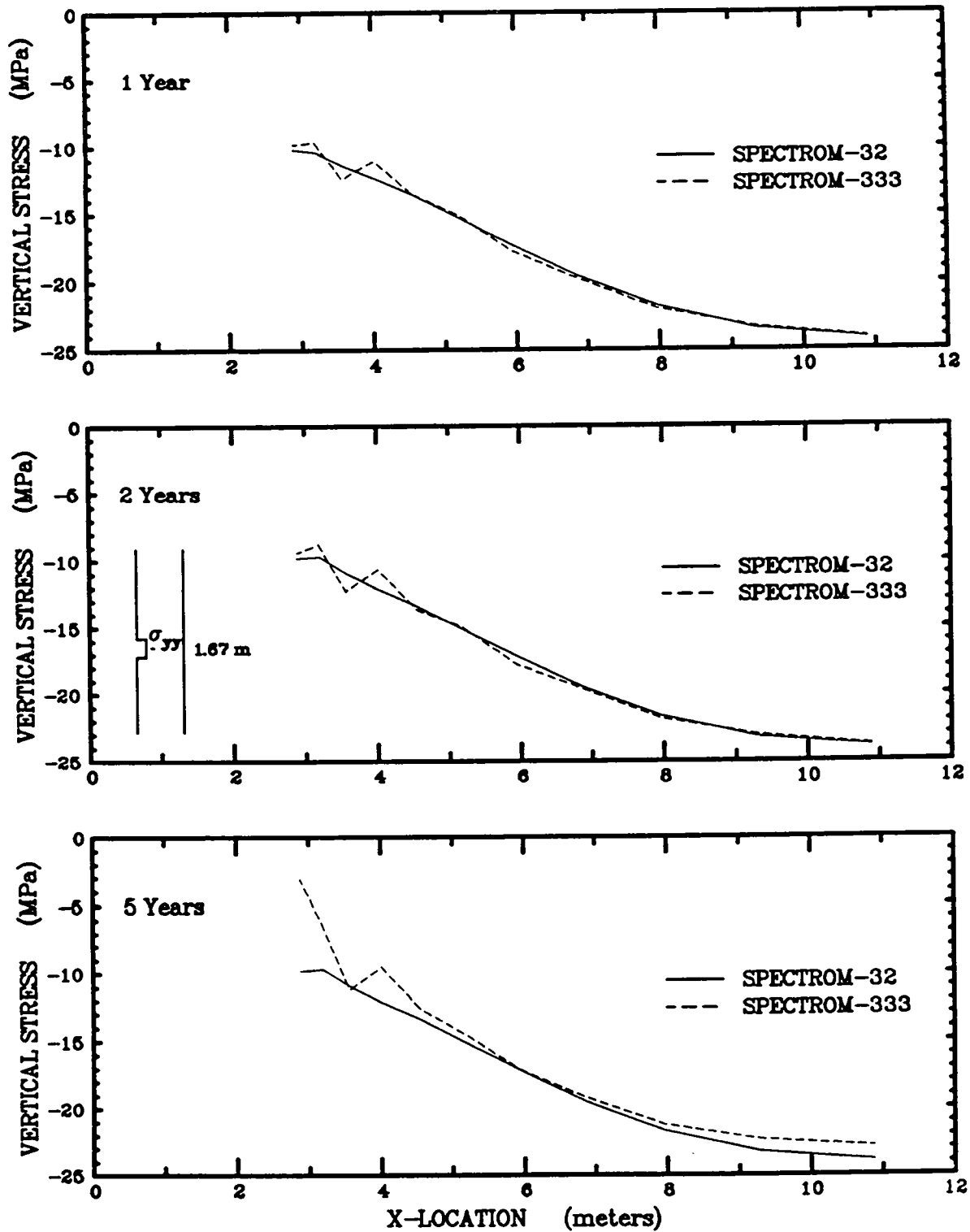
RSI-262-94-081

Figure 4-35. SPECTROM-333 simplified heated room deformed mesh at 5 years.



RSI-262-94-082

Figure 4-36. Effective stress profiles through the pillar of the simplified heated room.



RSI-282-94-083

Figure 4-37. Vertical stress profiles through the pillar of the simplified heated room.

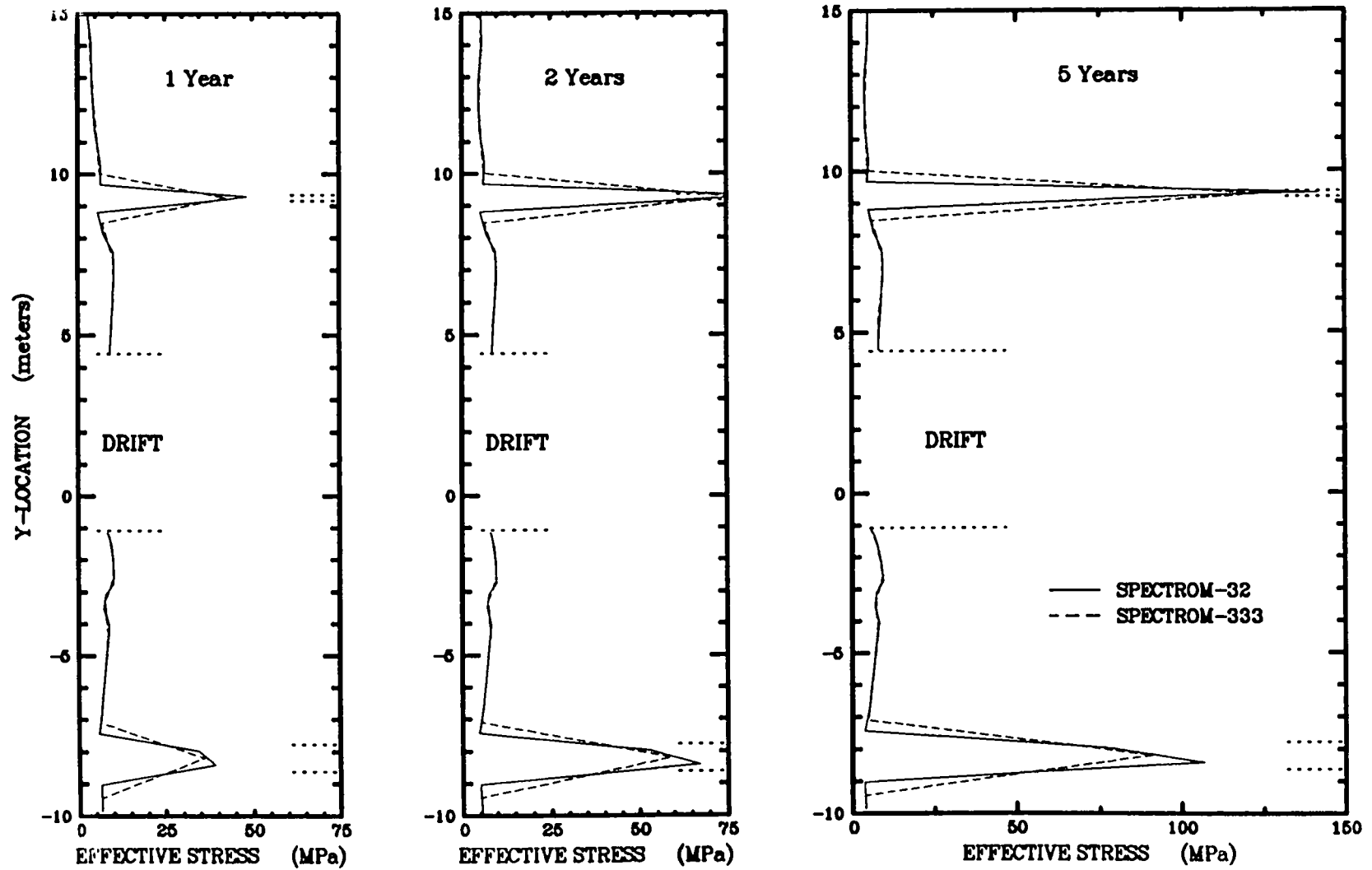


Figure 4-38. Effective stress profiles along the vertical centerline of the simplified heated room.

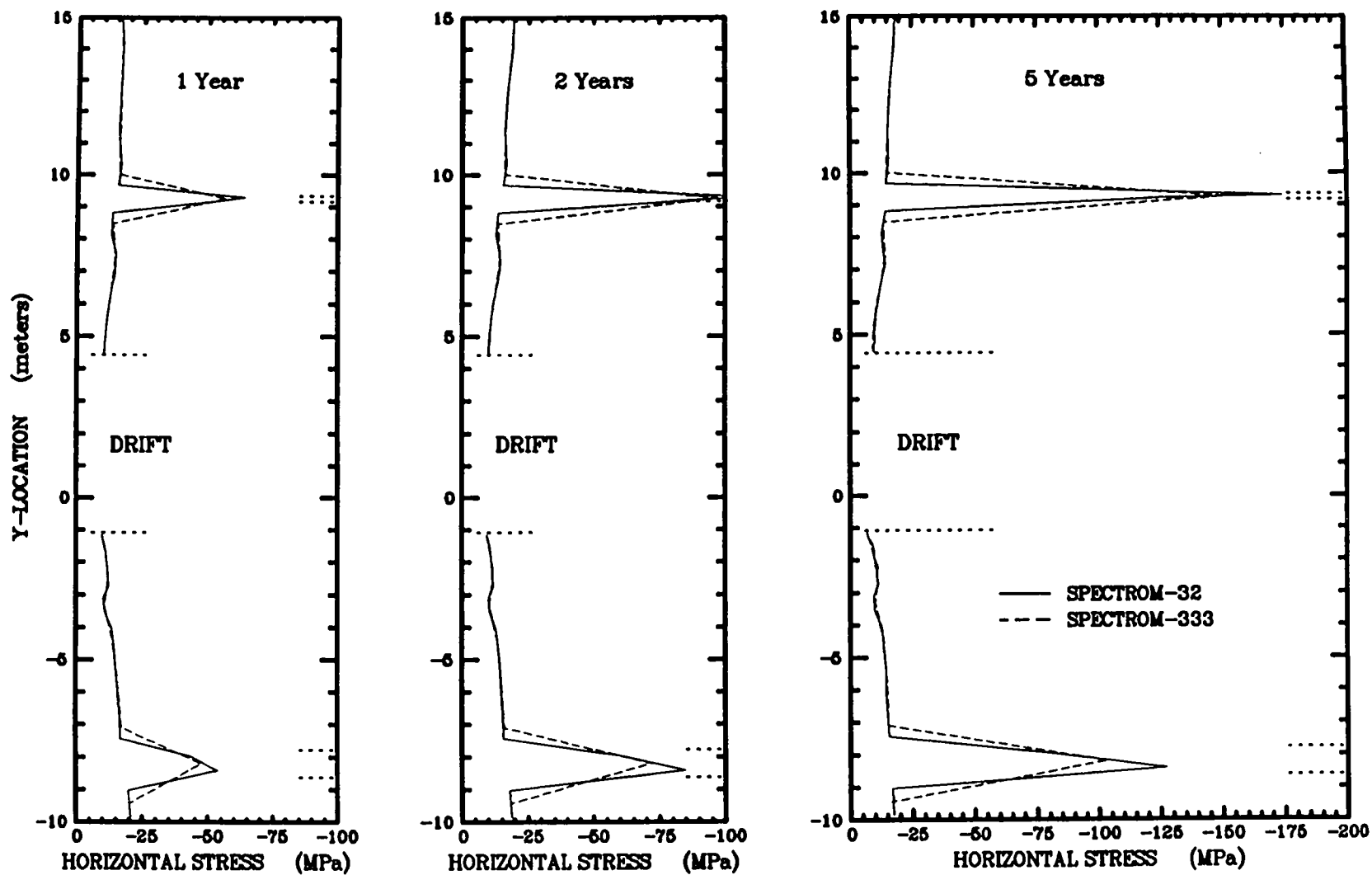


Figure 4-39. Horizontal stress profiles along the vertical centerline of the simplified heated room.

5.0 CONCLUSIONS

The **SPECTROM-32** and **SPECTROM-333** finite strain solutions to three boundary value problems are presented: (1) the WIPP Benchmark II isothermal room problem, (2) the WIPP Benchmark II heated room problem, and (3) the simplified heated calculation. A brief summary of the results obtained and observations made for the three analyses follow.

5.1 Benchmark II Isothermal Room

The **SPECTROM-32** predictions of the isothermal room vertical closures and horizontal displacements at the midpoint of the rib fall within the range of closures and displacements predicted by other researchers using other codes (e.g., Morgan et al., 1981). The **SPECTROM-333** prediction of vertical closure is greater than that predicted by the other representative codes; however, the predicted midpillar horizontal displacement falls within the range predicted by the other codes. The **SPECTROM-32** vertical closure is approximately 9 percent greater than the **JAC** solution and 32 percent greater than the **SANCHO** solution at 10 years. The vertical closure predicted by **SPECTROM-333** at 10 years is approximately 19 and 44 percent greater than the **JAC** and **SANCHO** solutions, respectively. The midpillar displacements predicted by **SPECTROM-32** and **SPECTROM-333** are approximately 4 and 26 percent greater than **JAC** and **SANCHO** solutions, respectively. The stresses predicted by **SPECTROM-32** and **SPECTROM-333** appear to follow the same trend and generally fall within the range of stresses predicted by other representative codes. The **SPECTROM-333** predictions of stress in the anhydrite beds are less than those predicted by the other codes. This discrepancy was not investigated but is probably the result of the single integration point used for the constitutive model integration. Results of the relative displacement across the four active slide lines do not seem unusual even though they tend to be larger than most of the results reported by Morgan et al. (1981).

5.2 Benchmark II Heated Room

Stress measures and relative slip across the active slide lines predicted by **SPECTROM-32** and **SPECTROM-333** for the heated room seem reasonable and appear to be in close agreement with the results reported by Morgan et al. (1981) for this problem. The vertical closure predicted by **SPECTROM-32** and **SPECTROM-333** are approximately 5 percent greater than the **JAC** solution and approximately 10 percent greater than the **SANCHO** solution at 10 years for this problem. The

SPECTROM-32 horizontal displacement at 10 years is approximately 10 percent greater than the **JAC** and **SANCHO** solutions; whereas, the **SPECTROM-333** solution is approximately 38 percent greater than the **JAC** and **SANCHO** solutions. The vertical room closure predicted by **SPECTROM-333** falls within the range predicted by other codes for the heated room. In contrast, the horizontal displacement at the rib midpoint predicted by **SPECTROM-333** is slightly greater than the displacements predicted by other representative codes. These observations are interesting since the vertical and horizontal closure trends predicted by **SPECTROM-333** for the heated room are essentially the opposite of the isothermal room closure trends when compared to other codes. The reasons for these differences were not investigated. However, a reasonable assumption points to mesh refinement and the fact that **SPECTROM-333** uses only one integration point for the constitutive models as possible causes. The **SPECTROM-32** vertical closure and horizontal displacement results fall within the range of results reported by Morgan et al. (1981).

5.3 Simplified Heated Room

Because the simplified heated problem was used to isolate possible sources of error and resolve discrepancies encountered during the parallel calculations, few results were reported by Munson and Morgan (1986) that could be used for comparison. Figure 4-32 presents a comparison of the vertical closure histories predicted by the finite element codes **SPECTROM-333**, **JAC**, **SANCHO**, and **SPECTROM-32**. Munson and Morgan (1986) noted that the small deformation solutions are approximately 20 percent higher than the large deformation solutions after 4.5 years, which indicates that large deformations are occurring and that a large deformation capability is needed for problems of this type. The **SPECTROM-32** and **SPECTROM-333** large deformation solutions are greater than the **SANCHO** and **JAC** large deformation solutions. After 5 years, the **SPECTROM-32** large deformation solutions are approximately 7 and 15 percent greater than the **SANCHO** and **JAC** large deformation solutions, respectively. The **SPECTROM-333** solution is less than 1 percent greater than the **SPECTROM-32** large deformation solution. The 5 percent difference between the **SANCHO** and **JAC** large deformation solutions at 5 years was largely attributed to inaccuracies resulting from the selection of time step sizes and tolerances for the **SANCHO** solution. Munson and Morgan (1986) noted that by decreasing the time step size and convergence tolerances, the **SANCHO** solution was obtained to within 1 percent of the **JAC** solution. Possible causes for the differences between the **JAC** and **SPECTROM** large deformation solutions were not investigated. However, one may hypothesize that changes in mesh refinement, time step size, and convergence tolerances could decrease the differences in the computed results. Other displacement and stress results reported for the two Benchmark problems were not available for

the simplified heated room problem for comparison; however, these results predicted by **SPECTROM-32** and **SPECTROM-333** are presented in Section 4.3 for future reference.

5.4 Summary

SPECTROM-32 and **SPECTROM-333** are demonstrated to have the nonlinear modeling capabilities needed for solving complex problems commonly analyzed for the WIPP program. The problems presented emphasize most of the nonlinear features known to influence the mechanical behavior of the repository. One objective of this report was to compare the results predicted by the **SPECTROM** codes with the results predicted by a number of independent researches using different computer codes. Agreement among several sets of results does not mean that they represent the correct solution; it merely indicates the probable correct solution. If the results differ significantly, potential reasons for the discrepancies can be identified and investigated. Results predicted by other codes were presented as a range at a given time and location. Results from two of the codes (**REM** and **STEALTH**) were not used for comparison because they were unrepresentative of the range of results predicted by the other seven codes. Although difficult to quantify, the term *agreement* (as used here) is not limited to mean that the results fall within the range of results predicted by other codes. In fact, none of the codes participating in the benchmark exercise predicted results that fall within the range of results predicted by the other codes for all of the results presented. Stated differently, if each of the codes' results were plotted against the range of results provided by the remaining codes, every code would fall outside of the range of results more than once. Therefore, assessment of the agreement of results must include all results collectively and not any one result by itself. Overall, reasonable agreement was obtained for the **SPECTROM-32** and **SPECTROM-333** solutions for the benchmark problems based on a global comparison with the results obtained by other codes which participated in the benchmark exercise.

Perhaps the most important response of the benchmark problems and the simplified heated room is the predicted closure of the room. The **SPECTROM-32** room closure results fall within the range of results predicted by the other participants of the benchmark exercise. The **SPECTROM-333** closure results are typically at or slightly greater than the upper end of the range of results. However, the **SPECTROM-333** results appear reasonable with the percentage difference in the closure response between **SPECTROM-32** and **SPECTROM-333** typically less than the predicted differences between **SANCHO** and **JAC** or **SANCHO** and **SPECTROM-32**. The most probable cause for this discrepancy is mesh refinement and the fact that **SPECTROM-333** uses only one integration point for the constitutive models.

In general, **SPECTROM-32** and **SPECTROM-333** predicted slightly more slip across the side lines than most of the other codes that participated in the WIPP Benchmark II exercise. There was little standardization among the participants of the WIPP Benchmark II exercise with six different slide line algorithms being used. This produced a significant range of slide line response. The slightly larger displacements predicted across the slide lines by the **SPECTROM** codes in comparison to the other codes' results can be attributed to the different slide line algorithm.

6.0 REFERENCES

- Anderson, C.A. 1976. "An Investigation of the Steady Creep of a Spherical Cavity in a Half Space," *Journal of Applied Mechanics*. Vol. 43, 254–258.
- Biffle, J.H. 1981. *Second Benchmark Problem for WIPP Structural Computation with the JAC Computer Program*. SAND81–0767. Albuquerque, NM: Sandia National Laboratories.
- Biffle, J.H., and M.L. Blanford, 1994. *JAC2D — A Two-Dimensional Finite Element Computer Program for the Nonlinear Quasistatic Response of Solids with the Conjugate Gradient Method*. SAND93-1891. Albuquerque, NM: Sandia National Laboratories.
- Branstetter, L.J., C.M. Stone, and R.D. Krieg. 1981. *WIPP Benchmark II Results Using SANCHO*. SAND81–0853. Albuquerque, NM: Sandia National Laboratories.
- Callahan, G.D., and K.L. DeVries, 1991. *Analyses of Backfilled Transuranic Waste Storage Rooms*. SAND91-7052. Albuquerque, NM: Sandia National Laboratories.
- Callahan, G.D., A.F. Fossum, and D.K. Svalstad. 1989. *Documentation of SPECTROM-32: A Finite Element Thermomechanical Stress Analysis Program*. DOE/CH/10378-2. RSI-0269. Rapid City, SD: RE/SPEC Inc.
- Chan, K.S., S.R. Bodner, A.F. Fossum, and D.E. Munson. 1992. "A Constitutive Model for Inelastic Flow and Damage Evolution in Solids Under Triaxial Compression," *Mechanics of Materials*. Vol. 14, 1–14.
- Chaudhary, A.B., J.E. Vakili, and H.R. Hume. 1987. *A Mathematical Formulation for Large Strain Analysis of Geologic Continua*. BMI/ONWI/–672. Hereford, TX: Office of Nuclear Waste Isolation, Battelle Memorial Institute.
- Cook, R.D. 1974. *Concepts and Applications of Finite Element Analysis*. New York, NY: John Wiley & Sons, Inc.
- Dienes, J.K. 1979. "On the Analysis of Rotation and Stress Rate in Deforming Bodies," *Acta Mechanica*. Vol. 32, 217–232.
- Gartling, D.K. 1981. *MERLIN — A Computer Program to Transfer Data Between Finite Element Meshes*. SAND81–0463. Albuquerque, NM: Sandia National Laboratories.
- Hearmon, R.F.S. 1961. *An Introduction to Applied Anisotropic Elasticity*. New York, NY: Oxford University Press.

- Hoger, A., and D.E. Carlson. 1984. "Determination of the Stretch and Rotation in the Polar Decomposition of the Deformation Gradient," *Quarterly of Applied Mathematics*. Vol. 42, Issue 2, 113–117.
- Irons, B., and S. Ahmad. 1980. *Techniques of Finite Elements*. West Sussex, England: Ellis Horwood Limited.
- Krieg, R.D. 1982. "A Unified Creep-Plasticity Model for Halite," *Mechanical Testing for Deformation Model Development*. ASTM STP 765. Eds. R.W. Rohde and J.C. Swearingen. Philadelphia, PA: American Society for Testing and Materials. 139–147.
- Krieg, R.D., H.S. Morgan, and T.O. Hunter. 1980. *Second Benchmark Problem for WIPP Structural Computations*. SAND80–1331. Albuquerque, NM: Sandia National Laboratories.
- Lekhnitskii, S.G. 1963. *Theory of Elasticity of an Anisotropic Elastic Body*. Ed. J.J. Brandstatter. San Francisco, CA: Holden-Day.
- Malvern, L.E. 1969. *Introduction to the Mechanics of a Continuous Medium*. Englewood Cliffs, NJ: Prentice-Hall, Inc.
- Matthies, H., and G. Strang. 1979. "The Solution of Nonlinear Finite Element Equations," *International Journal For Numerical Methods in Engineering*. Vol. 14, no. 11, 1,613–1,626.
- Morgan, H.S., R.D. Krieg, and R.V. Matalucci. 1981. *Comparative Analysis of Nine Structural Codes Used in the Second WIPP Benchmark Problem*. SAND81–1389. Albuquerque, NM: Sandia National Laboratories.
- Munson, D.E., and P.R. Dawson. 1982. *A Transient Creep Model for Salt During Stress Loading and Unloading*. SAND82–0962. Albuquerque, NM: Sandia National Laboratories.
- Munson, D.E., and H.S. Morgan. 1986. *Methodology for Performing Parallel Design Calculations (Nuclear Waste Repository Application)*. SAND85–0324. Albuquerque, NM: Sandia National Laboratories.
- Munson, D.E., A.F. Fossum, and P.E. Senseny. 1989. *Advances in Resolution of Discrepancies Between Predicted and Measured In Situ WIPP Room Closures*. SAND88–2948. Albuquerque, NM: Sandia National Laboratories.
- Norton, F.H. 1929. *Creep of Steel at High Temperatures*. New York, NY: McGraw-Hill Book Company.
- Owen, D.R.J., and E. Hinton. 1980. *Finite Elements in Plasticity: Theory and Practice*. Swansea, United Kingdom: Pineridge Press Limited.

- Pinsky, P.M., M. Ortiz, and K.S. Pister. 1983. "Numerical Integration of Rate Constitutive Equations in Finite Deformation Analysis," *Computer Methods in Applied Mechanics and Engineering*. 40, 137–158.
- Roy, S., A.F. Fossum, and R.J. Dexter. 1992. "On the Use of Polar Decomposition in the Integration of Hypoelastic Constitutive Laws," *International Journal of Engineering Science*. Vol. 30, no. 2, 119–133.
- Seegerlind, L.J. 1976. *Applied Finite Element Analysis*. New York, NY: John Wiley & Sons, Inc.
- Sjaardema, G.D., and R.D. Krieg. 1987. *A Constitutive Model for the Consolidation of Crushed Salt and Its Use in Analyses of Backfilled Shaft and Drift Configurations*. SAND87-1977. Albuquerque, NM: Sandia National Laboratories.
- Stone, C.M., R.D. Krieg, and Z.E. Beisinger. 1988. *SANCHO — A Finite Element Computer Program for the Quasistatic, Large Deformation, Inelastic Response of Two-Dimensional Solids*. SAND84-2618, Albuquerque, NM: Sandia National Laboratories.
- Svalstad, D.K., 1989. *Documentation of SPECTROM-41: A Finite Element Heat Transfer Analysis Program*. DOE/CH/10378-1. RSI-0266. Rapid City, SD: RE/SPEC Inc.
- Taylor, L.M., and D.P. Flanagan. 1987. *PRONTO 2D — A Two-Dimensional Transient Solid Dynamics Program*. SAND86-0594. Albuquerque, NM: Sandia National Laboratories.
- Timoshenko, S.P., and J.N. Goodier. 1970. *Theory of Elasticity*. 3rd ed. New York, NY: McGraw-Hill Book Company.
- Zienkiewicz, O.C. 1977. *The Finite Element Method*. 3rd ed. London, England: McGraw-Hill Book Company (UK) Limited.

APPENDIX A: MATERIAL CHARACTERIZATION

APPENDIX A: MATERIAL CHARACTERIZATION

The purpose of the benchmark exercise was to compare the results obtained directly with different codes. Direct comparison is difficult unless identical problems are performed. Characterization of the different materials used in the benchmark problems are explicitly described by Krieg et al. (1980) and are repeated here for completeness.

The stratigraphy in which both the isothermal and heated rooms are located consists of halite, argillaceous halite, anhydrite, polyhalite, 10 percent anhydrite-polyhalite mixed with 90 percent halite, and clay arranged as shown in Figure 3-2. This stratigraphy is for the upper level at the WIPP site and was established by Sandia National Laboratories and the WIPP Project Office contractors in November 1979 (Krieg et al., 1980). The static and dynamic coefficients of friction for the clay seams for the WIPP Benchmark II problems were chosen to be zero. The mechanical properties of the other layers have the values reported by Krieg et al. (1980). These properties are summarized in Table A-1. The creep constants, D , n , and Q in Table A-1, are constants in the secondary creep law description that follows (Equation A-3).

Table A-1. Mechanical properties for the Benchmark II problem^a
(upper level, nominal 655 m)

Material	Elastic Constants ^b		Creep Constants		
	ν	E (Pa)	D (Pa ^{-4.9} - s ⁻¹)	n	Q (kcal/mole)
Halite (H)	0.25	2.48×10^{10}	5.79×10^{-36}	4.9	12.0
Argillaceous Salt	0.25	2.48×10^{10}	1.74×10^{-35}	4.9	12.0
10% A-P, 90% H	0.25	2.65×10^{10}	5.21×10^{-36}	4.9	12.0
Anhydrite (A)	0.33	7.24×10^{10}	0.0	—	—
Polyhalite (P)	0.33	7.24×10^{10}	0.0	—	—
Clay Seam	Friction Slide Line: μ static = μ dynamic = 0.0				

^a From Krieg et al. (1980).

^b Poisson's ration, ν , and Young's modulus, E .

The thermal properties of the various layers are presented in Table A-2. These properties have been provided by Krieg et al. (1980) and were obtained from material property tests performed on salt samples from the WIPP site. Most of the tests were performed on halite. Very few tests were performed on the other materials, so the properties in Table A-2 for all materials except halite are estimates for the benchmark calculations but will be refined by further investigations. The thermal properties of the “equivalent thermal material” to simulate radiation across the room are also given in Table A-2. These properties have been provided by Krieg et al. (1980).

Table A-2. Thermal properties for the Benchmark II problem^a

Material	Density ρ kg/m ³	Specific Heat C_p J/kg-K	Coefficient of Linear Thermal Expansion, α K ⁻¹	Thermal Conductivity ^b Parameters	
				λ_o W/m-k	Γ
Halite (H)	2,167	860	45.0×10^{-6}	5.0	1.14
Argillaceous Salt	2,167	860	40.0×10^{-6}	4.0	1.14
10& A-P, 90% H	2,167	860	42.7×10^{-6}	5.0	1.14
Anhydrite (A)	2,167	860	20.0×10^{-6}	4.5	1.14
Polyhalite (P)	2,167	860	24.0×10^{-6}	2.0	1.00
“Equivalent Thermal Material”	1	1,000	—	50.0	0.00

^a From Krieg et al. (1980).
^b $k = \lambda_o(\theta/300)^\Gamma$ where θ is temperature in Kelvin.

NOTE: The equation in Table A-2 expressing thermal conductivity for the various materials was incorrect when specified for the Benchmark II problems. The correct equation is

$$k = \lambda_o \left(\frac{300}{\theta} \right)^\Gamma$$

However, the incorrect equation was used in the **SPECTROM-32** and **SPECTROM-333** solutions of the first two Benchmark II calculations so that a direct comparison could be made with previous solutions in which the incorrect equation was used.

The creep law used for the Benchmark II exercise is that adopted by Herrmann, Wawersik, and Lauson to describe the secondary creep of southeastern New Mexico salt (Herrmann et al., 1980). Primary creep is not considered in this problem. The constitutive model follows.

The strain rate is characterized by the following:

$$\dot{\epsilon}_{ij} = -\frac{\nu}{E} \dot{\sigma}_{kk} \delta_{ij} + \left(\frac{1 + \nu}{E} \right) \dot{\sigma}_{ij} + \dot{\epsilon}_{ij}^c \quad (\text{A-1})$$

where

$\dot{\sigma}_{ij}$ = Components of the stress rate tensor

ν = Poisson's ratio

E = Young's modulus

δ_{ij} = Kronecker delta

$\dot{\epsilon}_{ij}^c$ = Creep strain rate given by:

$$\dot{\epsilon}_{ij}^c = \left| \dot{\epsilon}_{kl}^c \right| \frac{\sigma'_{ij}}{\left| \sigma'_{mn} \right|} \quad (\text{A-2})$$

where

σ'_{ij} = Components of the deviatoric stress tensor.

and the stress and strain tensor norms used here are defined as

$$\left| \dot{\epsilon}_{ij}^c \right| = \left(\dot{\epsilon}_{ij}^c \dot{\epsilon}_{ij}^c \right)^{1/2}$$

$$\left| \sigma'_{ij} \right| = \left(\sigma'_{ij} \sigma'_{ij} \right)^{1/2}$$

For this case, in which only secondary (steady state) creep is considered, the magnitude of the creep strain rate can be expressed in terms of the effective creep strain rate $\dot{\bar{\epsilon}}$, or the effective stress, $\bar{\sigma}$, as follows:

$$\begin{aligned}
 |\dot{\epsilon}_{ij}^c| &= \sqrt{1.5} \dot{\bar{\epsilon}} \\
 &= \sqrt{1.5} D \bar{\sigma}^n \exp \frac{-Q}{R\theta}
 \end{aligned}
 \tag{A-3}$$

$\dot{\bar{\epsilon}}$ is defined as:

$$\dot{\bar{\epsilon}} = \left(\frac{2}{3} \dot{\epsilon}_{ij}^c \dot{\epsilon}_{ij}^c \right)^{1/2}
 \tag{A-4}$$

while $\bar{\sigma}$ is

$$\bar{\sigma} = \left(\frac{3}{2} \sigma'_{ij} \sigma'_{ij} \right)^{1/2}
 \tag{A-5}$$

D, n = Constants determined from data analysis

θ = Temperature, K

Q = Effective activation energy, cal/mole

R = Universal gas constant, 1.987 cal/mole-K.

Values for the parameters are given in Table A-1.

References for Appendix A

Herrmann, W., W.R. Wawersik, and H.S. Lauson. 1980. *Analysis of Steady State Creep of Southeastern New Mexico Bedded Salt*. SAND80-0558. Albuquerque, NM: Sandia National Laboratories.

Krieg, R.D., H.S. Morgan, and T.O. Hunter. 1980. *Second Benchmark Problem for WIPP Structural Computations*. SAND80-1331. Albuquerque, NM: Sandia National Laboratories.

DISTRIBUTION

Federal Agencies:

U.S. Department of Energy (6)
Office of Civilian Radioactive Waste
Management
Attn: Deputy Director, RW-2
Associate Director, RW-10/50
Office of Program and
Resources Management
Office of Contract Business
Management
Director, RW-22
Analysis and Verification Division
Associate Director, RW-30
Office of Systems and Compliance
Associate Director, RW-40
Office of Storage and
Transportation
Director, RW-4/5
Office of Strategic Planning and
International Programs
Office of External Relations
Forrestal Building
Washington, DC 20585

U.S. Department of Energy
Albuquerque Operations Office
Attn: National Atomic Museum Library
P.O. Box 5400
Albuquerque, NM 87185-5400

U.S. Department of Energy
Research & Waste Management Div.
Attn: Director
P.O. Box E
Oak Ridge, TN 37831

U.S. Department of Energy (6)
Carlsbad Area Office
Attn: V. Daub
G. Dials
M. McFadden
R. Lark
R. Bills
J. A. Mewhinney
P.O. Box 3090
Carlsbad, NM 88221-3090

U.S. Department of Energy
Attn: E. Young
Room E-178
GAO/RCED/GTN
Washington, DC 20545

U.S. Department of Energy
Office of Environmental Restoration
and Waste Management
Attn: J. Lytle EM-30
Forrestal Building
Washington, DC 20585-0002

U.S. Department of Energy (3)
Office of Environmental Restoration
and Waste Management
Attn: M. Frei, EM-34, Trevion II
Washington, DC 20585-0002

U.S. Department of Energy
Office of Environmental Restoration
and Waste Management
Attn: S. Schneider, EM-342, Trevion II
Washington, DC 20585-0002

U.S. Department of Energy (2)
Office of Environment, Safety and Health
Attn: C. Borgstrom, EH-25
R. Pelletier, EH-231
Washington, DC 20585

U.S. Department of Energy (2)
Idaho Operations Office
Fuel Processing and Waste Management
Division
785 DOE Place
Idaho Falls, ID 83402

U.S. Environmental Protection Agency (2)
Radiation Protection Programs
Attn: M. Oge
ANR-460
Washington, DC 20460

U.S. Nuclear Regulatory Commission
Division of Waste Management
Attn: H. Marson
Mail Stop 4-H-3
Washington, DC 20555

Boards:

Defense Nuclear Facilities Safety Board
Attn: D. Winters
625 Indiana Avenue NW, Suite 700
Washington, DC 20004

Nuclear Waste Technical Review Board (2)
Attn: Chairman
S.J.S. Parry
1100 Wilson Blvd., Suite 910
Arlington, VA 22209-2297

Advisory Committee on Nuclear Waste
Nuclear Regulatory Commission
Attn: R. Major
7920 Norfolk Avenue
Bethesda, MD 20814

State Agencies:

Attorney General of New Mexico
P.O. Drawer 1508
Santa Fe, NM 87504-1508

Environmental Evaluation Group (3)
Attn: Library
7007 Wyoming NE
Suite F-2
Albuquerque, NM 87109

New Mexico Energy, Minerals, &
Natural Resources Dept.
Attn: Library
2040 S. Pacheco
Santa Fe, NM 87505

New Mexico Environment Dept. (3)
Secretary of the Environment
Attn: Mark Weidler
1190 St. Francis Drive
Santa Fe, NM 87503-0968

New Mexico Bureau of Mines &
Mineral Resources
Socorro, NM 87801

New Mexico Environment Dept.
WIPP Project Site
Attn: P. McCasland
P.O. Box 3090
Carlsbad, NM 88221

Laboratories/Corporations:

Battelle Pacific Northwest Laboratories
Attn: R.E. Westerman, MSIN P8-44
Battelle Boulevard
Richland, WA 99352

INTERA, Inc.
Attn: G.A. Freeze
1650 University NE, Suite 300
Albuquerque, NM 87102

INTERA, Inc.
Attn: J.F. Pickens
6850 Austin Center Blvd., Suite 300
Austin, TX 78731

INTERA, Inc.
Attn: W. Stensrud
P.O. Box 2123
Carlsbad, NM 88221

Los Alamos National Laboratory
Attn: B. Erdal, INC-12
P.O. Box 1663
Los Alamos, NM 87544

RE/SPEC Inc.
Attn: Angus Robb
4775 Indian School Rd. NE, Suite 300
Albuquerque, NM 87110-3927

RE/SPEC Inc. (10)
Attn: G.D. Callahan
P.O. Box 725
Rapid City, SD 57709-0725

Southwest Research Institute (2)
Center for Nuclear Waste Regulatory
Analysis
Attn: P.K. Nair
6220 Culebra Road
San Antonio, TX 78228-0510

Tech Reps Inc. (4)
Attn: J. Chapman (2)
T. Peterson (2)
5000 Marble NE, Suite 222
Albuquerque, NM 87110

Westinghouse Electric Corp. (5)
Attn: Library
C. Cox
L. Fitch
B.A. Howad
R. Kehrman
P.O. Box 2078
Carlsbad, NM 88221

S. Cohen & Associates
Attn: Bill Thurber
1355 Beverly Road
McLean, VA 22101

**National Academy of Sciences,
WIPP Panel:**

Howard Adler
Oxygrase, Inc.
7327 Oak Ridge High
Knoxville, TN 37909

Ina Alterman
Board on Radioactive Waste
Management
GF456
2101 Constitution Ave.
Washington, DC 20418

Rodney C. Ewing
Department of Geology
University of New Mexico
Albuquerque, NM 87131

Charles Fairhurst
Department of Civil and Mineral
Engineering
University of Minnesota
500 Pillsbury Dr. SE
Minneapolis, MN 55455-0220

B. John Garrick
PLG Incorporated
4590 MacArthur Blvd., Suite 400
Newport Beach, CA 92660-2027

Leonard F. Konikow
U.S. Geological Survey
431 National Center
Reston, VA 22092

Carl A. Anderson, Director
Board on Radioactive Waste Management
National Research Council
HA 456
2101 Constitution Ave. NW
Washington, DC 20418

Christopher G. Whipple
ICF Kaiser Engineers
1800 Harrison St., 7th Floor
Oakland, CA 94612-3430

John O. Blomeke
720 Clubhouse Way
Knoxville, TN 37909

Sue B. Clark
University of Georgia
Savannah River Ecology Lab
P.O. Drawer E
Aiken, SC 29802

Konrad B. Krauskopf
Department of Geology
Stanford University
Stanford, CA 94305-2115

Della Roy
Pennsylvania State University
217 Materials Research Lab
Hastings Road
University Park, PA 16802

David A. Waite
CH₂M Hill
P.O. Box 91500
Bellevue, WA 98009-2050

Thomas A. Zordon
Zordon Associates, Inc.
3807 Edinburg Drive
Murrysville, PA 15668

Universities:

University of New Mexico
Geology Department
Attn: Library
141 Northrop Hall
Albuquerque, NM 87131

University of Washington
College of Ocean & Fishery Sciences
Attn: G.R. Heath
583 Henderson Hall, HN-15
Seattle, WA 98195

Libraries:

Thomas Brannigan Library
Attn: D. Dresp
106 W. Hadley Street
Las Cruces, NM 88001

Government Publications Department
Zimmerman Library
University of New Mexico
Albuquerque, NM 87131

New Mexico Junior College
Pannell Library
Attn: R. Hill
Lovington Highway
Hobbs, NM 88240

New Mexico State Library
Attn: N. McCallan
325 Don Gaspar
Santa Fe, NM 87503

New Mexico Tech
Martin Speere Memorial Library
Campus Street
Socorro, NM 87810

WIPP Public Reading Room
Carlsbad Public Library
101 S. Halagueno Street
Carlsbad, NM 88220

Foreign Addresses:

Studiecentrum Voor Kernenergie
Centre d'Énergie Nuclaire
Attn: A. Bonne
SCK/CEN Boeretang 200
B-2400 Mol
BELGIUM

Atomic Energy of Canada, Ltd.
Whiteshell Laboratories
Attn: P. Goodwin
Pinewa, Manitoba
CANADA ROE 1L0

Francois Chenevier (2)
ANDRA
Route du Panorama Robert Schumann
B.P.38
92266 Fontenay-aux-Roses, Cedex
FRANCE

Jean-Pierre Oliver
OECD Nuclear Energy Agency
Division of Radiation Protection and
Waste Management
38 Boulevard Suchet
75016 Paris
FRANCE

Claude Sombret
Centre d'Études Nucléaires
de la Vallée Rhone
CEN/VALRHO
S.D.H.A. B.P. 171
30205 Bagnols-Sur-Ceze
FRANCE

Commissariat à l'Énergie Atomique
Attn: D. Alexandre
Centre d'Études de Cadarache
13108 Saint Paul Les Durance Cedex
FRANCE

Bundesanstalt für Geowissenschaften
und Rohstoffe
Attn: M. Langer
Postfach 510 153
D-30631 Hannover
GERMANY

Bundesministerium für Forschung und
Technologie
Postfach 200 706
5300 Bonn 2
GERMANY

Institut für Tieflagerung
Attn: K. Kuhn
Theodor-Heuss-Strasse 4
D-3300 Braunschweig
GERMANY

Gesellschaft für Anlagen und
Reaktorsicherheit (GRS)
Attn: B. Baltes
Schwertnergasse 1
D-50667 Cologne
GERMANY

Physikalisch-Technische
Bundesanstalt
Attn: P. Brenneke
Postfach 3345
D-3300 Braunschweig
GERMANY

Shingo Tashiro
Japan Atomic Energy Research Institute
Tokai-Mura, Ibaraki-Ken, 319-11
JAPAN

Netherlands Energy Research
Foundation ECN
Attn: L.H. Vons
3 Westerduinweg
P.O. Box 1
1755 ZG Petten
THE NETHERLANDS

Svensk Kärnbränsleforsörjning AB
Attn: F. Karlsson
Project KBS (Kärnbränslesakerhet)
Box 5864
S-102 48 Stockholm
SWEDEN

Nationale Genossenschaft für die
Lagerung Radioaktiver Abfälle (2)
Attn: S. Vomvoris
P. Zuidema
Hardstrasse 73
CH-5430 Wettingen
SWITZERLAND

AEA Technology
Attn: J.H. Rees
D5W/29 Culham Laboratory
Abington, Oxfordshire OX14 3DB
UNITED KINGDOM

AEA Technology
Attn: W.R. Rodwell
044/A31 Winfrith Technical Centre
Dorchester, Dorset DT2 8DH
UNITED KINGDOM

AEA Technology
Attn: J.E. Tinson
B4244 Harwell Laboratory
Didcot, Oxfordshire OX11 0RA
UNITED KINGDOM

D.R. Knowles
British Nuclear Fuels, plc
Risley, Warrington, Cheshire WA3 6AS
1002607 UNITED KINGDOM

Internal:

<u>MS</u>	<u>Org.</u>	
0827	1502	P.J. Hommert
1324	6115	P.B. Davies
1320	6119	E.J. Nowak
1322	6121	J.R. Tillerson
1322	6121	D.E. Munson (10)
1322	6121	F.D. Hansen
1395	6700	P. Brewer
1335	6705	M. Chu
1395	6707	M. Marietta
1335	6000	W. Weart
1395	6701	L. Shephard
1341	6306	A.L. Stevens
1328	6342	D.R. Anderson
1395	6743	V.H. Slaboszewicz
1341	6347	D.R. Schafer
1341	6348	J.T. Holmes
1328	6741	H.N. Jow
1330	6352	C.B. Michaels (2)
1330	6352	NWM Library (20)
9018	8523-2	Central Technical Files
0899	13414	Technical Library (5)
0619	12615	Print Media
0100	7613-2	Document Processing for DOE/OSTI (2)